UCRL-18706

cy 2

LIBRARY AND
DOCUMENTS SECTION

MÖSSBAUER RESONANCE STUDIES OF GOLD COMPOUNDS

Marjorie Omori Faltens
(Ph. D. Thesis)

February 1969

TWO-WEEK LOAN COPY

This is a Library Circulating Copy which may be borrowed for two weeks. For a personal retention copy, call Tech. Info. Division, Ext. 5545

LAWRENCE RADIATION LABORATORY
UNIVERSITY of CALIFORNIA BERKELEY

UCRL-18706

UCRL-18706

UNIVERSITY OF CALIFORNIA

Lawrence Radiation Laboratory
Berkeley, California

AEC Contract No. W-7405-eng-48

MÖSSBAUER RESONANCE STUDIES OF GOLD COMPOUNDS

Marjorie Omori Faltens

(Ph.D. Thesis)

February 1969

TABLE OF CONTENTS

ABSTRACT vii

I. INTRODUCTION 1

II. MÖSSBAUER EFFECT 2

A. General Background 2

B. Hyperfine Interactions 5

1. Isomer Shift 5

2. Nuclear Zeeman Splitting 7

3. Quadrupole Splitting 7

III. COORDINATION CHEMISTRY OF GOLD 12

A. Chemical Characteristics of Gold 12

B. Chemical Bonding in Gold Compounds 16

IV. EXPERIMENTAL TECHNIQUE AND APPARATUS 25

A. Source 25

B. Absorber Preparation 27

1. Tetrafluoroaurate(III), $[AuF_4]^-$ 30

2. Gold(III) trifluoride, AuF_3 31

3. Gold(III) trichloride, $AuCl_3$ 31

4. Gold(I) chloride, AuCl 32

5. Cesium aurous auric chloride, $Cs_2Au(I)Au(III)Cl_6$ ... 32

6. Sodium and potassium tetrachloraurate(III), $NaAuCl_4$ and $KAuCl_4$ 33

7. Gold(III) tribromide, $AuBr_3$ 33

8. Gold(I) bromide, AuBr 34

9. Potassium tetrabromoaurate(III), $KAuBr_4$ 34

10. Gold(III) iodide, AuI_3 35

11. Gold(I) iodide, AuI 35

12. Potassium dicyanoaurate(I), $KAu(CN)_2$ 36

13. Gold(I) cyanide, AuCN 36

14. Potassium trans-dicyanodihaloaurate(III) 37

15. Potassium tetracyanoaurate(III), $KAu(CN)_4$ 38

16. Sodium dithiosulfatoaurate(I), $Na_3Au(S_2O_3)_2$..... 38

17. Gold sulfides, Au_2S, Au_2S_2 and Au_2S_3 39

C. Apparatus 41

1. Radiation Detector System 41

2. Drive System 42

3. Velocity Transducer 45

4. Cryostat 52

D. Data Processing 55

V. EXPERIMENTAL AND THEORETICAL RESULTS 60

A. Results of the Mössbauer Effect Experiments 60

1. Gold(III) trifluoride, AuF_3 60

2. Tetrafluoroaurate(III), $[AuF_4]^-$ 62

3. Gold(III) trichloride, $AuCl_3$ 65

4. Gold(I) chlorine, AuCl 70

5. Sodium and potassium tetrachloroaurate(III), $NaAuCl_4$ and $KAuCl_4$ 72

6. Cesium Aurous Auric Chloride $Cs_2Au(I)Au(III)Cl_6$.... 76

7. Gold(III) tribromide, $AuBr_3$ 80

8. Gold(I) bromide, AuBr 82

9. Potassium tetrabromoaurate(III), $KAuBr_4$ 82

10. Gold(I) iodide, AuI 84

11. Gold(III) iodide, AuI_3 89

12. Gold(I) cyanide, AuCN 91

13. Potassium dicyanoaurate(I), $KAu(CN)_2$ 93

14. Potassium tetracyanoaurate(III), $K[Au(CN)_4]$ 95

15. Potassium trans-dicyanodihaloaurate(III), $Au(CN)_2X_2$ (X=Cl,Br,I) 99

16. Sodium dithiosulfatoaurate(I), $Na_2Au(S_2O_3)_2$..... 104

17. Au(III) cis-dicyanoethylene-1,2-dithiolate anion, $[AuS_4C_4(CN)_4]^-$ 106

18. Gold(III) -- sesquioxide, Au_2O_3 109

19. Gold sulfides: Au_2S, Au_2S_2 and Au_2S_3 112

B. General Observations About the Results 117

1. Isomer Shift 120

2. Quadrupole Splitting 124

3. Relationship of the Isomer Shifts and Quadrupole Splittings 128

C. Calculation of Nuclear Electron Density 134

D. Calculation of the Electric Field Gradient 137

1. Electric Field Gradient for 5d Electrons 140

2. Electric Field Gradient for 6p Electrons 143

E. Discussion 151

VI. SUMMARY 161

APPENDIX A 163

Error Analysis 163

APPENDIX B 168

Evaluation of $\langle 1/r^3 \rangle$ Calculations 168

APPENDIX C 173

Electric Field Gradients 173

1. The Main Sources of Electric Field Gradients 173

2. Calculation of Electric Field Gradients 175

APPENDIX D 182

The Calculation of q^{latt} Values 182

APPENDIX E 185

Evaluation of Crawford-Schawlow Effect 185

ACKNOWLEDGMENTS 189

REFERENCES 190

MÖSSBAUER RESONANCE STUDIES OF GOLD COMPOUNDS

Marjorie O. Faltens

Lawrence Radiation Laboratory
University of California
Berkeley, California 94720

January 1969

ABSTRACT

Mössbauer experiments were performed at liquid helium temperature on linear gold(I) compounds and square-planar gold(III) compounds. A linear relationship was established between the isomer shift and quadrupole splitting values for both the aurous and auric compounds. These results are explained in terms of the comparable electric field gradient values of the 5d and 6p electrons of gold and the differences in the ionic character of the compounds. The nuclear factor $\delta R/R$ for Au 197 was determined to be 3.1×10^{-4}. A scale was establihsed to indicate the number of 6s electrons on gold which corresponds to a given isomer shift and the number of 6p electrons and 5d electron holes which are responsible for the observed quadrupole splittings.

I. INTRODUCTION

The Mössbauer effect has proven to be a valuable tool in the fields of experimental chemistry and physics.[1,2] In particular, the Mössbauer effect provides a sensitive method of investigating the changes in the electronic environment of the Mössbauer nucleus as a function of the atoms to which it is bonded. Information about the electronic structure of an atom is accessible by several nuclear resonance techniques (e.g., NQR, NMR) but the results often involve ambiguities concerning the importance of ionic character and bond hybridization. The Mössbauer effect is unique in that it observes both the effects of the s electrons (isomer shift) and the unbalance of p and d electrons (quadrupole splitting); thus facilitating the interpretation of the results.

Interest in the present studies was initiated when it was found by D. A. Shirley[3] et al. that the quadrupole splittings of the square-planar gold(III) halides were much less than those of the corresponding linear gold(I) halides. Townes and Dailey[4,5,6] had proposed--with supporting evidence from lighter atoms--that the electric field gradients and thus the quadrupole splittings are mainly due to valence p electrons. Since gold(III) has two 6p valence electrons in the molecular plane and gold(I) has one 6p electron along the symmetry axis, it was expected that both oxidation states of gold would have similar values of quadrupole splittings. The large differences in the quadrupole splittings of the two oxidation states are explained by taking the 5d electrons into consideration.

II. MÖSSBAUER EFFECT

A. General Background

Several comprehensive reviews on the theory and application of the Mössbauer effect are available in the literature.[1,7,8,9] We will therefore limit this section to the discussion of the Mössbauer effect as related to the present investigation. The Mössbauer γ-ray resonance is a consequence of the recoil-free fraction of γ rays emitted and absorbed by the Mössbauer nucleus.

When a free atom at rest emits a γ ray between isomeric states whose energies differ by energy E_t, the atom recoils with an energy of E_R which is given by

$$E_R = E_t^2/2mc^2 \quad . \tag{1}$$

Here, m is the mass of the atom and c is the speed of light. The resultant energy of the γ ray, E_γ, is then

$$E_\gamma = E_t - E_R \quad . \tag{2}$$

Similarly, the γ ray energy, $E_{\gamma'}$, which is required to excite a nucleus of mass m to an isomeric state that is E_t higher is

$$E_{\gamma'} = E_t + E_R \quad . \tag{3}$$

This results in a $2E_R$ energy discrepancy from exact resonance conditions. E_R for Au 197 is about 1.6×10^{-2} eV. Although the

energy lost in the recoil is small, this energy loss is significant when compared to the inherently narrow natural linewidth, Γ_n, of the γ ray. Γ_n can be determined from the uncertainty principle if the average lifetime, τ, of the isomeric state is known:

$$\Gamma_n \tau = \hbar \tag{4}$$

$\hbar$ is Plank's constant divided by 2π. The natural linewidth of Au 197, which has a half life of $1.82 \pm 0.10 \times 10^{-9}$ seconds,[10] is 0.0972 ± 0.054 cm/sec. This is equivalent to $2.51 \pm 0.04 \times 10^{-7}$ eV. $2\Gamma_n$ is the minimum observable linewidth in the limit of zero absorber thickness. The experimental linewidths are generally wider. The ideal observable linewidth for Au 197 is 0.194 ± 0.10 cm/sec. Shirley, et al.[11] discuss absorbers of finite thickness.

The lines are sufficiently narrow that the γ ray emission and absorption lines do not overlap and a resonance is not observed. When the nucleus is embedded in a solid or crystallite, the recoil energy may be greatly diminished because the crystal may recoil as a whole. M is the mass of the

$$E_R \text{ (crystallite)} = E_\gamma^2/2Mc^2 \tag{5}$$

crystallite, which can approach 10^{18} atomic masses or more. As E_R gets vanishingly small, there is, quantum mechanically, a finite probability that no phonons will be excited in the crystal lattice and that therefore the γ ray will carry away the entire transition energy, E_t. The

fraction of these recoil-free events, f, is approximated by

$$f = \exp\left[-\frac{6E_R}{k\Theta_D}\left(\frac{1}{4} + \left(\frac{T}{\Theta_D}\right)^2 \int_0^{\Theta_D/T} \frac{x\,dx}{e^x - 1}\right)\right] \tag{6}$$

where T is the ambient temperature and k is the Boltzman's constant. Θ_D, the Debye temperature, is a characteristic of the crystal. For metals such as gold, possessing low Debye temperatures (Θ_D = 165°K), low ambient temperatures are required to obtain an acceptable recoil-free fraction of γ ray transitions. All of our experiments were performed at 4.2°K. At this temperature, the recoil-free fraction of the 77 keV γ ray for gold in platinum metal (our source) is 0.27 ± 0.03.[12] The shape of the absorption line is given by a Lorentz curve:

$$\sigma(E) = \sigma_{m'} \frac{(\Gamma/2)^2}{(E-E_0)^2 + (\Gamma/2)^2} \tag{7}$$

where Γ is the total linewidth of the absorption line. $\sigma_{m'}$ is the effective cross section for absorption and is defined as[11]

$$\sigma_{m'} = \frac{\lambda^2(2I^*+1)}{2\pi(2I+1)} \frac{1}{(1+\alpha)} \tag{8}$$

λ is the wave length of the radiation, I^* and I are the spins of the excited and ground states respectively. α is the internal conversion coefficient for the competing mode of decay. α is equal to 3.94 ± 0.14 for Au 197.[11]

B. Hyperfine Interactions

Due to the narrow linewidth of the resonance γ ray, the hyperfine structure of the nuclear transitions can be analyzed by the Mössbauer effect. The nuclear energy levels are perturbed by the surrounding electrons in the solid giving rise to three possible hyperfine interactions: the electric monopole, $\mathcal{H}_{IS}$; the magnetic dipole, $\mathcal{H}_M$; and the electric quadrupole interaction, $\mathcal{H}_Q$. The Hamiltonian for the interactions is

$$\mathcal{H} = \mathcal{H}_{IS} + \mathcal{H}_M + \mathcal{H}_Q \quad . \tag{9}$$

We shall discuss the three effects in turn.

The perturbation of the nuclear energy levels by the above interactions destroys the resonance conditions, but resonance can be restored by imparting a small Doppler velocity, v, to the γ ray of energy E. The change in the energy, ΔE, of the modulated γ ray is given by:

$$\Delta E = E\, v/c \tag{10}$$

where c is the speed of light. The velocity is taken as positive when the source approaches the absorber.

1. Isomer Shift

The nuclear energy levels are perturbed by the coulombic interaction between the nuclear and electronic charges in the nucleus. The isomer shift, IS, is the difference between the energy changes in the absorber, δE_{abs}, and the source, δE_s. The IS, given in Eq. (11) is a function of the mean nuclear charge radii, R_{ex} and R_g, of the

excited and ground states respectively and is also a function of the electron densities in the nuclei, $\sum_{abs} \psi(0)^2$ and $\sum_{s} \psi(0)^2$, of the absorber and source respectively.

$$IS = \delta E_{abs} - \delta E_s = \frac{4\pi Z e^2 R^2 c}{5E_\gamma} S'(Z) \left[\frac{R_{ex}-R_g}{R}\right]\left[\sum_{abs} \psi(0)^2 - \sum_{s} \psi(0)^2\right] \tag{11}$$

The constants have their usual significance.[13] The quantity in the first square brackets is the nuclear factor which is the same for any absorber-source pair of a given isotope. The quantity in the second square brackets is an atomic factor which reflects the electronic configuration about the nuclei of the source and absorber. R_{ex} for the 77 keV isomeric state of Au 197 is larger than R_g, so the nuclear factor is positive for our studies.[12] The electron density in the nucleus is chiefly governed by the number of s electrons since only they have non-zero probability density at the nucleus.* The inner d electrons can affect the charge density at the nucleus by screening the s electrons. In our experiments, the source was always Au 197 in platinum metal, thus $\sum_{s} \psi(0)^2$ was held constant and only $\sum_{abs} \psi(0)^2$

*Relativistic $p_{1/2}$ electrons also have a finite density in the nucleus. In Section V-C, the results show that the charge density of the $p_{1/2}$ electrons in the nucleus of gold is about 4% of that of the s electrons.

was varied. Therefore, a positive IS (where the absorption maximum occurs when the source is moving toward the absorber) indicates that $\sum_{abs} \psi(0)^2$ is greater than $\sum_{s} \psi(0)^2$.

For Au 197, Eq. (11) simplifies to

$$IS(cm/sec) = 5.39 \cdot 10^{-24}\ \delta R/R \Delta\psi(0)^2_{relativistic} \tag{12}$$

where

$$\Delta\psi(0)^2 \equiv \sum_{abs} \psi(0)^2 - \sum_{s} \psi(0)^2 \tag{13}$$

and δR is the difference between R_{ex} and R_g.

2. Nuclear Zeeman Splitting

The interaction of the nuclear magnetic moment, μ, and the effective magnetic field, H_{eff}, is given by:

$$H_M = -\frac{\mu}{I}\ H_{eff}\ . \tag{14}$$

This lifts the degeneracy of the spin I state into $2I + 1$ levels. The magnetic dipole transitions (M1) are governed by the following selection rule, $\Delta m = 0, \pm 1$. m is the projection of I on the symmetry axis. Since our compounds are all diamagnetic, we shall not elaborate on this hyperfine interaction.

3. Quadrupole Splitting

The quadrupole splitting arises from the interaction between the nuclear quadrupole moment, Q, and the electric field gradient,

$q(= \partial^2 V/ z^2)$. The Hamiltonian for this interaction is given by Eq. (15):[14]

$$H_Q = \frac{eqQ}{4I(2I-1)}\left[3I_z^2 - I(I+1) + \eta(I_x^2 - I_y^2) \right] \quad . \tag{15}$$

Here e is the electron charge, I the nuclear spin and I_z the projection of I on the z-axis. η, the asymmetry parameter, is given by:

$$\eta = \left(\frac{\partial^2 V}{\partial x^2} - \frac{\partial^2 V}{\partial y^2} \right) \Big/ \left(\frac{\partial^2 V}{\partial z^2} \right) \quad . \tag{16}$$

The convention is to select the x, y and z axes so that

$$\left| \frac{\partial^2 V}{\partial z^2} \right| \geqslant \left| \frac{\partial^2 V}{\partial x^2} \right| \geqslant \left| \frac{\partial^2 V}{\partial y^2} \right| \tag{17}$$

then η will take on values between zero and unity. If the crystal is axially symmetric, $\eta = 0$ and $m = I_z$ and the states of $\pm m$ are degenerate. Then ΔE is given by Eq. (18) and is non-zero for spin $I \geqslant 1$. For Au 197, only the ground state with spin $I = 3/2$ is perturbed by the quadrupole interaction:

$$\Delta E = \frac{|eqQ|}{4I(2I-1)} \left(3I_z^2 - I(I+1) \right) \left(1 + \frac{\eta^2}{3} \right)^{1/2} \quad . \tag{18}$$

Figure II-1 depicts the lifting of the energy degeneracy of the $I = +3/2$ state. The quadrupole splitting, QS, which is the difference between the energy changes of the ground and excited states is equal to $eqQ/2$ for Au 197 axially symmetric compounds.

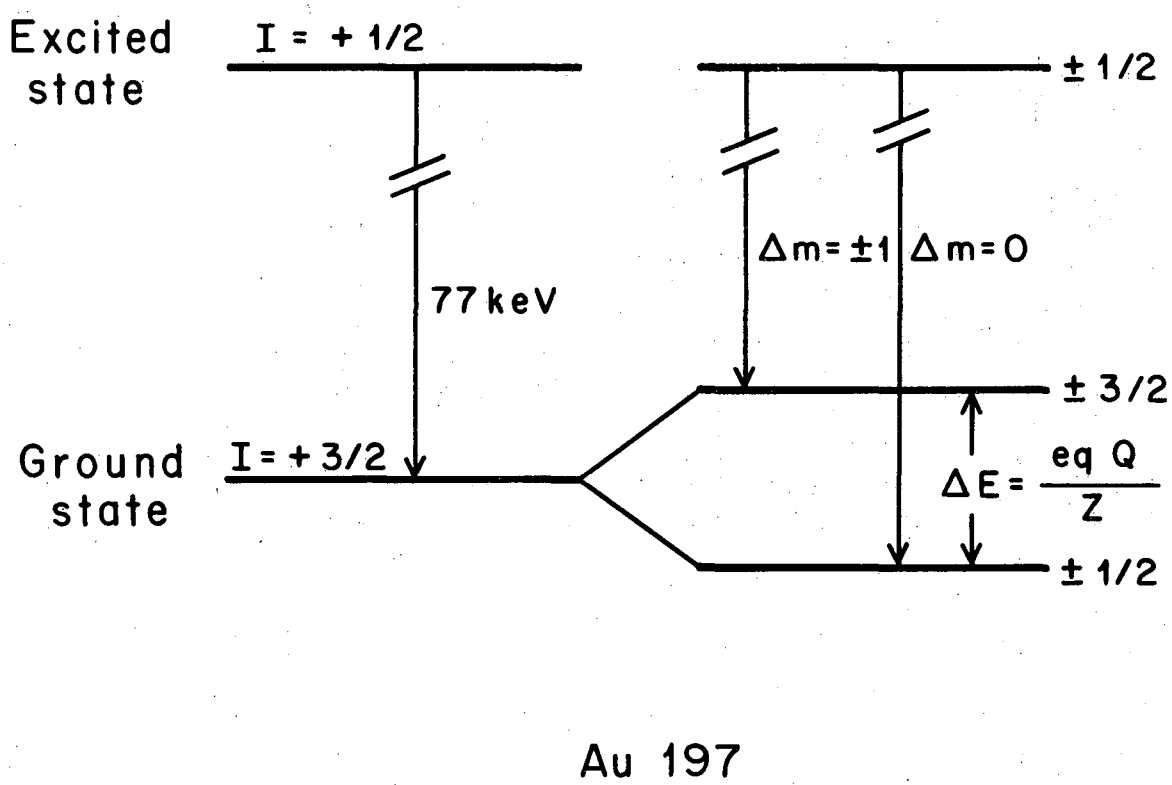

XBL691-1783

Fig. II-1. Splitting of nuclear energy level of Au 197 due to non-zero electric field gradient.

The electric quadrupole coupling interaction, like the isomer shift, is a function of both a nuclear and an atomic factor: the quadrupole moment which is a measure of the deviation of the nuclear charge distribution from spherical symmetry and the electric field gradient, q, which is a function of the electronic distribution on the vicinity of the nucleus. For a given isotope, Q is a constant ($Q = +0.594 \pm .01 \times 10^{-24} cm^2$) for the 77 keV isomeric state of Au 197);[15] therefore, we can deduce information about the interatomic bonds from the quadrupole splittings for compounds of the same isotope.

Several of our gold compounds have asymmetric QS doublets.* One conceivable source of the unequal line intensities is the existence of more than one chemical species of gold. Since gold generally forms fairly unstable compounds, this is always a possibility. We made special precautions against decomposition of our absorbers. An anisotropic absorber (or source) could also cause unequal line intensities. To help guard against this possibility, we carefully ground our samples. If the asymmetry parameter is non-zero, the transition components are no longer pure σ and π. For the single crystal, the intensities of the absorption lines are no longer equal. For the powder sample, however, the intensities are averaged over-all angles and the observed intensities are equal.

The third and less trivial possibility is the Gol'danskii effect. This effect has been treated in the literature[16,17,18,19] obviating an extensive development here.

---

*The three gold sulfides and $AuS_4C_4(CN)_4$ show the greatest asymmetry.

It has been shown that the ratio of the π- to the σ-transition intensities for an isotropic polycrystalline sample is:[18]

$$\frac{i\pi(\text{total})}{i\sigma(\text{total})} = \frac{\int_{-1}^{1} i\pi(\Theta)d\cos\Theta}{\int_{-1}^{1} i\sigma(\Theta)d\cos\Theta} = 1 \quad . \tag{19}$$

If the recoil-free fraction of the γ-transitions have angular dependence, we have

$$\frac{i\pi(\text{total})}{i\sigma(\text{total})} = \frac{\int_{-1}^{1} i\pi(\Theta)f\cos\Theta(d\cos\Theta)}{\int_{-1}^{1} i\sigma(\Theta)f\cos\Theta(d\cos\Theta)} \neq 1$$

resulting in unequal line intensities in the QS doublet. Gol'danskii, et al.[17,19] have experimentally tested and confirmed such an effect.

III. COORDINATION CHEMISTRY OF GOLD

A. Chemical Characteristics of Gold

The chief chemical characteristic of gold is its extreme inactivity. Neither oxygen nor strong acids attack gold, and the halogens at ordinary temperatures react with it very slowly, if at all. All gold compounds are easily decomposed. Due to its chemical inactivity, gold occurs naturally in only two forms: as native or metallic gold and as a component of the telluride minerals. Gold can be dissolved in a very dilute aqueous solution of potassium cyanide to form the stable dicyanoaurate(I) complex ion, $[Au(CN)_2]^-$. However, it does so only to the extent of $\sim$2 g of gold per liter. Aside from aqueous potassium cyanide, gold will only dissolve in the presence of the strongest oxidizing agent, especially those which contain chloride (as in aqua regia) and so form the stable chloride complex anion, $[AuCl_4]^-$.

Although the existence of divalent and tetravalent gold compounds has been reported, the principle valencies of gold are only +1 and +3. The much rarer +2 and +4 states are discussed briefly at the end of this section.

The wide occurrence of the +1 and +3 oxidation states complicates the chemistry of gold. With two possible valencies, there is the possibility of the atom being oxidized or reduced from one state to the other by its surroundings and the further problem of the aurous (+1) state disproportionating into the auric (+3) state and the free metal:

$$3\ Au(+1) \longrightarrow Au(+3) + 2\ Au(metal) \quad . \qquad (1)$$

This poses a special problem because the exceptional stability and insolubility of the metal promotes its separation.

Gold manifests some unusual chemical behavior. The order of stability of most metal halide complexes decreases in the following order:

$$F^- \gg Cl^- > Br^- > I^- \quad . \qquad (2)$$

Gold, however, is a member of a small group of metals which have a reversed order of complex stability. This makes it apparent that the stabilities of the gold complexes are directly related to their covalent character. Indeed, aurous fluoride AuF, (which should be highly ionic) does not exist due to thermo-instabilities.[20] AuF_3 and $[AuF_4]^-$ are extremely unstable. In general, a given gold(III) compound is more stable than the corresponding gold(I) compound. One exception is the instability of AuI_3 as compared to the relative stability of AuI.

The instability of AuI_3 may be partly attributed to steric crowding. From simple geometric considerations, the square-planar configuration of gold(III) compounds would require the radii ratio of the gold ion to the ligand ion, r+/r-, to be equal to or greater than 0.414. As seen in Table I, this requirement is met by all the ligands except the iodide ion (r+/r- = 0.394) and the carbon atom in the cyanide ion (r+/r- = 0.328). The cyanide complexes are stabilized by multiple

Table I. Ionic charge and ionic radii information for the ligands.

Ligand	Bonding Atom	Charge	Ionic Radius[22]	$\frac{r(Au+3)}{r(ligand)}$ *
F^-	F	-1	1.36	0.625
Cl^-	Cl	-1	1.81	0.460
Br^-	Br	-1	1.95	0.436
I^-	I	-1	2.16	0.394
O^{-2}	O	-2	1.40	0.608
$S_2O_3^{-2}$	S	-2	1.84	0.462
CN^{-1}	C	-4	2.60	0.328
Au^{+1}		+1	1.37	
Au^{+3}		+3	0.85[23]	

* It should be noted that none of the gold compounds are purely ionic; a fact which would increase the value of these ratios.

bonding. The iodide complex has no such stabilizing possibility. The possible existance of a low energy charge transfer band in AuI_3, which is similar to $[AuI_4]^-$, may also account for this instability. There is evidence from charge transfer spectra studies of $[AuCl_4]^-$ and $[AuBr_4]^-$, that $[AuI_4]^-$ would have a charge transfer band in the infrared region, causing it to decompose spontaneously at room temperature.[21]

Gold forms covalent bonds in great preference to ionic bonds. Not only are all gold compounds largely covalent, but apparently they all form complexes to increase their coordination number from one to two for the aurous state and from three to four in the auric state. Therefore, most gold compounds can accurately be considered coordination compounds in which the number of bonds (the coordination number) formed by one of the atoms is greater than that expected from the valency considerations. The atoms or groups of atoms attached to the central (gold) atom are referred to as ligands and are said to be coordinated or complexed to the central (metal) atom in the first coordination sphere.

Although +1 and +3 are the only important oxidation states of gold, other oxidation states have been reported. Therefore, for the sake of being complete, we will briefly discuss the +2 and +4 oxidation states.

Divalent gold complexes complexes have been reported[24] but we were not able to prepare it in sufficient quantity to observe a Mössbauer effect. Gold(I) dithiocarbamates, when treated with thiuram disulfide, are reported to yield gold(II) species in solution. It

would have an odd number of unshared electrons and thus would be paramagnetic. If the gold complex is isomorphous to the silver congener (which is drawn below), the gold(II) complex would have linear bonding with a square-planar coordination (Easley).[25] Divalent silver has a $4d^9$ electronic configuration.

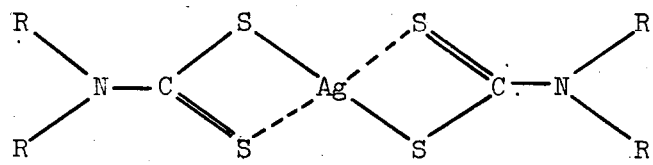

The only known tetravalent gold compound, AuF_4, was prepared by Rao and associates.[26] It is a pale yellow substance which is highly paramagnetic with μ = 3.9 B.M. at 293°K. AuF_4 was found to be amorphous to x-rays and no detailed structural information is available.

B. Chemical Bonding in Gold Compounds

Before discussing the hybridization of gold bonds, it will be instructive at this juncture to present the geometrics of the s, p and d atomic orbitals. The diagrams in Fig. III-1 indicate the surfaces of constant probability density.

The s orbital is spherically symmetric, while the three degenerate p orbitals (p_x, p_y and p_z) have positive and negative lobes along the respective axes and are mutually perpendicular.

There are three mutually perpendicular d orbitals (d_{xy}, d_{yz} and d_{xz}), each with four alternating plus and minus lobes in the respective planes. The lobes are at 45° angles with the respect to the Cartesian coordinate axes. A fourth d orbital, $d_{x^2-y^2}$, which is

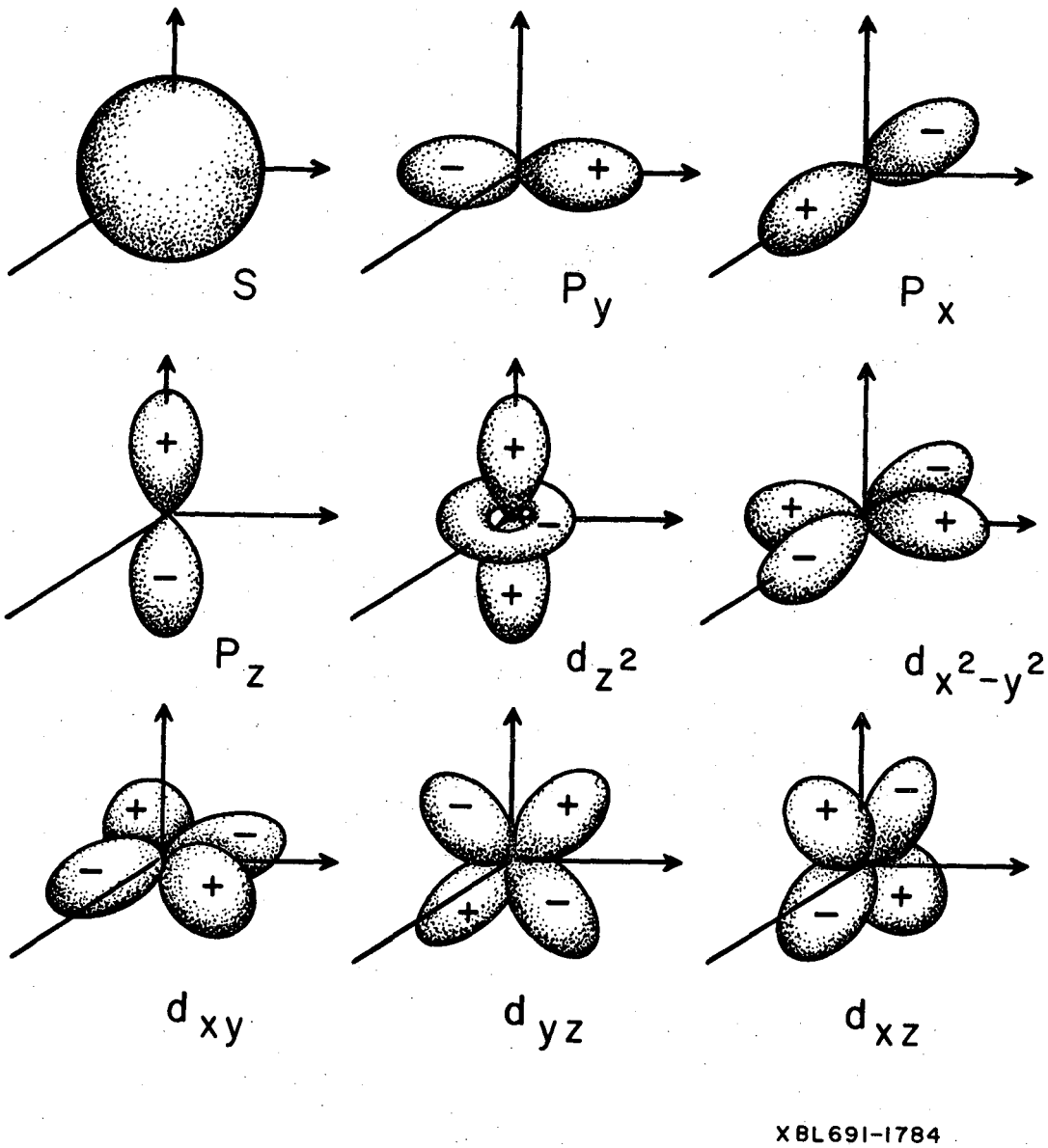

Fig. III-1. Configurations of the s, p and d atomic orbitals.

orthogonal to the first three, lies along the x-y axes with four lobes alternating in sign. Finally, there is the d_{z^2} orbital which has positive lobes along the z-axis and a negative collar around the z-axis in the x-y plane. In the absence of a perturbing ligand field, the five d orbitals of a given d shell are degenerate.

Pauling has developed much of the current valence-bond treatment of coordination compounds which successfully predicts the configurations of gold complexes. According to the valence-bond treatment, the central gold atom will make available a number of orbitals equal to its coordination number for the formation of covalent bonds with ligand orbitals. The strength of the bond is a function of the degree of overlap of the orbitals. The amount of overlap of the gold bonds with the ligand bonds is maximized by hybridizing the required number of gold atomic orbitals to form a new set of equivalent bonding orbitals possessing definite directional properties.

In valence-bond notation, gold(I) has a filled 5d inner shell, or core, of ten unshared electrons, and hydridizes the 6s and $6p_z$ orbitals for bonding. The orbitals are arbitrarily oriented along the ± z directions. Having a filled $5d^{10}$ core and no unpaired electrons, the aurous complexes are diamagnetic. The sp-hybrid orbitals are

$$\psi{+}Z = 1/\sqrt{2}\ (6s-6p_z)$$
$$\psi{-}Z = 1/\sqrt{2}\ (6s+6p_z)\ . \qquad (3)$$

The sp-hybrid orbitals consist of equal parts of normalized 6s and $6p_z$ wavefunctions of the gold atom. The configuration of the sp-hybrid orbitals are shown in Fig. III-2(a).

In bonding, the two bonding molecular orbitals can be approximated by the following expression:

$$\psi_{[AuL_2]^-} = \alpha\, 1/\sqrt{2}\ (6s \pm 6p_z)_{Au} \mp \beta\psi_L \quad . \tag{4}$$

The wave function of the ligand is denoted by ψ_L. The upper signs are for one bond and the lower signs are for the other. If one pair of signs were reversed, the resulting orbitals would be antibonding.

To facilitate the discussion of the bonding electrons, we will take the ligand, L, to be chlorine. We then have

$$\psi_{[AuCl_2]^-} = \alpha\, 1/\sqrt{2}\ (6s \pm 6p_z)_{Au} \mp \beta(3p_z)_{Cl} \quad . \tag{5}$$

Each bond involves two electrons which are spin-paired. Therefore, a total of four electrons participate in the two bonds. For $[AuCl_2]^-$ in $CsAuCl_2$, for example, the sources of the four electrons are:

Gold atom	1 electron
One each from both Cl atoms	2 electrons
Metal cation (Cs+)	1 electron
	4 electrons .

This electron count will facilitate the discussion of electric field gradients in Section V-D.

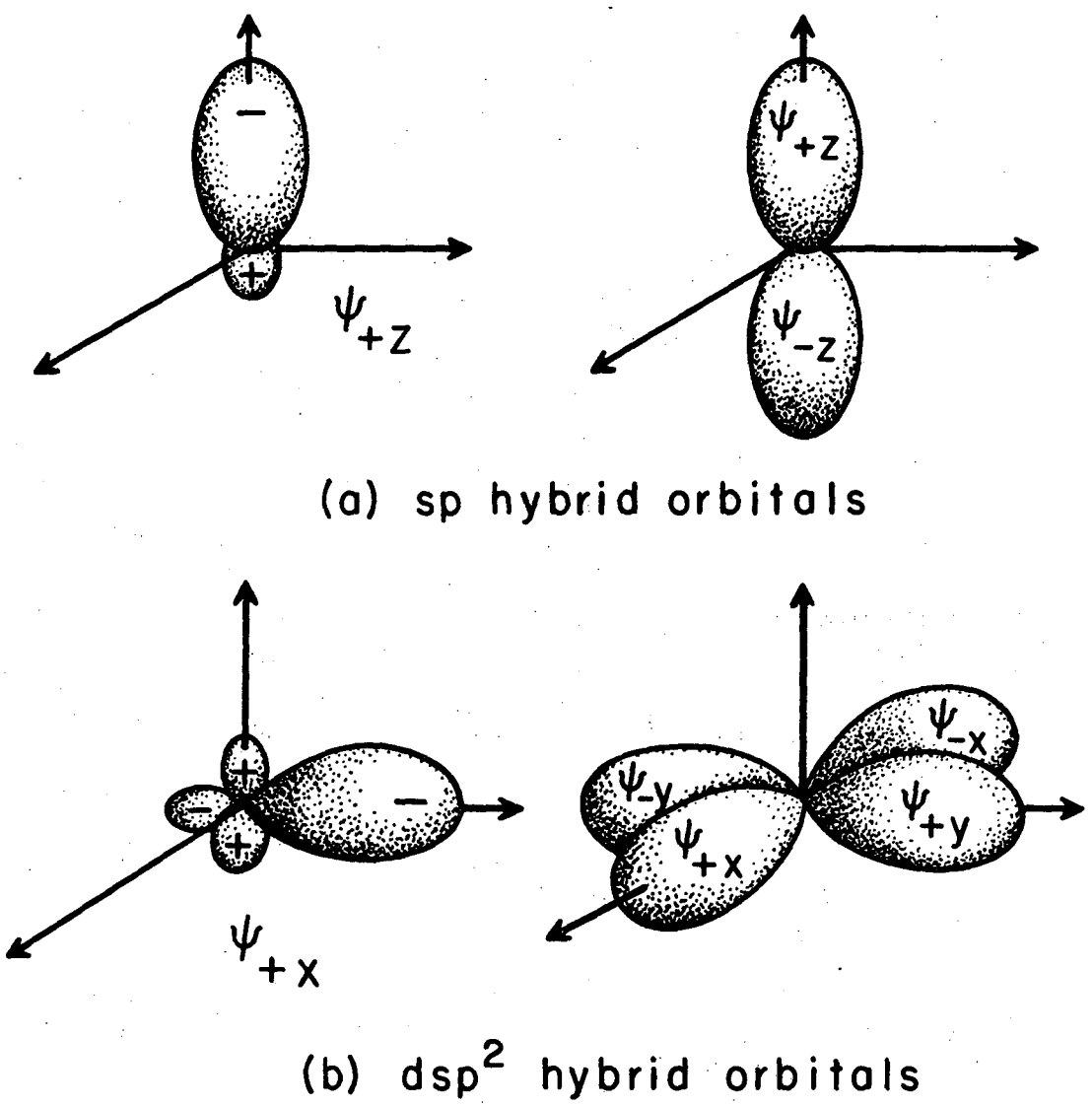

Fig. III-2. Configuration of the (a) sp and (b) dsp^2 hybrid orbitals.

For the AuCl polymer, it takes a little more care to account for all four bonding electrons. Each chlorine atom bridges two gold atoms in a zig-zag chain. In the diagram below, the bonding of the polymer is indicated by the electron pairs between the atoms. The gold electron is denoted by an open circle and each chlorine electron is given by an x.

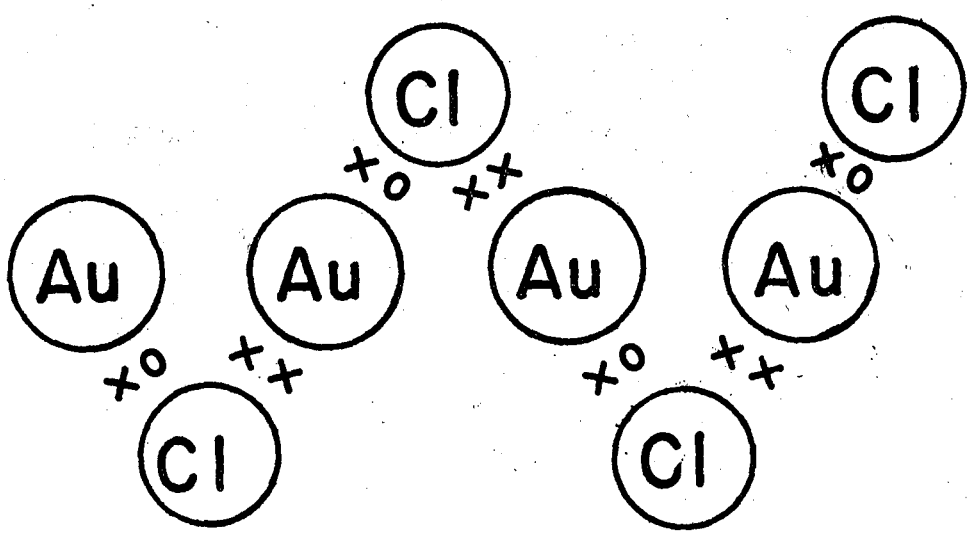

O gold bonding electrons

X chlorine bonding electrons

If the bonds are considered to be formed in the x-y plane of chlorine, the two chlorine bonding orbitals would be $3p_x$ and $3p_y$. One orbital will have a single electron and thus form a normal bond with gold. The

second, however, will be doubly occupied and will thus contribute both of the required electrons to form a bond with gold. The electron count would then be: one electron from the gold atom, one electron from the first chlorine atom and two electrons from the second chlorine atom to make a total of four electrons. The electrons from gold atoms are denoted by open circles, o, and those from chlorine atoms are denoted by the crosses, x.

Gold(III) has a $5d^8$ core of eight unshared electrons which are all spin-paired, resulting in diamagnetic complexes. For bonding, gold(III) forms four dsp^2 hybrid orbitals by utilizing its $5d_{x^2-y^2}$, 6s, $6p_x$, and $6p_y$ atomic orbitals. The orbitals, which have square-planar symmetry, can be taken along the $\pm x$ and $\pm y$ directions. Their configuration and orientations are indicated in Fig. III-2(b). The compositions of the four dsp^2 hybrid orbitals are

$$\begin{aligned}
\psi_{+X} &= 1/2(6s) - 1/\sqrt{2}(6p_x) - 1/2(5d_{x^2-y^2}) \\
\psi_{-X} &= 1/2(6s) + 1/\sqrt{2}(6p_x) - 1/2(5d_{x^2-y^2}) \\
\psi_{+Y} &= 1/2(6s) - 1/\sqrt{2}(6p_y) + 1/2(5d_{x^2-y^2}) \\
\psi_{-Y} &= 1/2(6s) + 1/\sqrt{2}(6p_y) + 1/2(5d_{x^2-y^2}) \quad .
\end{aligned} \tag{6}$$

The four molecular orbitals for gold(III) compounds are similar to the $[AuCl_4]^-$ molecular orbitals which are given below.

$$\psi_{[AuCl_4]^-} = \begin{array}{l} \{1/2(6s) \pm 1/\sqrt{2}(6p_x) - 1/2(5d_{x^2-y^2})\}_{Au} \mp (3p_x)_{Cl} \\ \\ \{1/2(6s) \pm 1/\sqrt{2}(6p_y) + 1/2(5d_{x^2-y^2})\}_{Au} \mp (3p_y)_{Cl} \end{array} . \quad (7)$$

Again, as in the case of the gold(I) molecular orbitals, the upper signs represent one molecular orbital and the lower signs represent the other. The eight required electrons for the four bonds are supplied by the following atoms

Gold atom	3 electrons
Metal cation(Na+)	1 electron
Four chlorines, one each	4 electrons
	8 electrons .

In the gold(III) dimers such as $(AuCl_3)_2$, the four terminal halides (Cl) contribute one electron each to the bonds. The two bridging halides (Cl), however, utilize two p orbitals, as in the example of the AuCl polymer. The bonding electron count for $(AuCl_3)_2$ is

Gold atom	3 electrons
Two terminal chlorines one each	2 electrons
One bridging chlorine one electron	1 electron
Other bridging chlorine filled 3p orbital	2 electrons
	8 electrons .

The bonding electrons in $(AuCl_3)_2$ are depicted in the diagram below:

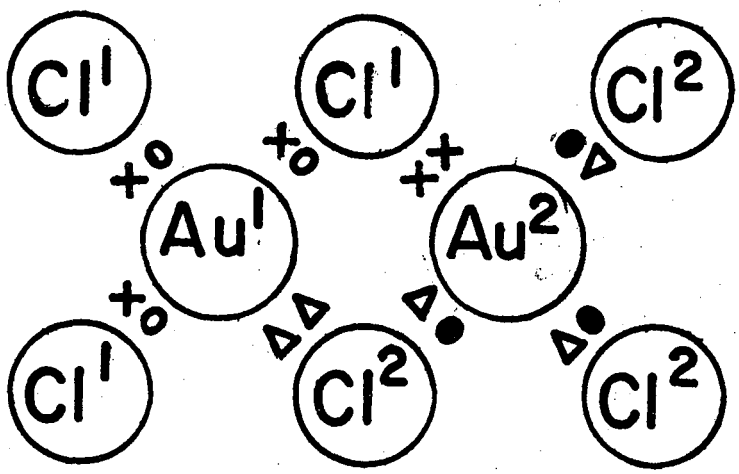

O gold 1 bonding electrons

● gold 2 bonding electrons

✕ chlorine 1 bonding electrons

Δ chlorine 2 bonding electrons

From the bond-strength criterion of maximum overlap of orbitals, the valence-bond theory correctly predicts that the tervalent gold complexes are in general more stable than the corresponding univalent gold complexes. The relative bond strengths of the sp and dsp^2 hybrid orbitals are 1.732 and 2.694 respectively.*

---

*The bond strengths are taken relative to the s orbital. See Pauling's Nature of the Chemical Bond, Reference 22.

IV. EXPERIMENTAL TECHNIQUE AND APPARATUS

Our Mössbauer apparatus basically consists of a source, an absorber and a detector, plus a means of imparting a Doppler velocity to the source (or absorber) to modulate the resonance gamma ray energy. This velocity drive system includes a linear drive amplifier and an instantaneous velocity monitor for the moving source (or absorber). All of our experiments were performed at liquid helium temperature (4.2°K) in a three-wall cryostat. These basic systems are described below. A block schematic diagram of the electronic equipment is given in Fig. IV-1.

A. Source

Pt 197, which populates the 77.345 ± .004 keV[27] isomeric state of Au 197, was obtained by thermal neutron bombardment of Pt 196. The latter was purchased as a powder in 65% enrichment from the Oak Ridge Radioisotopes Division. The Pt 196 powder was solidified by heating it in a zinc oxide crucible at 1750°C for ten minutes in a vacuum. (This is a few degrees below its melting point. At the actual melting point of platinum, 1769°C, we found that the metal wets the crucible.) The solid source could then be moved with respect to the absorber with little danger of extraneous movements due to bouncing of unsecured powder particles. The active source was contained in Mylar tape which could subsequently be dissolved with benzene. The spent source could be re-irradiated several times.

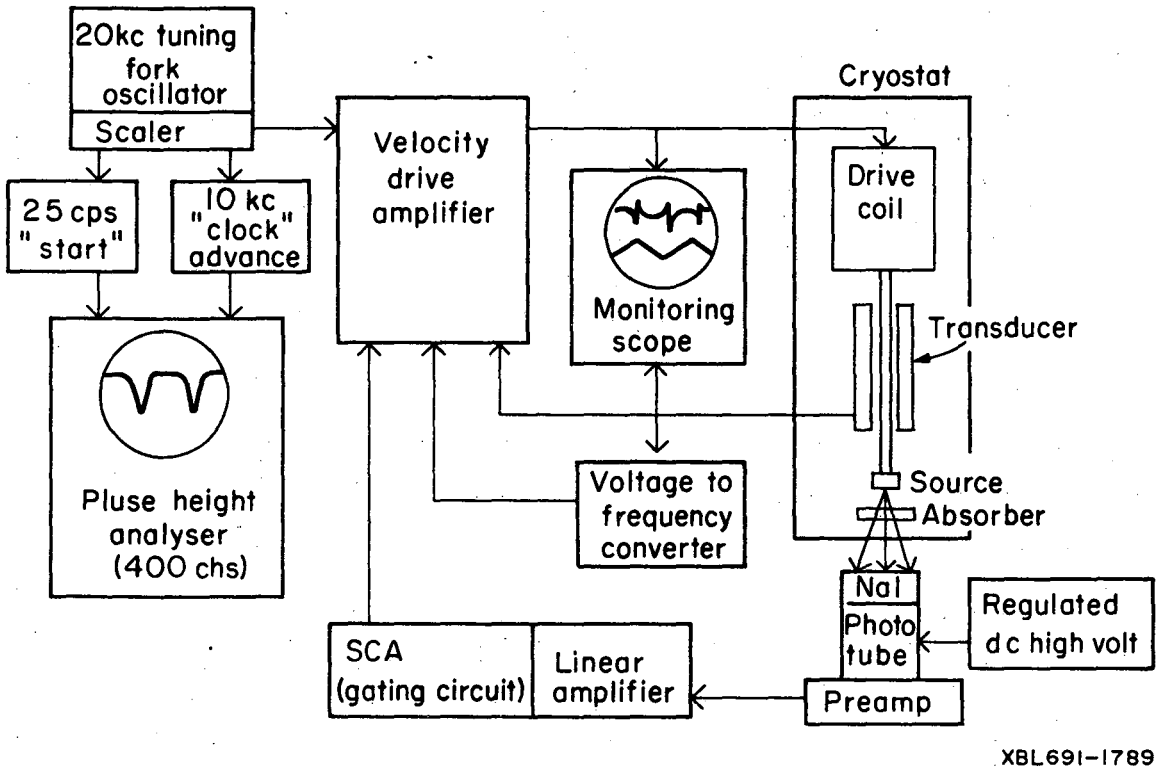

Fig. IV-1. Schematic diagram of Mössbauer effect electronic circuitry.

Pieces of Pt 196 weighing about 10 mg. each were sent to the General Electric Vallecitos reactor for an 18-hour irradiation in a flux of 2×10^{14} neutrons/cm^2/sec. When Vallecitos was not available, a 24-36 hour irradiation at a flux of about 2×10^{13} neutrons/cm^2/sec was obtained at the University of California's reactor in Livermore, California. These sources were used in the form received from the reactors, without further heat treatment or chemical modifications. The absorbers were gold nuclei in various chemical compounds. The decay scheme for Au 197 is given in Fig. IV-2.

B. Absorber Preparation

All of the gold compounds, except where indicated, were prepared in this laboratory and the methods of preparation are given below. Generally, the samples were prepared in the wet a few hours before the Mössbauer experiment was performed so as to keep the decomposition to a minimum. The absorbers were stored at dry ice or liquid nitrogen temperatures and when necessary were kept in the dark to avoid either photo- or thermo-decomposition. A half-gram sample of powdered absorber was placed in a lucite or teflon container which pressed the powder into an uniform disc of 2 cm^2 area. A photograph of these containers* is

---

*Lucite absorber holders were used except in the cases of highly reactive AuF_3 and $[BrF_2]^+[AuF_4]^-$, at which time we used teflon absorber holders. The cylinder, cover and rim-press shown in the 2nd row of Fig. IV-3 was commonly used. The fully assembled absorber holder is the forth item in the 2nd row. The lucite absorber holder in the top row is used when only a small sample is available. The teflon absorber holder is indicated in the photograph.

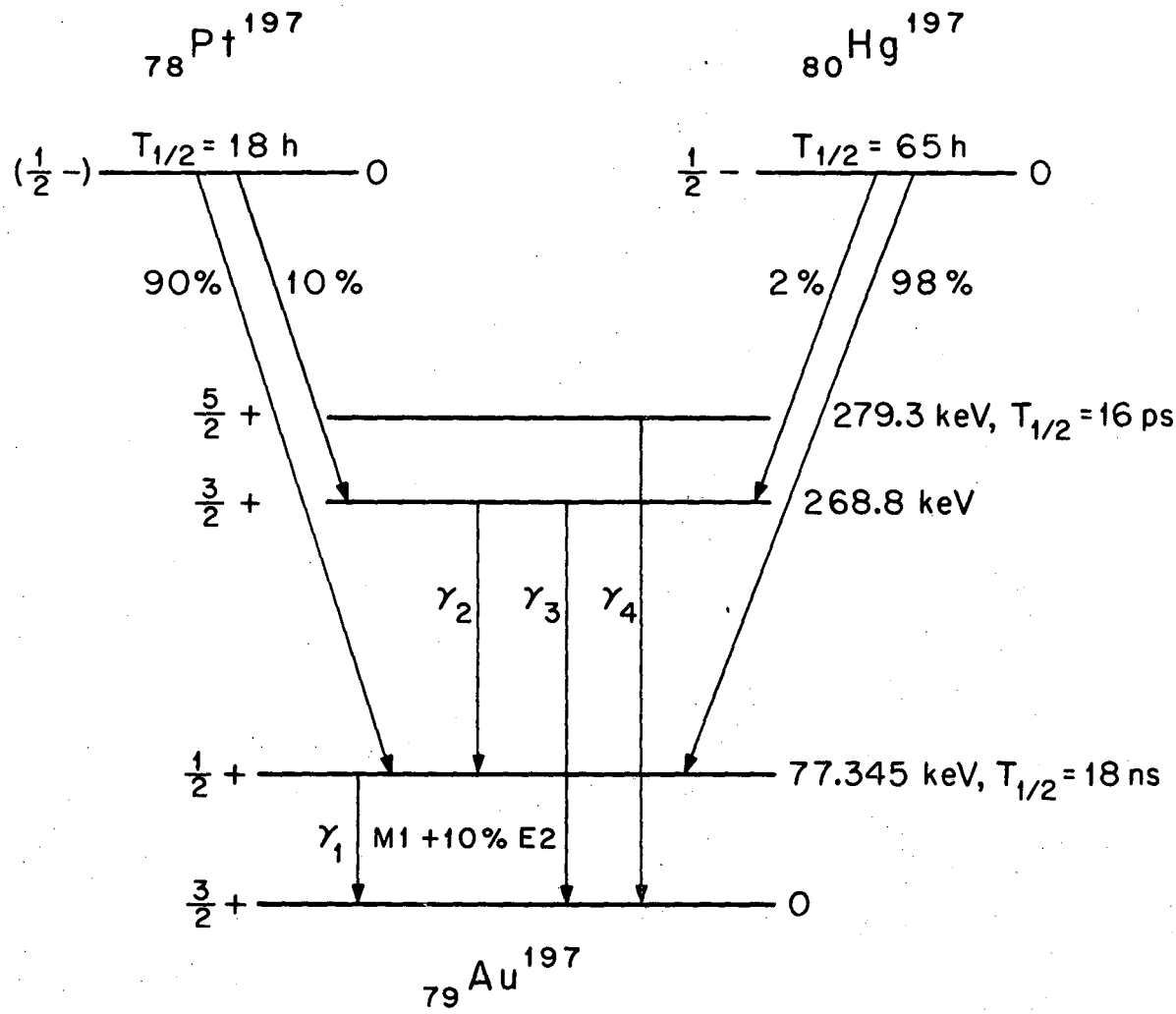

γ_1 = 77.345 keV

γ_2 = 191.5 keV

γ_3 = 268.8 keV

γ_4 = 279.3 keV

XBL691-1786

Fig. IV-2. Decay scheme of Au 197 Mössbauer nucleus (Lederer, et al.[28]).

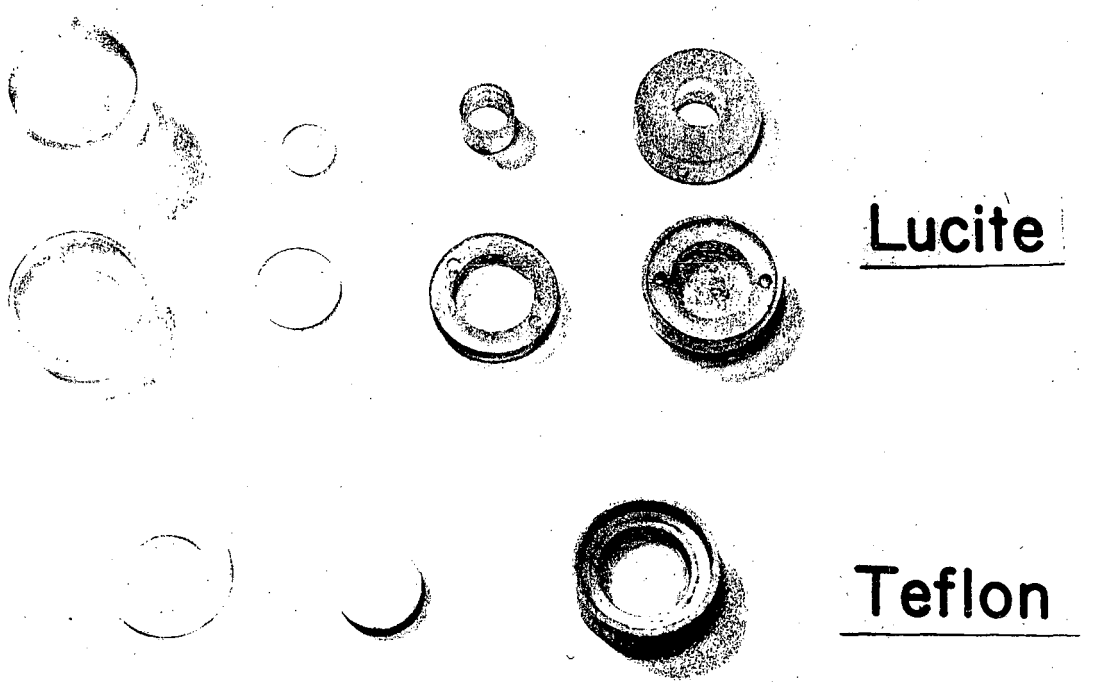

Fig. IV-3. Photograph of the Lucite and Teflon absorber holders.

given in Fig. IV-3. Once in the cryostat, where conditions of inert atmosphere (He gas) and low temperature (4.2°K) prevailed, decomposition was virtually arrested.

The compounds were characterized by chemical analysis and x-ray diffraction patterns when possible. In the following Sections, the compounds are enumerated along with their chemical characteristics and methods of preparation.

1. Tetrafluoroaurate(III), $[AuF_4]^-$

Because of the high reactivity and toxicity of BrF_3 and the ease with which moisture reacts with the gold fluorides, the preparation* was done in a Monel reaction vacuum system. One gram of 30-mesh gold powder was placed in a translucent "Kel-F" reaction vessel† and dried by evacuating the heated vessel overnight. Ten to fifteen milliliters of BrF_3 were transferred into the vessel and allowed to react at room temperature. The light yellow BrF_3 turned dark red to black with bromine as it was liberated in the reaction

$$\underset{\text{mustard yellow}}{\text{Au metal}} + \underset{\text{light yellow}}{2BrF_3} \longrightarrow \underset{\text{bright yellow}}{AuBrF_6} + \underset{\text{dark red}}{\tfrac{1}{2}\,Br_2} \quad . \qquad (1)$$

*The details of the preparation has been reported by A. G. Sharp.[44]

†Kel-F is a non-reactive fluoro-organic substance. The reaction tubes were purchased from Argonne National Laboratories.

The bromine was removed periodically by collecting it into a liquid nitrogen cold finger. The completion of the reaction was marked by the cessation of bromine liberation and subsequent coloration. The bright yellow $AuBrF_6$ was isolated by heating the reaction vessel to 50°C and removing the excess BrF_3 into a cold finger. This final step took approximately six hours. The sample was prepared as an absorber by putting it into a non-reactive Teflon absorber holder.

2. Gold(III) trifluoride, AuF_3

Gold trifluoride was prepared by converting $AuBrF_6$ in the following reaction,

$$\underset{\text{bright yellow}}{AuBrF_6} \xrightarrow{120^\circ C} \underset{\text{paprika orange}}{AuF_3} + \underset{\text{light yellow}}{BrF_3} \uparrow \qquad (2)$$

by heating the system to 120°C in a vacuum for about an hour. This compound, like $AuBrF_6$, was transferred into a Teflon absorber holder in a dry-box. The chemical analysis gave a ratio of gold-to-fluoride of 1.0/3.0.

3. Gold(III) trichloride, $AuCl_3$

The auric chloride was prepared from chlorauric acid, $HAuCl_4$, by heating it in a tube furnace in an atmosphere of dry chlorine gas. The chlorauric acid, which is commercially available as gold chloride, can be prepared by dissolving gold in aqua regia. The reaction is:

$$\underset{\text{golden orange}}{HAuCl_4 \cdot 4H_2O} \xrightarrow[175^\circ C]{Cl_2} \underset{\text{brownish red}}{AuCl_3} + HCl \uparrow + H_2O \uparrow \quad . \qquad (3)$$

Chlorine gas was dried by passing it through two sulfuric acid scrubbing towers. The trichloride reacts readily with moisture in the air. A typical analysis gave a chlorine-to-gold molar ratio of 2.46/1.00. This ratio was low in Cl due to loss of Cl_2 during analysis.

4. Gold(I) chloride, AuCl

By heating auric chloride to 235°C in an atmosphere of dry hydrogen chloride gas, one can decompose it into aurous chloride

$$\underset{\text{brownish red}}{AuCl_3} \xrightarrow{235^\circ C} \underset{\text{light yellow}}{AuCl} + Cl_2 \uparrow \quad . \tag{4}$$

Aurous chloride reacts readily with atmospheric moisture to form auric chloride. At elevated temperatures, AuCl will disproportionate into $AuCl_3$ and gold metal. The presence of $AuCl_3$ can be detected by its intense brownish-red color. Gold metal can be recognized by its darker mustard-yellow color. It has been suggested that aurous chloride can be purified of auric chloride by rinsing it with anhydrous ether. This procedure imparts a pale but distinct green tinge to the compounds: aurous chloride turns to this color upon standing for a few days in a desiccator. We used the compound as it came from the tube furnace. A typical analysis gave a chlorine-to-gold molar ratio of 1.05/1.00.

5. Cesium aurous auric chloride, $Cs_2Au(I)Au(III)Cl_6$

The preparation of black $Cs_2Au(I)Au(III)Cl_6$ requires a large excess of CsCl and a dilute solution of gold complex to avoid the deposition of the sparingly soluble yellow $CsAuCl_4$. In the preparation,

we mixed 2 grams of AuCl with 12 grams of CsCl in a beaker containing 300 cc 6N HCl. The mixture was boiled, cooled, filtered, and allowed to crystallize. The details of the preparation is given by Wells.[29]

6. Sodium and potassium tetrachloraurate(III), $NaAuCl_4$ and $KAuCl_4$

These two salts were purchased from Alfa Inorganics, Inc. $NaAuCl_4$ is light bright-yellow and $KAuCl_4$ is a deep golden-yellow color.

7. Gold(III) tribromide, $AuBr_3$

By combining and mechanically stirring aqueous liquid bromine and 30-mesh gold powder, one obtains $AuBr_3$ by the following reaction

$$\underset{\text{mustard yellow}}{Au} + \underset{\text{dark red}}{3/2\ Br_2} \longrightarrow \underset{\text{black}}{AuBr_3} \quad . \tag{5}$$

Chemical analysis yields an average bromine-to-gold molar ratio of 2.96/1.00.

In an attempt to prepare bromauric acid, $HAuBr_4 \cdot xH_2O$, we reacted gold powder with an acid mixture of three-parts HBr and one-part nitric acid. After the brown nitrous oxide, NO_2, stopped evolving, the dark reddish-brown solution was decanted to check for unreacted gold powder. The solution was then evaporated to dryness in air. However, chemical analysis gave a ratio of bromine-to-gold of 3.04-to-1.00 indicating that $AuBr_3$ was probably formed. The physical appearance was that of $AuBr_3$, black.

8. Gold(I) bromide, AuBr

Aurous bromide was prepared by heating auric bromide at 100°C in an atmosphere of dry argon gas:

$$\underset{\text{black}}{AuBr_3} \xrightarrow[\text{dry}]{100^\circ C} \underset{\text{gray-yellow}}{AuBr} + Br_2 \uparrow \quad . \tag{6}$$

Above 115°C, AuBr decomposes into its elements. This reaction, which takes approximately a half-day, was carried out in a tube furnace. AuBr is soluble in water in which it disproportionates into $AuBr_3$ and metallic gold. A chemical analysis gave a gold-to-bromide molar ratio of 1.006/1.000.

9. Potassium tetrabromoaurate(III), $KAuBr_4$

The compound $KAuBr_4$ was prepared according to the method outlined by Bailar.[30] The reaction can be summarized as follows

$$KBr + Au + 3/2\ Br_2 \xrightarrow{55^\circ C} \underset{\substack{\text{dark}\\ \text{reddish-brown}}}{KAuBr_4 \cdot 2H_2O} \quad . \tag{7}$$

The actual molar ratio of bromine-to-gold used was four-to-one. The $KAuBr_4$ was dissolved in methanol and filtered through sintered glass followed by evaporation to dryness at 40°C in a stream of air. The chemical analysis gave the following molar ratios: K/Au/Br = 1.02/1.00/3.97.

10. Gold(III) iodide, AuI_3

Auric iodide, AuI_3, decomposes into gold metal and aurous iodide, AuI, at 25°C. We made several attempts to prepare AuI_3 at 0°C by slowly pouring an aqueous solution of chlorauric acid into an aqueous solution of potassium iodide:

$$[AuCl_4]^- + 4I^- \longrightarrow [AuI_4]^- + 4Cl^- \qquad (8)$$

$$3[AuI_4]^- + [AuCl_4]^- \longrightarrow 4AuI_3 + 4Cl^- \quad . \qquad (9)$$

At first, a brownish precipitate forms, which Prescott and Johnson suggest is $KAuI_4$, an intermediate product.[31] It quickly reacts with the excess $[AuCl_4]^-$ to form AuI_3. This precipitate was filtered through a medium sintered glass funnel and washed with ice water. The brownish precipitate turns into a dark dull green clay-like substance, AuI_3. Auric iodide decomposes into aurous iodide on standing in air. Although a typical analysis gave an iodine-to-gold molar ratio of about 2.8/1.0, and the color was that of AuI_3, we believe that the substance was essentially converted into aurous iodide and the extra iodine existed in elemental form. See the discussion of the results in Section V.

11. Gold(I) iodide, AuI

Aurous iodide is more easily prepared than the other gold halides. It is precipitated by slowly adding a dilute solution of KI to an equivalent amount of chlorauric acid, $HAuCl_4$, in aqueous solution. The reaction is

$$3I^- + [AuCl_4]^- \longrightarrow AuI + 3Cl^- + I_2 \quad . \qquad (10)$$

bright orange — lemon yellow

This yellow, finely-divided substance has a tinge of green. A typical analysis gave an iodine-to-gold molar ratio of 1.05/1.00.

12. Potassium dicyanoaurate(I), $KAu(CN)_2$

$KAu(CN)_2$ can be prepared from elemental gold by the "old cyanide process" used by gold miners. The chemical reactions involved are probably,

$$Au + O_2 + 2H^+ + 4(CN)^- \longrightarrow 2[Au(CN)_2]^- + HOOH \qquad (11)$$

$$HOOH + 4(CN)^- + 2Au \longrightarrow 2[Au(CN)_2]^- + 2(OH)^- \quad . \qquad (12)$$

Gold powder in a dilute aqueous solution of KCN was vigorously stirred with a magnetic stirrer. A stream of air was bubbled through the solution. About five grams of 30-mesh gold powder can be dissolved overnight. The $KAu(CN)_2$ was purified by recrystallization from water.

13. Gold(I) cyanide, AuCN

AuCN was prepared by heating an acidic aqueous solution of $KAu(CN)_2$ at 50°C:

$$H^+ + [Au(CN)_2]^- \xrightarrow{50°C} AuCN + HCN \uparrow \quad . \qquad (13)$$

Gold(I) cyanide is sparingly soluble in water. No chemical analysis was done due to difficulty in dissolving AuCN.

14. Potassium trans-dicyanodihaloaurate(III)

a. $KAu(CN)_2Cl_2$. The halogen-cyanide mixed complexes were prepared by the method outlined by J. M. Smith *et al.*[32] The chlorine-cyanide complex was formed by dissolving 0.02 moles of $KAu(CN)_2$ in 100 cc water and 30 cc methanol solution. The solution was mechanically stirred while chlorine gas was being bubbled through it. This was continued overnight to insure a complete reaction. The solution was then evaporated until very pale yellow crystals began to appear, after which the solution was chilled with ice and the complex was filtered and collected. The $KAu(CN)_2Cl_2$ was recrystallized from water. The analysis gave the following molar ratios: K/Au/Cl/CN = 1.03/1.00/1.99/1.99.

b. $KAu(CN)_2Br_2$. The bromine-cyanide mixed complex was prepared by mixing an aqueous solution of $KAu(CN)_2$ with an excess amount of liquid bromine which had been dissolved in methanol. The mixture was mechanically stirred overnight then partially evaporated, chilled in ice and filtered. The chemical analysis gave the following molar ratios: K/Au/Br/CN = 1.03/1.00/2.05/1.98.

c. $KAu(CN)_2I_2$. Like its chlorine and bromine congeners, it was prepared from $KAu(CN)_2$. An aqueous solution of $KAu(CN)_2$ was stirred with a solution of iodine which was dissolved in methanol. After reacting overnight, this solution was partially evaporated, chilled to 0°C and the crystals were collected by filtering. A chemical analysis gave: K/Au/I/CN = 1.02/1.00/2.04/2.05.

15. Potassium tetracyanoaurate(III), $KAu(CN)_4$

$KAu(CN)_4$ was prepared by treating 0.02 moles of $KAu(CN)_2Br_2$ with 0.04 moles KCN in 60 cc methanol:

$$\underset{\text{bright yellow}}{KAu(CN)_2Br_2} + 2KCN \xrightarrow{CH_3OH} \underset{\text{colorless}}{KAu(CN)_4} + \underline{KBr} \quad .$$

The yellow solution was stirred until it turned colorless. Then the solution was evaporated down to 15 cc and filtered to remove the white crystals of KBr. After carefully evaporating the clear solution to dryness, it was recrystallized from water. The chemical analysis gave: K/Au/CN = 1.08/1.00/4.02. This sample tested positive for Br^- which is probably from residual KBr impurity. This would account for the slight excess potassium in the chemical analysis.

16. Sodium dithiosulfatoaurate(I), $Na_3Au(S_2O_3)_2$

The reactions involved in the preparation of the gold thiosulfate complex can be summarized as follows

$$3(OH)^- + [AuCl_4] \longrightarrow Au(OH)_3 + 4Cl_4^- \qquad (15)$$

$$Au(OH)_3 + 4Na_2S_2O_3 \longrightarrow 3NaOH + Na_2S_4O_6 + Na_3Au(S_2O_3)_2 \ . \qquad (16)$$

The details of the preparation are given by J. Brown.[33] We started by adding 21 grams of $HAuCl_4 \cdot 4H_2O$ to about 75 ml of water. To this solution, we added a 40% (by weight) solution of NaOH dropwise until a vivid

red-orange precipitate started to form. This solution was then poured into a mechanically stirred solution of 50 grams $Na_2(S_2O_3)\cdot 5H_2O$ in 100 ml of water, causing no visible change. The direction of pouring is important because if the solutions are mixed in the reverse order, the insoluble black precipitate of gold sulfide results. While still stirring vigorously, 4M HNO_3 was added dropwise at such a rate that any red coloration caused by the addition of each drop of acid disappeared completely before the next was added. The acid was added until all of the red-orange precipitate had dissolved and the red coloration no longer appeared. The solution, which amounted to about 200 cc, was filtered through a "fine" sintered glass funnel and to it was added 800 cc of ethyl alcohol. The white fluocculent precipitate which formed was collected on a similar glass funnel and washed with ethanol (about 100 cc), then recrystallized twice by dissolving the gold thiosulfate in the minimum of water and then adding about two volumes of ethanol and allowing the crystals to grow overnight.

17. Gold sulfides, Au_2S, Au_2S_2 and Au_2S_3

The three gold sulfide compounds were reasonably stable and sparingly soluble in water. They are all dark substances.[35]

a. Au_2S. Au_2S is a steel-gray sulfide with a solubility product[34] of less than 10^{-3}. It dissolves in aqua regia, potassium cyanide, and sulfide solutions. The compound was prepared by bubbling H_2S through an aqueous solution of aurous cyanide:

$$2[Au(CN)_2]^- + H_2S + 2H^+ \xrightarrow{H_2O} Au_2S + 4HCN\uparrow \quad . \qquad (17)$$

The insoluble precipitate was washed with dilute HCl solution to avoid peptizing the precipitate. The initially dark reddish-brown precipitate soon turned steel-gray. The chemical analysis gave the following molar ratio: Au/S = 2.04/1.00.

b. $\underline{Au_2S_2}$. This gold sulfide was prepared by reacting H_2S with an aqueous solution of auric chloride

$$8AuCl_3 + 9H_2S + 4H_2O \longrightarrow 4\underline{Au_2S_2} + 24HCl + H_2SO_4 \quad . \qquad (19)$$

Chemical analysis gives Au/S = 1.000/1.007.

c. $\underline{Au_2S_3}$. This compound was prepared[35] by passing H_2S through a solution of chlorauric acid in anhydrous ether. The precipitate was washed with more of the anhydrous ether. Chemical analysis gave the following molar ratio: Au/S = 1.00/1.65. This ratio is a little high in sulfur, which may be from occluded H_2S. The reaction for the preparation is

$$2[AuCl_4]^- + 3H_2S \xrightarrow[\text{ether}]{\text{anhydrous}} Au_2S_3 + 6H^+ + 8Cl^- \quad . \qquad (18)$$

C. Apparatus

1. Radiation detector system

For detecting the γ-rays, we used NaI(Tl) scintillation detectors which were mounted on Amperex XP1010 photomultiplier tubes. A one-inch thick NaI crystal, which was purchased from the Harshaw Chemical Company, was used for the detection of the 77-keV γ-ray of Au 197. At 77 keV, the resolution was about 17%. We found that our lithium-drifted germanium counter had too low an efficiency to be practical. Its high resolution was offset by its count rate, which was about 1/8 that of the NaI assembly. For the low energy γ ray of Fe 57, we used a 2mm-thick NaI crystal for optimum resolution. At 5.9 keV, the resolution was approximately 50%.

The γ-ray pulses were amplified by the Amperex photomultiplier which was powered by a regulated dc high-voltage power supply. The photomultiplier tube was usually operated at between 1000 and 1200 volts, where the resolution of the required γ ray was optimized. After passing through a preamplifier, the scintillation pulses were amplified in a Golding linear amplifier which contained a single channel analyzer for gating on the γ ray of interest. For gating purposes, the γ-ray spectrum was displayed on the Packard analyzer in the pulse-height analyzer mode. The gated γ-ray pulses were subsequently stored in the appropriate channels in the Packard analyzer to produce a Mössbauer spectrum.

2. Drive system

Briefly, the linear closed-loop drive system consists of a loudspeaker drive coil and a velocity transducer along with the necessary electronics. The drive coil provides an acceleration which is proportional to the applied current. The voltage output of the velocity transducer is proportional to the instantaneous velocity of the suitably coupled rod-magnet on which the source is firmly mounted. The drive coil, drive magnet, transducer, bar magnet, source and absorber are contained in the drive capsule which is illustrated in Fig. IV-4(a). Figure IV-4(b) is a photograph of the drive capsule.

A 20-kc tuning-fork oscillator (purchased from the American Time Products) is used to synchronize the PHA start-advance pulses with the velocity wave form. The frequency stability of the tuning fork oscillator is better than ±0.02% over the temperature interval between 15°C and 45°C. The PHA is operated in the multiscalar (time) mode with its channels being sequentially addressed by a 10-kc pulse derived from the above oscillator. A channel of the PHA is capable of receiving and storing pulses from the SCA during the period when it is being addressed. The 10-kc pulse advance frequency is further divided by the number of PHA channels (400) to produce a 25-cps square-wave which is used to re-initialize the analyzer after all 400 channels have been scanned and for the closed-loop drive system. This common frequency source effectively synchronizes the channel numbers and the instantaneous velocity of the source. A 25-cps triangular-wave is produced by integrating the above square wave which has first been amplitude-stabilized

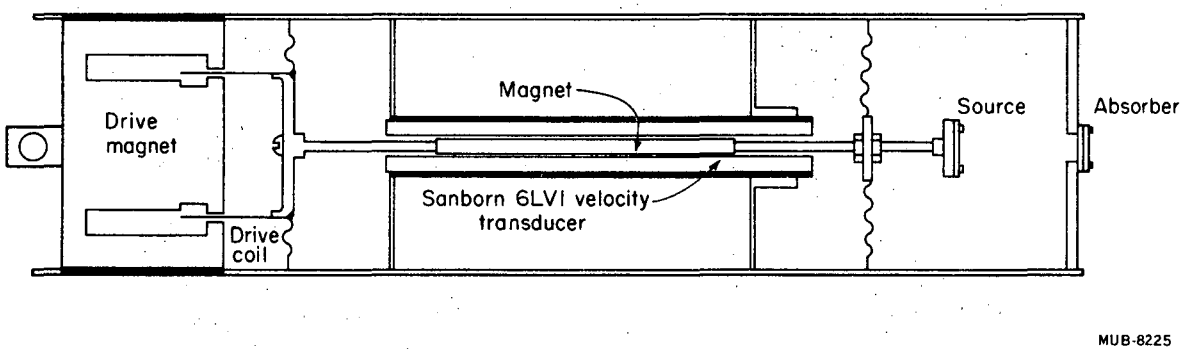

Fig. IV-4(a). The electromechanical drive capsule (Zane[36]).

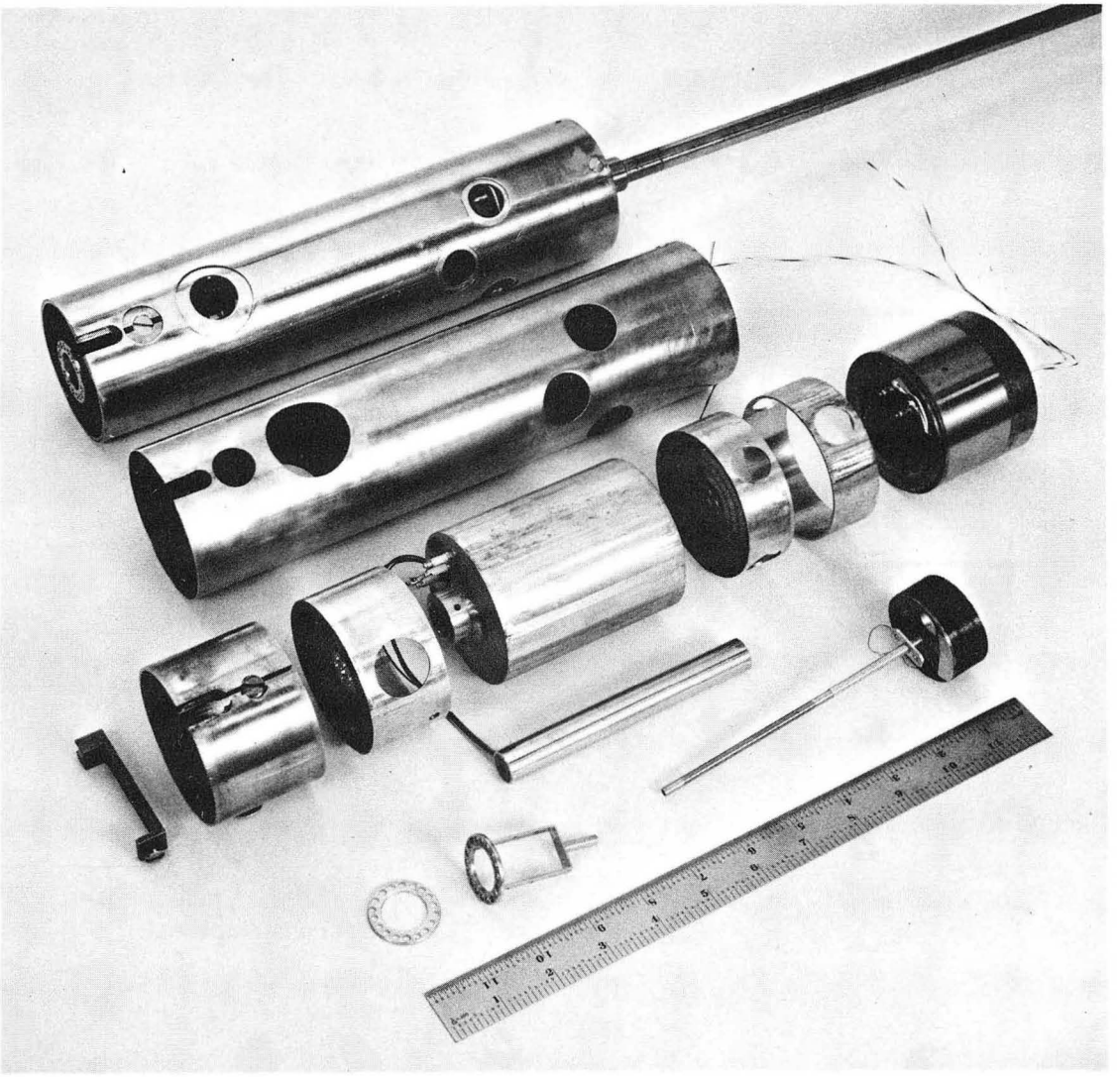

Chem 3640

Fig. IV-4(b). Photograph of the drive capsule assembly (Wickman[37]).

by a precision squaring circuit. The amplitude fluctuation is specified as being less than 0.001%/1°C.

The 25-cps reference triangle wave form is then fed into the closed-loop negative-feedback drive system to drive the loudspeaker coil. It was found that an additional small parabolic correction term to the triangle wave was needed to linearize the velocity. This parabolic wave was obtained by integrating the reference triangle wave and was therefore automatically synchronized with the system. When the feedback drive system is properly balanced, the deviation from linearity of the velocity wave form is less than 1% over 90% of the velocity range. The drive assembly is capable of attaining velocities of about ± 20 cm/sec. A schematic of the linear velocity drive amplifier is given in Fig. IV-5.

3. Velocity transducer

The velocity of the transducer is determined by converting the transducer's instantaneous output voltage to a corresponding frequency by using a modified VIDAR 260B voltage-to-frequency converter. These frequency counts are stored in the PHA in multiscaler mode controlled by the scaler advance, as when collecting the Mossbauer spectra. The velocity profile is fitted with an nth-degree polynomial (usually n equals 4) which is used to convert the channel numbers to the corresponding velocities. The VIDAR generates frequencies between 0 and 100 kc with the zero voltage (therefore zero velocity) at 50 kc. The 50 kc ∓ 50 kc frequency span can be set equal to selected voltages from ± 50 mv up to ±2000 mv.

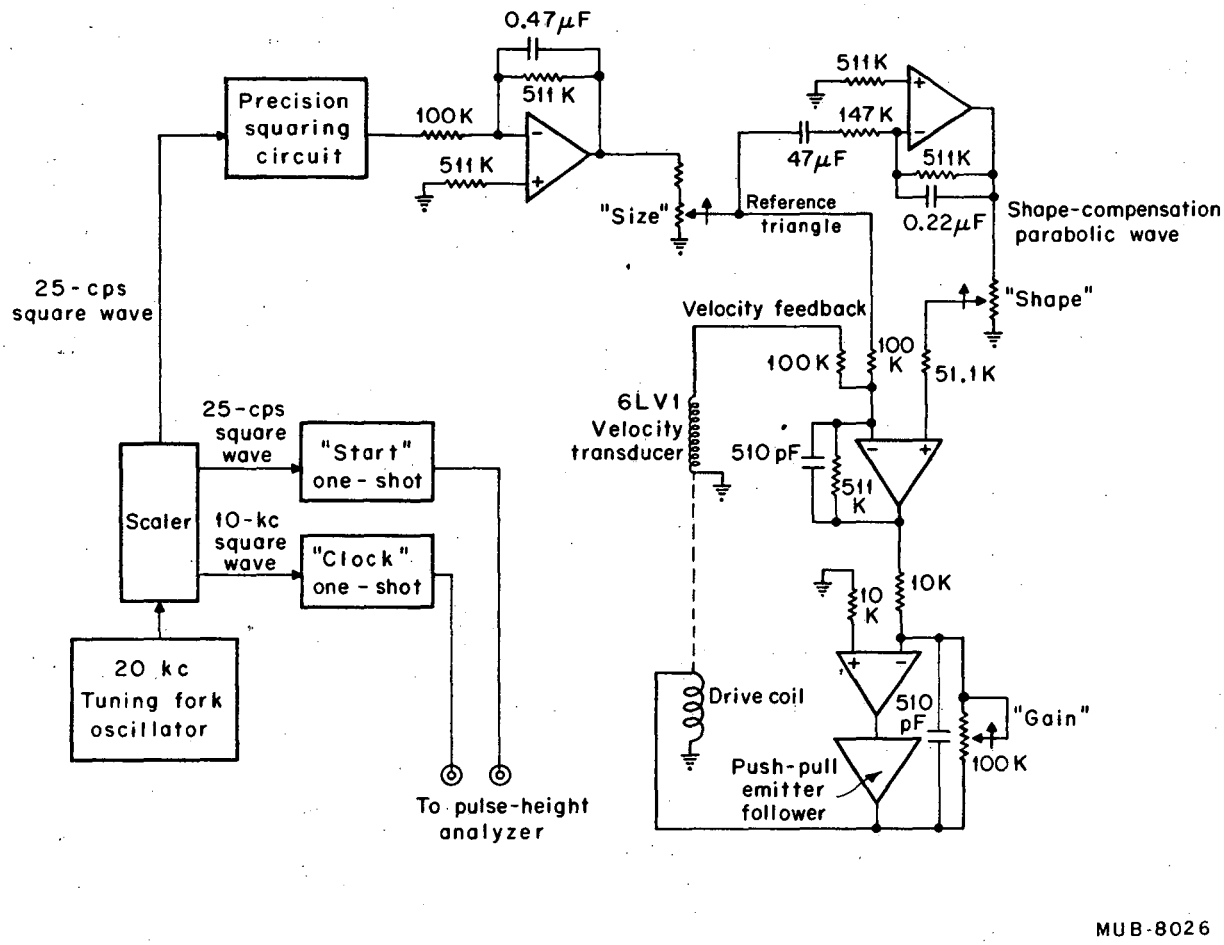

Fig. IV-5. Block diagram of multiscalar mode Mossbauer effect system. (Zane[36]).

The transducer voltage output is collected with the transducer both "on" and "off". When the transducer is "on", the frequency profile reflects the voltage output of the 25-cps velocity triangle wave of the source (or absorber). When the transducer is "off", the average of the frequency counts in all the channels determines the channel of zero velocity. The calculated average, $(I\ ,\ \text{"off"})_{calc}$, is given by Eq. (20),

$$(I\ ,\ \text{"off"})_{calc} = \frac{(50\ \text{kcps})(\text{counting time, sec.})}{(\text{number of channels})} \quad . \tag{20}$$

The experimentally-determined average of the counts for zero voltage, $(I\ ,\ \text{"off"})_{ave}$, is less than the calculated value due to the finite dead time of the analyzer. A dead time correction factor, $\Delta = \frac{(I\ ,\ \text{"off"})_{calc}}{(I\ ,\ \text{"off"})_{ave}}$, is applied to the velocities. The velocity of channel i, vel_i, is then

$$vel_i = \left\{ \frac{(I\ ,\ \text{"on"})_i - (I\ ,\ \text{"off"})_{ave}}{(\text{peak voltage of VIDAR})} \right\} \left\{ \begin{matrix} \text{Transducer} \\ \text{Calibration} \\ \text{cm/sec/volt} \end{matrix} \right\} \Delta \quad . \tag{21}$$

The actual $(I\ ,\ \text{"on"})_i$ values used is derived from an nth-degree polynomial fit explained above. The peak voltage is the scale which was selected on the VIDAR at the time of the experiment. The transducer calibration is explained below in this section.

It is noted that since the start pulse is generated at the same frequency as the velocity wave, and the scaler advance operates at 10 kc,

two mirror-image Mössbauer spectra are collected in the 400 channels. The two spectra can then be used to check and correct for the time lag which might occur between the VIDAR output (apparent velocity) and the transducer output (true velocity). If the true velocity lags the VIDAR velocity in time, the centroids of the two spectra will not agree. The correction for this time lag is made by taking the algebraic mean of the two centroids, since the deviations which are caused by a lag would be in the opposite sense. The effect of a time lag is illustrated in Fig. IV-6. If the actual centroids are located at points a and b on the velocity triangle, they would appear to be located at points a' for spectrum I and b' for spectrum II. This would result in velocity errors of the opposite sense. The correction is applied by taking the algebraic mean of a' and b'.

The transducers were calibrated by obtaining the well known six-line Mössbauer spectrum of Fe 57 and determining the velocity separation of the two outer Zeeman components. Klein and Zane[38] obtained a 1.0658 ± 0.004 cm/sec separation of the outer two Zeeman lines from laser interferometer calibrations at room temperature. This velocity separation is in excellent agreement with that reported by Preston et al. of 1.0657 cm/sec. Hanna et al. had previously determined the splitting of the outer Zeeman components at room and liquid helium temperatures as 1.0608 cm/sec and 1.0885 cm/sec respectively. Hanna's values were used to convert the laser room temperature value to one applicable at 4.2° K. This separation is 1.0939 cm/sec.

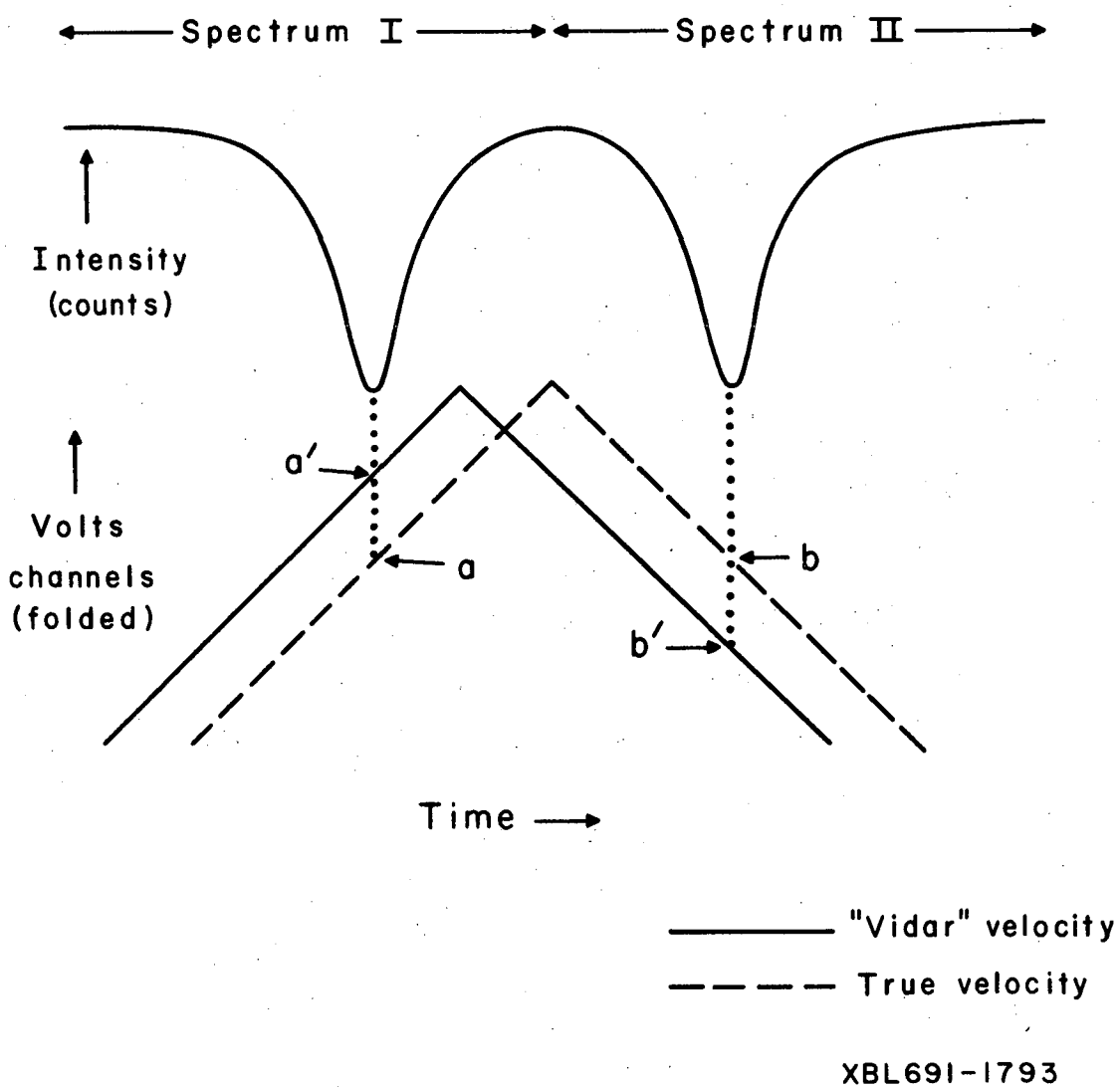

Fig. IV-6. Diagram showing effect of possible time lag between true velocity and apparent velocity.

We used a 1.1-millicurie single-line source which had been prepared by plating and annealing Co 57 into 0.001" thick copper metal. The absorber was a piece of enriched (> 90%) Fe 57 foil (1.9 mg. Fe 57/cm^2). Both the source and absorber were purchased from New England Nuclear.

At 4.2°K, the Sanborn 6LVI transducers which we used had an unacceptably short lifetime. We designed two systems to resolve this problem: 1) new sturdier transducers which were wound at the Lawrence Radiation Laboratory and 2) a long push-rod extension of the drive capsule which was built with a geometry that permits the transducer to be kept out of the cold region of the cryostat. Both systems were successful and the first of these modifications was used for these experiments. Figure IV-7 gives a diagram of the extended drive capsule. The push-rod portion centers into the assembly drawn above it.

The Sanborn transducer consists of two separate coils made of approximately 43 gauge wire. Our coils were wound with 38 gauge copper magnet wire in one countinous piece, reversing the direction of the winding at the center. As much wire as possible (about 6400 turns per half coil) was wound on the bobbin to maximize the sensitivity. The bobbin was turned from a single piece of bakelite and the wound coil was secured to the mu-metal outer cylinder with Dow Corning silicon rubber.

A push-rod extension had been previously built and found acceptable and was easily adapted to our system. With the 24 inch extension of the drive capsule, the transducer and drive coil are situated in that portion of the vacuum chamber which extends above the cryostat. The extension is friction-secured to the original drive capsule by an expansion band.

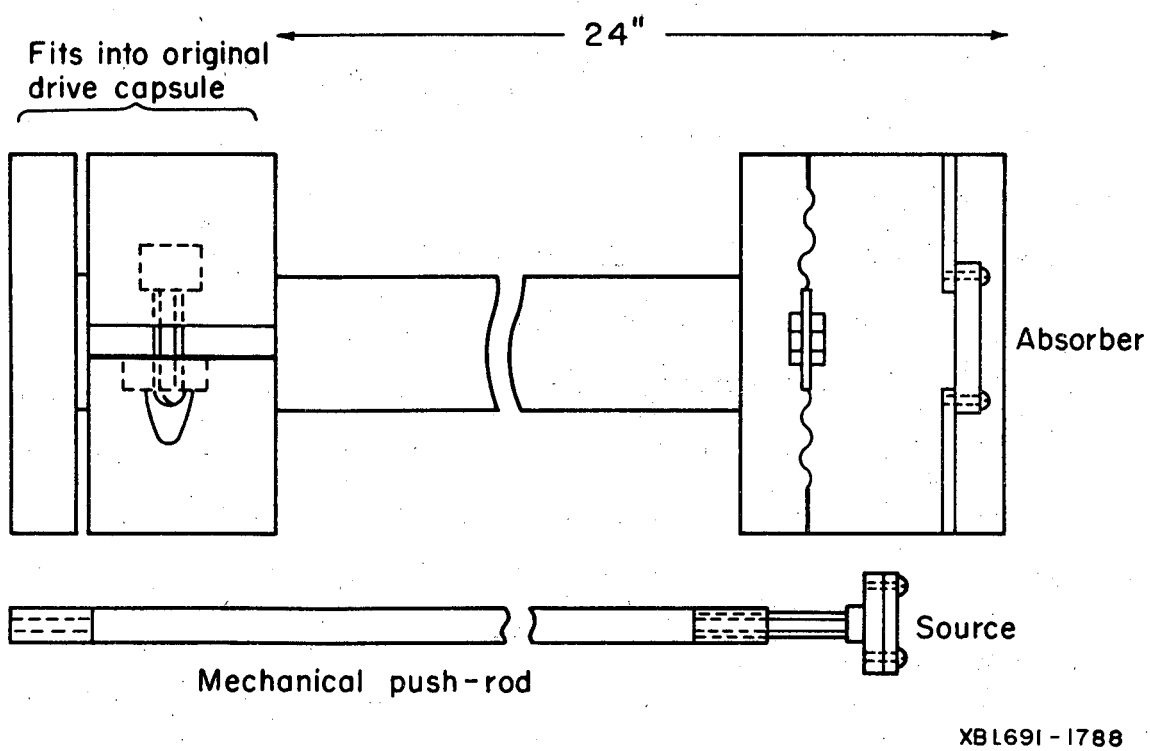

Fig. IV-7. Diagram of the extended drive capsule

The lightweight moving portion was made of 0.006 inch thick stainless steel metal of 3/8 inch O.D.

4. Cryostat

The cryostat is a three-wall dewar with liquid nitrogen and liquid helium pots (cavities). We kept approximately 2 mm Hg of helium exchange gas in the inner vacuum chamber where the drive capsule is situated. This inner chamber is separated from a 77°K heat-shield by three thin aluminum-coated Mylar windows. The outer vacuum jacket has an indium-sealed beryllium window which minimizes the attenuation of low energy γ rays. The source was located approximately 7 inches from the detector. After thermal equilibrium was reached, the cryostat maintained its low temperature for about 24 hours. The geometry of the cryostat is given in Fig. IV-8. A is the absorber, S the source and C the drive capsule. The relative dimensions of the long push-rod extension drive capsule is indicated at the right of the cryostat. Figure IV-9 is a photograph of the Mössbauer apparatus. The drive capsule was pulled out of the vacuum chamber and is shown at the right of the cryostat to illustrate its relative dimensions.

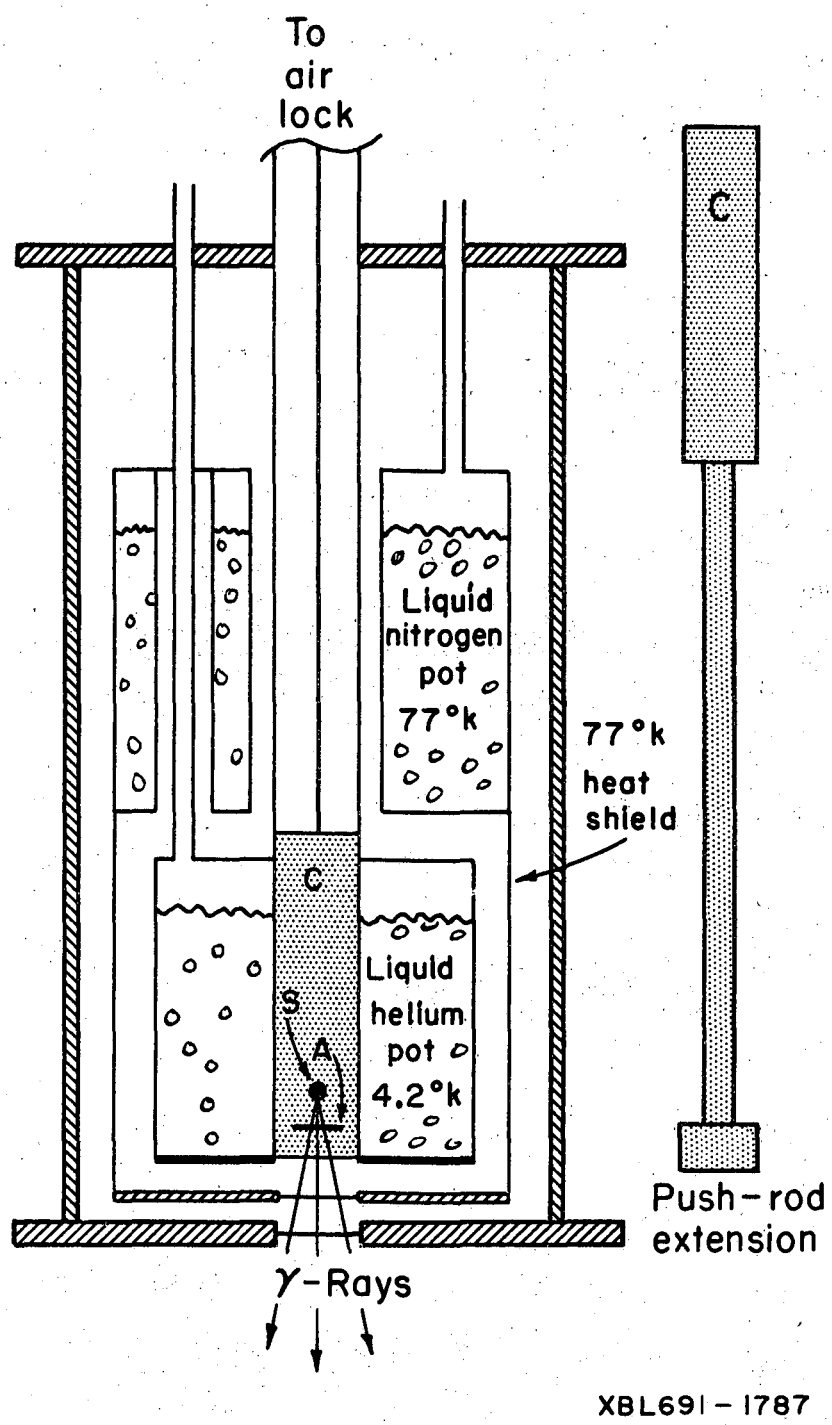

Fig. IV-8. Diagram of Mössbauer experiment cryostat. The drive capsule, C, is positioned in the cryostat. S is the source and A is the absorber.

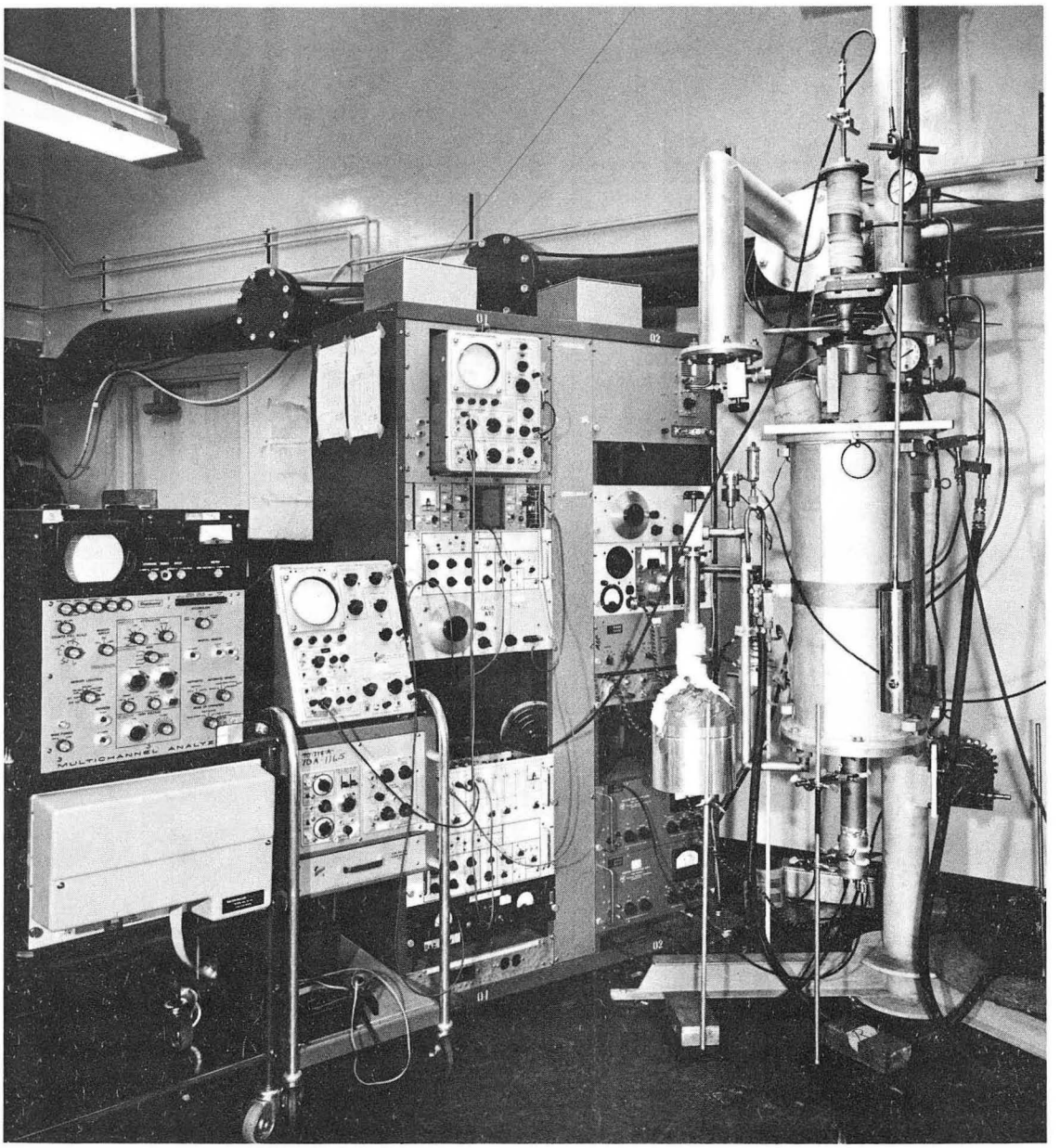

Chem 3641

Fig. IV-9. Photograph of the electronic equipment of Mössbauer experiments.

D. Data Processing

Data analysis was facilitated by high-speed computers. Initially, we used the IBM 7094 with which we had problems of adequate computer space in core. We eventually converted to the CDC 6600. The program for fitting Lorentz curves to the Mössbauer spectra, FLOR, is written as a subroutine to VARMIT, a least-squares fitting program. The report by W. C. Davidon includes the mathematical details of the method.[40]

For most gold compounds, the individual linewidths, Γ, are not narrow enough compared to the quadrupole splitting separations to give resolved component lines. FLOR facilitates the resolution of those lines and determines their intensities ($I(i)$), linewidths ($\Gamma(i)$), and line positions ($v_0(i)$). Figure IV-10 illustrates these parameters.

The absorption line shapes are assumed to be Lorentzian and each line is fitted to the formula:

$$I(i) = K(i) \left[\frac{(\Gamma(i)/2)^2}{(v-v_0(i))^2 + (\Gamma(i)/2)^2} \right] \tag{22}$$

$K(i)$ is a constant. If N is the number of absorption maxima, then the theoretical velocity spectrum I is given by

$$I = \text{Base} - \sum_{i=1}^{N} I(i) \quad . \tag{23}$$

The total number of parameters, NPAR, is $(3N + 1)$ and is given in FLOR in the following order:

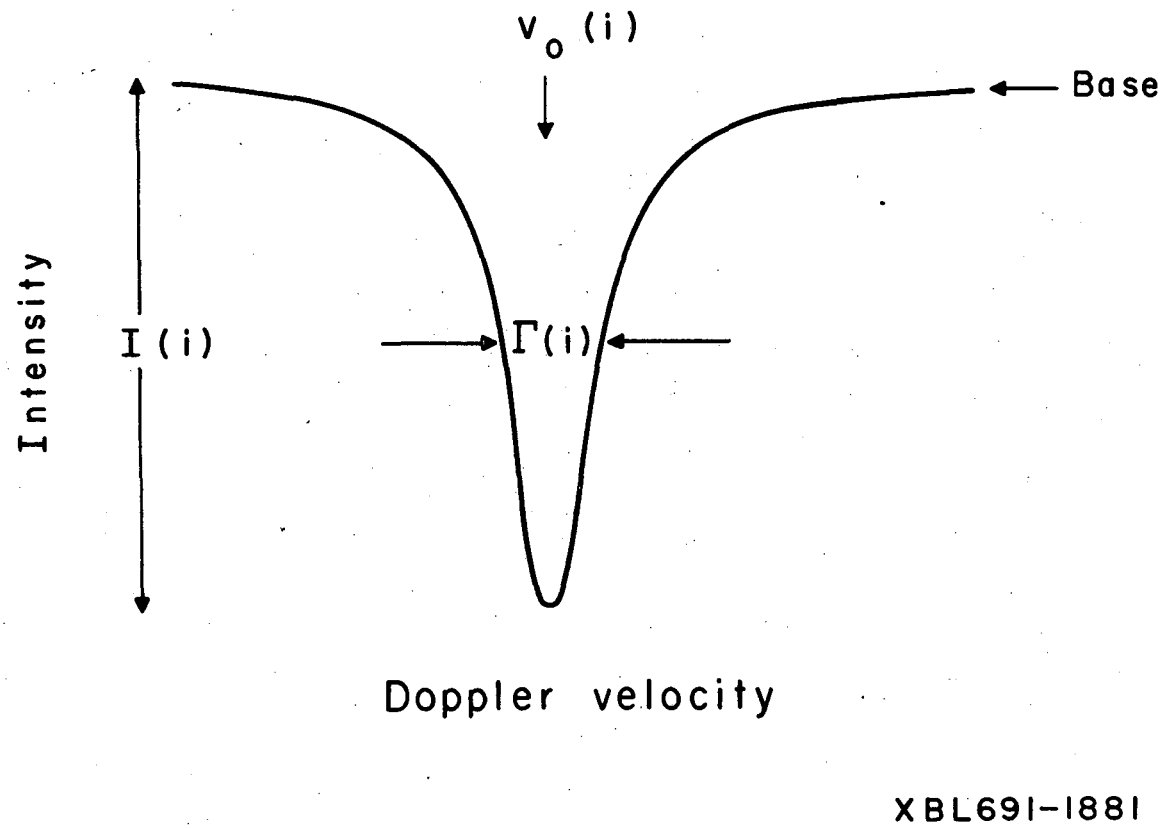

Fig. IV-10. The parameters of FLOR, the CDC 6600 computer program for fitting Lorentz curves to the Mössbauer spectra.

$$\text{Base}, \Gamma(i), I(1), v_0(1), \Gamma(2), I(2), v_0(2), \ldots, v_0(N) \quad . \tag{24}$$

There is a provision for setting the value of any parameter to a fixed constant and also for imposing linear constraints among the parameters as governed by the Hamiltonian. These provisions are especially important when the resolution of the Mössbauer spectrum is poor and a good fit could not otherwise be made.

The program utilizes a linearly-independent square "constraint" matrix with the dimension equal to NPAR. The programmer provides as input a set of linear constraint vectors, $CNTS_k$, whose coefficients satisfy Eq. (25).

$$CNTS_k = \sum_{l=1}^{3N+1} c_{kl} = 0 \tag{25}$$

The coefficient of the lth parameter in the kth constraint is c_{kl}. The program generates the required number of linearly-independent "dummy" constraints to complete the square (3N+1, 3N+1) constraint matrix. This matrix spans the NPAR dimensional vector space.

In addition to the values of the parameters, the program determines the root-mean-square statistical uncertainties, RMSU. The RMSU is a statistical error indication and is equal to the square root of the diagonal elements of the H (inverse Hessian) matrix

$$RMSU_i = \sqrt{\langle H_{ii} \rangle} \quad . \tag{26}$$

These RMSU values are reasonable for the baseline and intensities of the individual lines. For linewidths and line positions, the RMSU values are usually quite small. Actually, these RMSU values are very close in value to the standard deviations which can be calculated by the method of maximum likelihood. This method is based on Poisson statistics and is more accurate than the least-squares method for the treatment of data from an experiment with poor statistics. However, in the limit of high statistics, as with our Mössbauer experiments (about 10^6 counts), both methods converge. Being quite small, both the RMSU and standard deviation values are usually a poor indication of the reproducibility of the data. Therefore, we have reported the most probable error instead.

For a set of experimental results, the probable error, pe, is given by Eq. (27).

$$pe = 0.6745\sqrt{\sum_{i=1}^{M} \frac{(\bar{x} - x_i)^2}{M}} \qquad (27)$$

M is the number of measurements, $\bar{x}$ the average value of the measurements, and x_i's are the individual measurements. By definition, pe is the 50% confidence limit. That is, given a single additional experiment, there is a 50-50 chance that it's results will be within the pe of the previous identical experiments.

When possible, we performed several experiments on each compound. A given experiment yields two mirror-image spectra. Generally, for purposes of determining the errors, each image was considered individually.

In the case of IS, however, we first averaged the results of the two images, as explained in Section IV-C-3.

A discussion of errors is given in Appendix A.

V. EXPERIMENTAL AND THEORETICAL RESULTS

A. Results of the Mössbauer Effect Experiments

The results of our Mössbauer experiments on diamagnetic gold compounds are given in this chapter. The experiments were performed at 4.2°K with a moving source of Pt 197 which beta decays to the 77.345 keV isomeric state of Au 197. The stationary absorbers contained the various gold compounds. The errors that are indicated are the most probable errors. Another given Mössbauer experiment on the same gold compound would have a 50 percent chance of yielding results that are within the probable error. The evaluation of errors is discussed in Appendix A. The interpretation of these results are given in the following sections.

1. Gold(III) trifluoride, AuF_3

Gold trifluoride is a "paprika" orange crystalline substance with hexagonal symmetry, which has been characterized by a single-crystal X ray structural determination.[41] The space group[42] is $P6_1$ or $P6_12$, with cell dimensions of $a = 5.149$ Å and $c = 16.26$ Å. There are 6 molecules in the unit cell. The first coordination sphere has square-planar symmetry. The details of its structure are shown in Fig. V-1.

The bond lengths and bond angles are:[41]

Au - F (bridging) = 2.04 Å

Au - F (non-bridging) = 1.91 Å

Au - F (cross-linking) = 2.69 Å

$\angle$Au - F = 116°

The AuF_3 units form an infinite hexagonal helix.

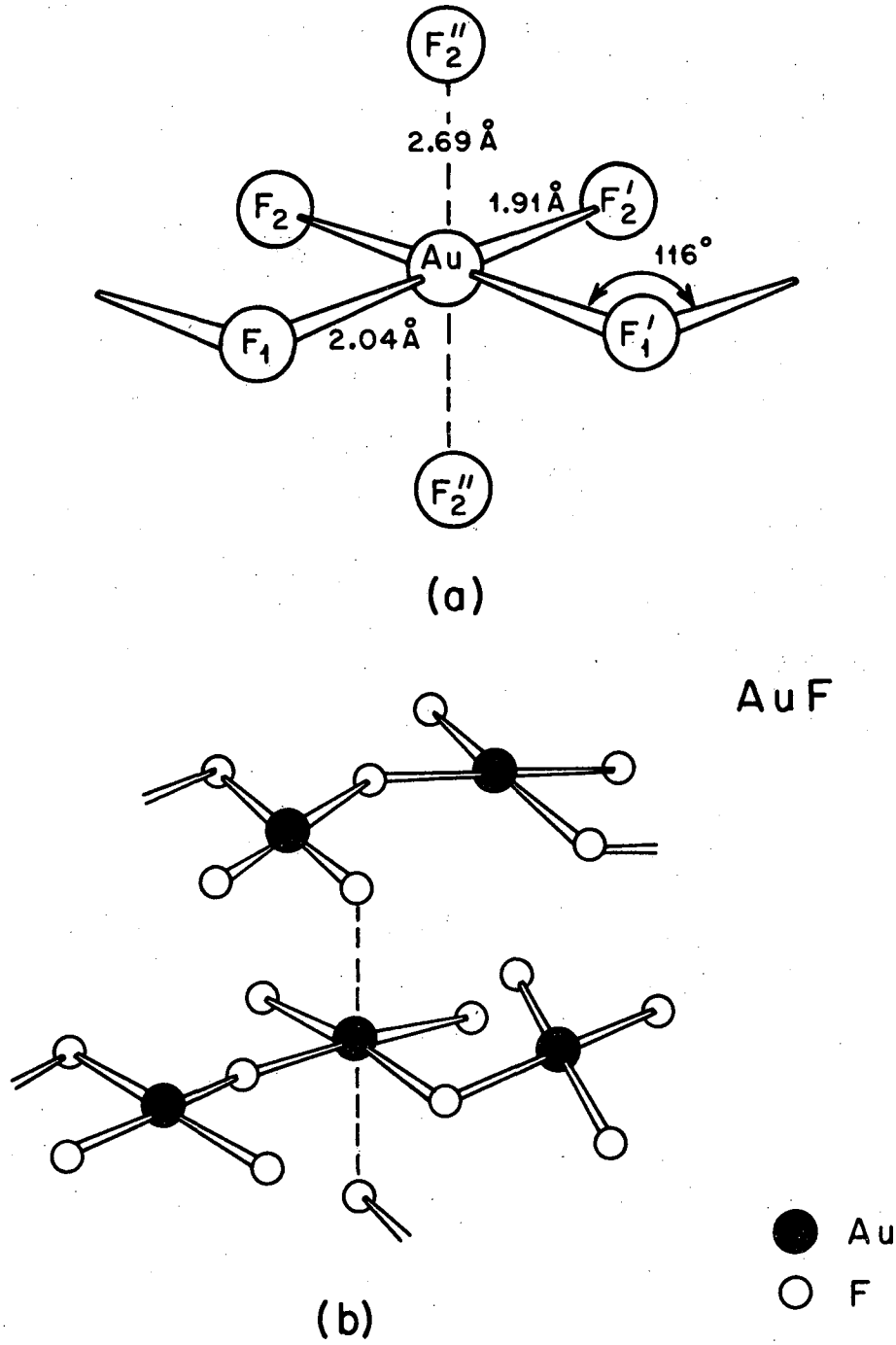

Fig. V-1. The coordination of gold in AuF_3 (Einstein[42]).

The Mössbauer spectrum for AuF_3 at 4.2°K is given in Fig. V-2. The line drawn through the data points is the least-squares fit of two Lorentz lines. Because of the square-planar symmetry about the gold atom in AuF_3, the two Lorentz lines were constrained to have equal linewidths and equal absorption intensities. The linewidth determined by the fit was 0.232 (0.002) cm/sec. The IS with respect to gold-in-platinum is -0.107 (0.001) cm/sec and the QS is 0.274 (0.002) cm/sec. Roberts et al.[43] reported an IS value of -1.3 ± 0.2 mm/sec, which is in agreement with our value within experimental error. They observed no quadrupole splitting. Three runs were made on this compound. The gold density of the common absorber was 163.9 mg/cm^2. A chemical analysis disclosed a fluorine to gold molar ratio of 3.00.

2. Tetrafluoroaurate(III), $[AuF_4]^-$

From the reactivity of $AuBrF_6$, Sharp[44] suggests that the compound is not formulated as $[AuF_2]^+[BrF_4]^-$ but rather as $[BrF_2]^+[AuF_4]^-$. The gold(III) tetrafluoride ion is yellow and hydrolizes in atmospheric moisture. The particular structure has not been characterized, but it is most likely that the $[AuF_4]^-$ anion is square-planar as was found for the anions of the $A^+[AuF_4]^-$ compounds, for A = Na, K, Mo, and Rb. Debye powder photos have been taken of the $A^+[AuF_4]^-$ compounds.[26]

In Fig. V-3 is shown the Mossbauer spectrum for $[BrF_2]^+[AuF_4]^-$ at 4.2°K. The line drawn through the data points is the least-squares fit of two Lorentz lines. We assumed that the symmetry of the complex was square-planar and fitted the data with two Lorentz lines which were constrained to have both equal width and equal intensity. The linewidth

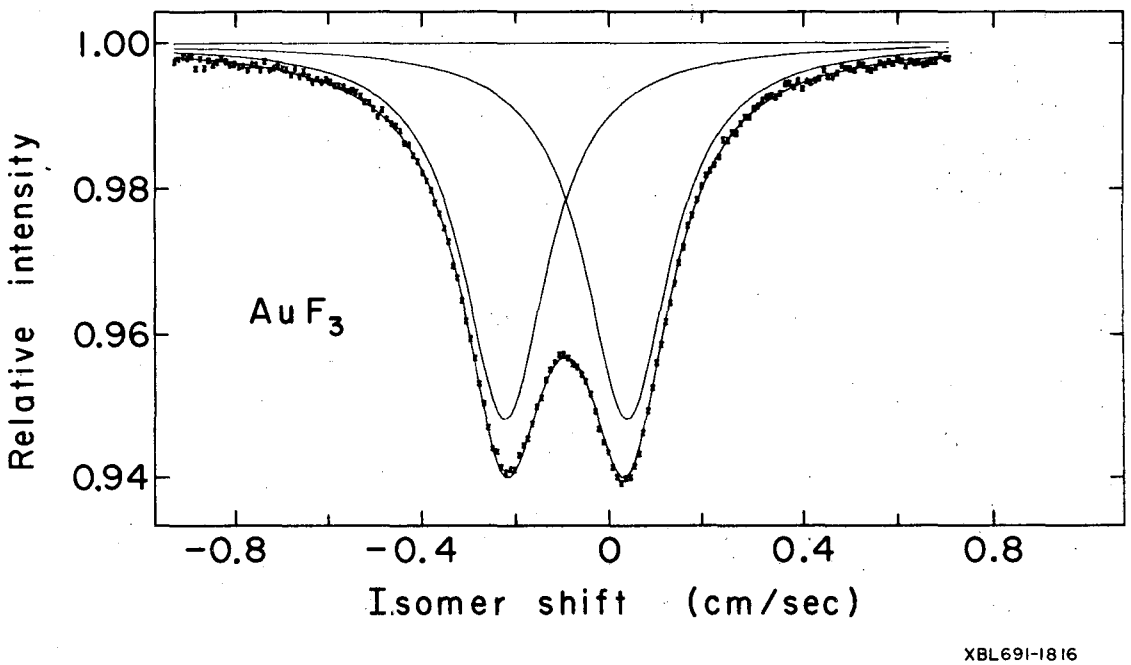

Fig. V-2. Mössbauer spectrum of Au 197 in AuF_3.

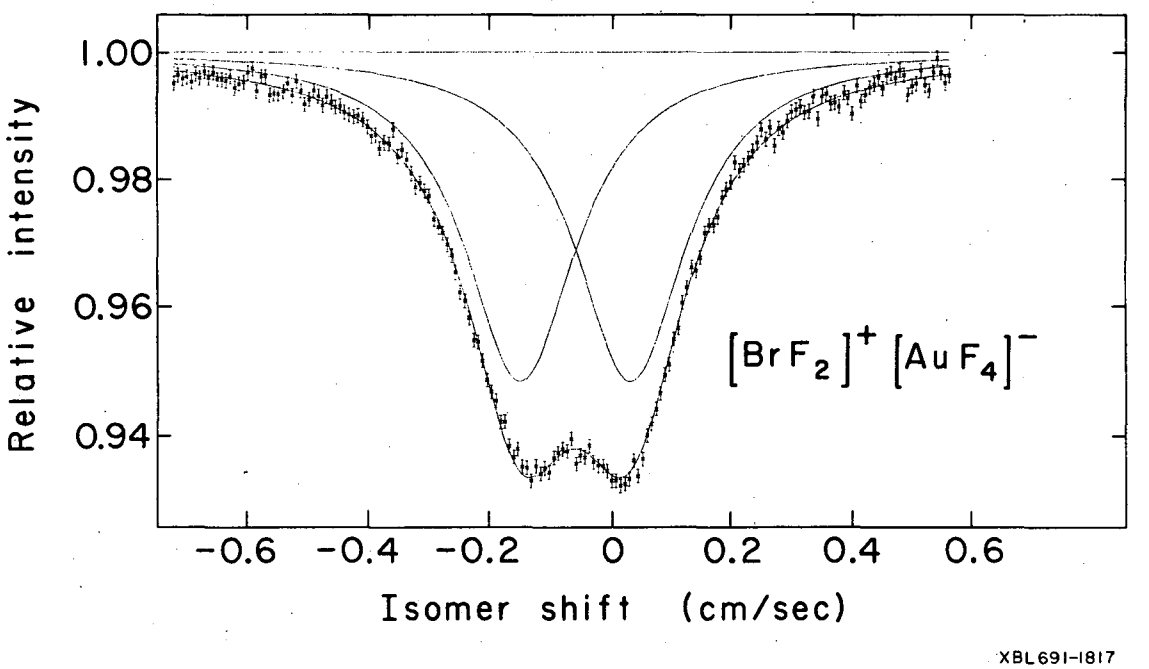

Fig. V-3. Mössbauer spectrum of Au 197 in $[BrF_2]^+[AuF_4]^-$.

determined by the fit was 0.228 (0.040) cm/sec. The IS with respect to gold in platinum is -0.069 (0.002) cm/sec and the QS is 0.182 (0.002) cm/sec. These recent results are in good agreement with earlier results that we obtained on a different apparatus. Roberts et al.[43] performed a Mössbauer experiment on $KAuF_4$. They observed an IS of 0 ± 0.02 mm/sec and no quadrupole splitting. Since the symmetry of the first coordination sphere around gold is thought to be square-planar in both compounds, the results were expected to be in closer agreement.

We considered the results of only the first of three runs performed on our latest sample of $[BrF_2]^+[AuF_4]^-$ as there was some evidence of sample decomposition. The first experiment had the best resolution of the three runs. The absorber contained 160.2 mg/cm^2 of gold and no chemical analysis was attempted on the decomposed sample.

3. Gold(III) trichloride, $AuCl_3$

Gold trichloride is a dark reddish-brown crystalline substance of monoclinic symmetry. It has been characterized by a single-crystal X ray[45] determination to be of the $P2_1/c$ space group with the following cell dimensions: a = 5.67, b = 11.04, and c = 6.44 Å.[45] Angle β = 113.3°. The substance reacts with moisture and may be photosensitive. The first coordination sphere has square-planar symmetry and the crystal consists of distinct dimer molecules Au_2Cl_6.

The bond lengths and bond angles are:

Au - Cl (terminal) = 2.25 and 2.23 ± 0.02 Å

Au - Cl (bridging) = 2.33 and 2.34 ± 0.02 Å

Au - Au (closest) = 3.55 ± 0.02 Å

Cl-Au-Cl (terminal chlorines) = 90°

Cl-Au-Cl (bridging chlorines) = 86° .

We note here that the average Au-Cl distance is 2.29 ± 0.02 Å. It was found that in the CsAu(I) Au(III)Cl_6 compound, the Au(III)-Cl distance is 2.31 Å. The two bond lengths are equal within experimental error. See Fig. V-4 for structural diagrams of the unit cell and the coordination of gold.

The Mössbauer spectra for $AuCl_3$ at 4.2°K are given in Fig. V-5 (a) and (b). The profile of two Lorentz lines is drawn through the spectrum for $AuCl_3$ in run 128 while the profile of run 173 consists of three Lorentz lines. In the preparation of the compound for run 173, it appears that the sample had undergone some decomposition into gold metal. Therefore, the spectrum was fitted with three lines, one of which represents the line for gold metal with an IS of -0.12 cm/sec. The $AuCl_3$ portion of the two runs was fitted with two Lorentz lines whose linewidths and intensities were constrained to be equal. The IS is +0.057 (0.009) cm/sec and the QS is 0.075 (0.008) cm/sec. The linewidth is 0.241 (0.020) cm/sec. Shirley, et al.[3] observed an Au-to-Pt IS of 0.037 (0.015) cm/sec and no quadrupole splitting for $AuCl_3$. Roberts et al.[43] report an Au-to-Pt IS of 0.9 ± 0.2 mm/sec and no quadrupole splitting. Our IS result is within experimental error of the result of Shirley but is not in good agreement with that of Roberts.

The areal density of gold in run 128 was 253.5 mg/cm^2 and the areal density in run 173 was 202.1 mg/cm^2. A chemical analysis of the sample from run 173 gave a chlorine-to-gold molar ratio of only 2.36.

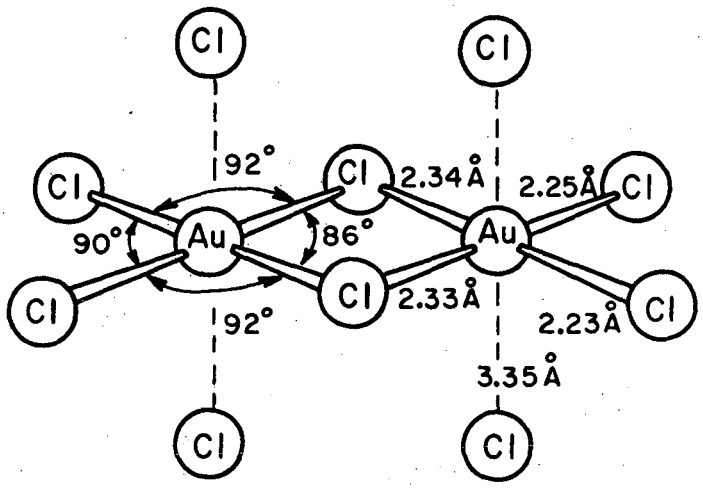

(a)

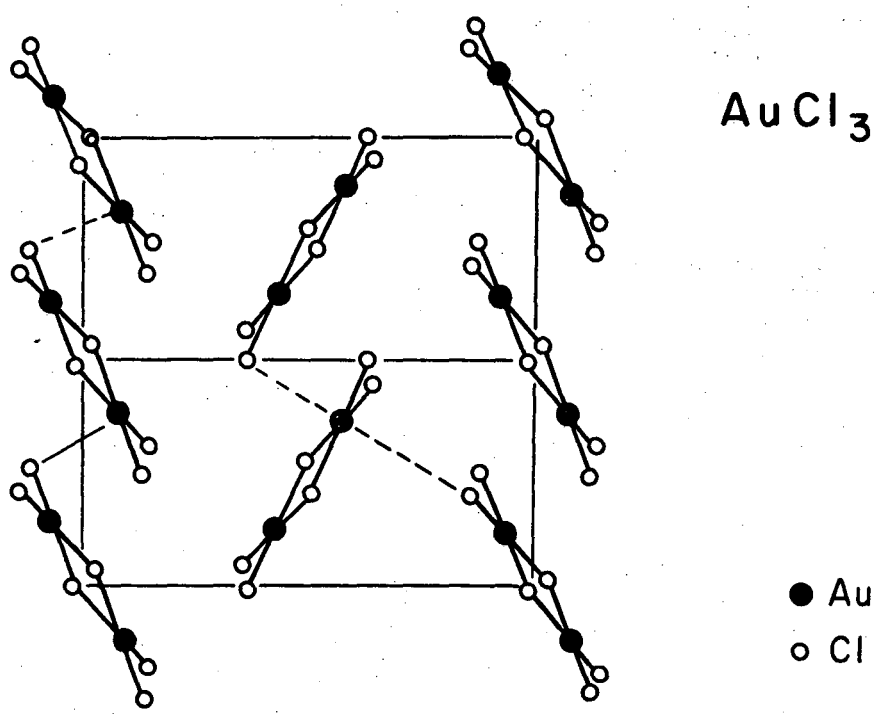

(b)

XBL691-1791

Fig. V-4. Coordination of gold in $AuCl_3$. (Clark, et al.[45])

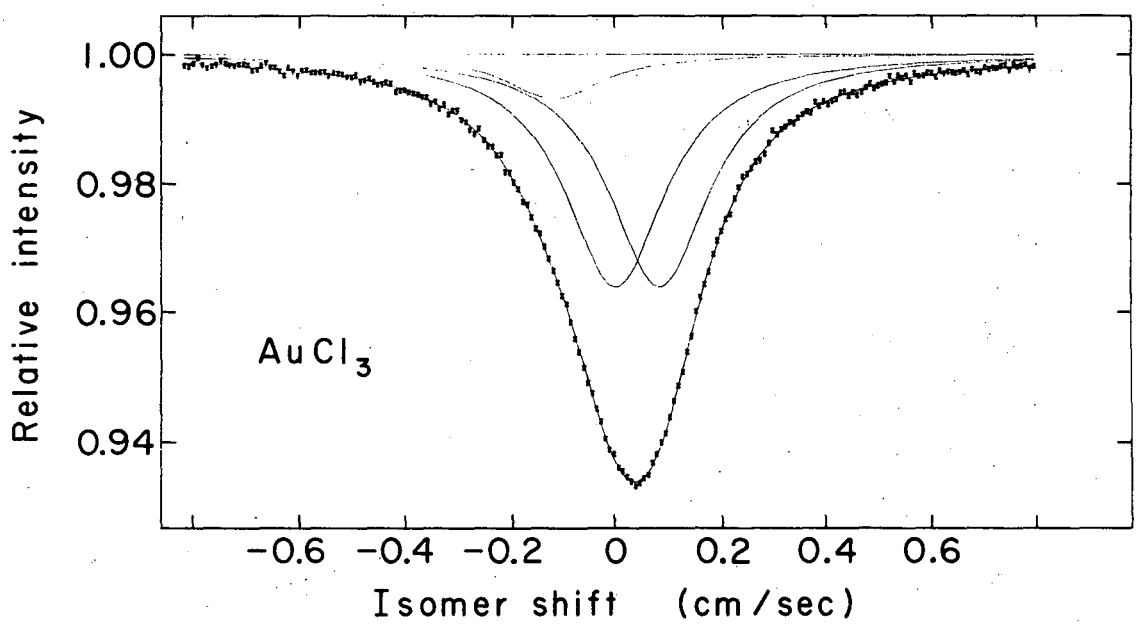

XBL691-1818

Fig. V-5. Mössbauer spectrum of Au 197 in $AuCl_3$.
(a) Experiment 173.

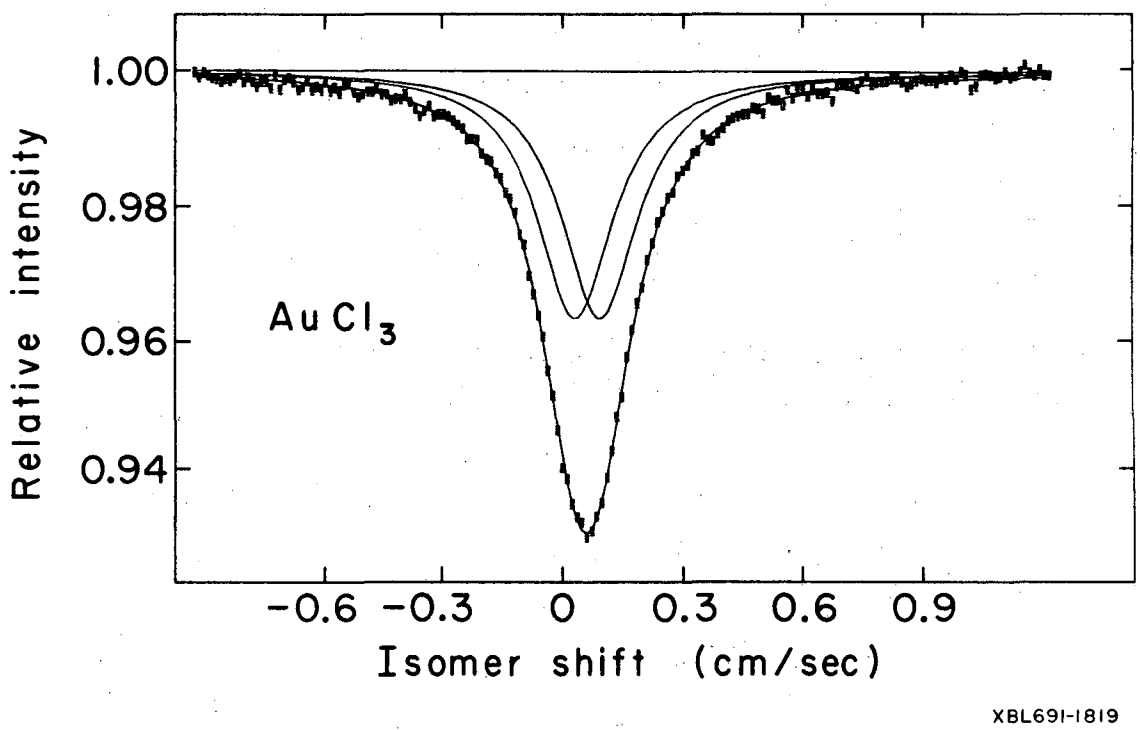

Fig. V-5. Mössbauer spectrum of Au 197 in $AuCl_3$.
(b) Experiment 128.

The theoretical molar ratio is 3.00 and thus this lower ratio helps substantiate the possibility that the sample contained metallic gold.

4. Gold(I) chlorine, AuCl

Gold chlorine, a light yellow, highly unstable substance of orthorhombic symmetry belongs to one of the following possible space groups; D_2^6, D_{2v}^{11}, D_{2v}^{14}, D_{2h}^{19}. It has only been characterized by an X-ray[46] powder pattern. Gold(I) chloride has four molecules in the unit cell and the cell dimensions are: a = 6.41, b = 3.36, and c = 9.48 Å. No bond lengths have been determined. We deduce from the bond lengths of the linear $[Cl\text{-}Au\text{-}Cl]^-$ complex in CsAu(I) Au(III)Cl_6,[47] that the bond length for AuCl should be close to 2.3 Å.

From the dynamics of the reversible reaction between chlorine gas and gold at 500°C, Blitz[48] showed that at these temperatures the vapor was essentially Au_2Cl_2. He found no evidence of the formation of $AuCl_2$ (as with copper and silver) or of $KAuCl_2$.[49] We assume that the aurous chloride forms a polymer similar to aurous iodide, yielding a linear configuration of the first coordination sphere similar to Fig. V-15 for aurous iodide.

The Mössbauer spectrum for AuCl at 4.2°K is shown in Fig. V-6. The line through the data points is the least-squares fit of two Lorentz curves. The lines, as resolved by the fit, were of width 0.196 (0.004) cm/sec. Because of the axial symmetry of AuCl polymers, the two Lorentz lines were constrained to have equal linewidths and absorption intensities. Shirley et al.[3] performed a Mössbauer experiment on AuCl and obtained values of IS and QS which agree with our values within experimental error.

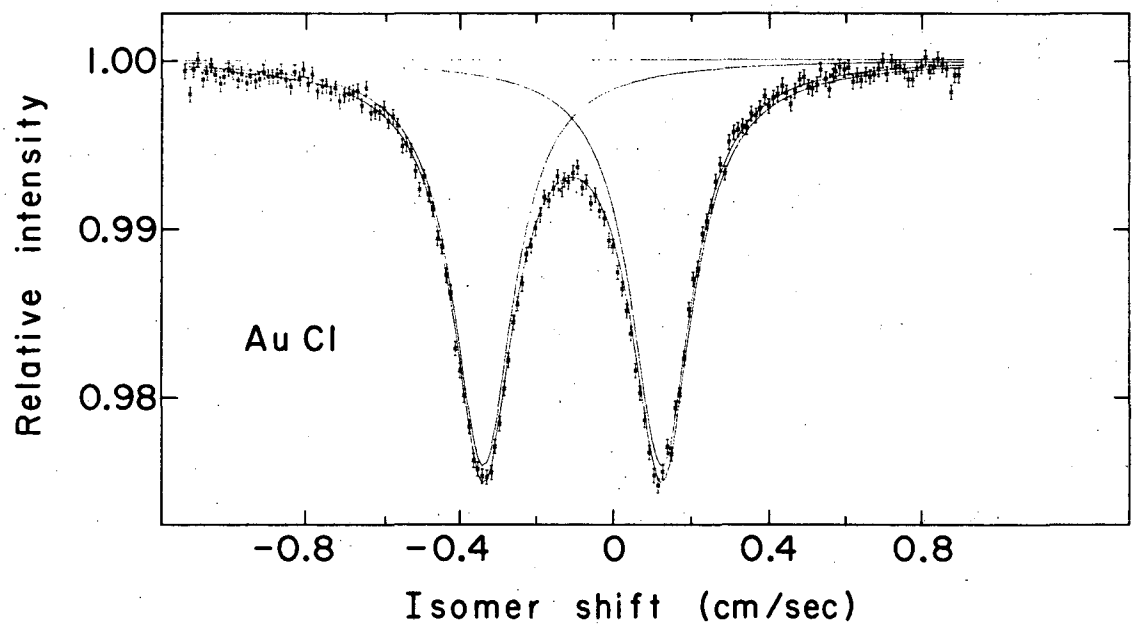

XBL691-1820

Fig. V-6. Mössbauer spectrum of Au 197 in AuCl.

Machmer[50] observed a pure quadrupole spectrum of Au 197 in AuCl and obtained a nuclear quadrupole coupling of 514 MHz which corresponds to a smaller QS value than ours. To facilitate the comparison of the quadrupole splitting values, we list them in the table below. Included in the table are the values of the triplet observed by Macher in AuCl at 300°K.

	Isomer Shift	Quadrupole Splitting
This work	-0.142 (0.001) cm/sec	0.465 (0.001) cm/sec
Shirley	-0.161 (0.020) cm/sec	0.434 (0.040) cm/sec
Machmer	---	514.15 Mz = 0.4120 cm/sec 514.346Mz = 0.4122 cm/sec 514.754Mz = 0.4125 cm/sec

We performed the Mössbauer experiment on AuCl four times and obtained good agreement for the QS each time. AuCl is an unstable, hydroscopic substance which easily undergoes decomposition into $AuCl_3$ and gold metal. We feel that in our vacuum cryostat at 4.2°K, AuCl probably did not decompose appreciably during a single run. The difference in the ambient experimental temperatures may account for part of the discrepancy in the QS values between the Mössbauer experiments and the more accurate nuclear quadrupole resonance technique.

Of the two absorber samples we used, one had a gold density of 180.25 mg/cm^2, the other of 160.06 mg/cm^2. A chemical analysis disclosed gold to chlorine molar ratios of 1.05 and 1.02.

5. Sodium and potassium tetrachloroaurate(III), $NaAuCl_4$ and $KAuCl_4$

The sodium salt of the gold(III) chloride ion (di-hydrate) is light bright-yellow with orthorhombic symmetry. The structure has been

determined by Bonamico et al.[51]. The compound belongs to the Pnma, D_{2n}^{16} space group. There are four complex ions in a unit cell with cell dimensions: a = 12.818, b = 7.067, c = 8.993 ± 0.005 Å. The symmetry of the first coordination is square-planar with an average Au-Cl bond distance of 2.28 Å. The structure of the $[AuCl_4]^-$ ion is constructed in Fig. V-7 from bond length and bond angle values of Bonamico, et al.[51]. The bond lengths and bond angles are:

Au - Cl(1) = 2.288 ± 0.005Å
Au - Cl(2) = 2.260 ± 0.005Å
Au - Cl(3) = 2.283 ± 0.005Å
Au - Cl(4) = 2.278 ± 0.005Å

Cl(1)-Au-Cl(2) = 90.2 ± 0.2°
Cl(1)-Au-Cl(4) = 89.6 ± 0.2°
Cl(2)-Au-Cl(3) = 89.2 ± 0.2°
Cl(3)-Au-Cl(4) = 90.9 ± 0.2°

The potassium salt of the gold(III) chloride ion is a deeper golden yellow than the sodium salt. It has monoclinic symmetry and belongs to the D_{2h}^5-$P2_1/a$ group.[52] There are four complex ions in the unit cell which has the following dimensions: a = 12.18, b = 6.35, c = 8.67 Å and β = 95°24'. Although no detailed structural data are available for the potassium salt, the coordination of gold is probably square-planar as it is in the sodium salt.

The Mössbauer spectrum for $K[AuCl_4]$ at 4.2°K is shown in Fig. V-8. The line drawn through the data points is the least-squares fit of two

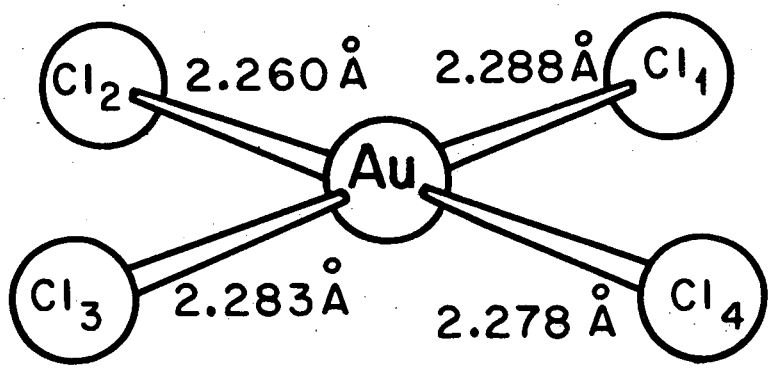

$[AuCl_4]^-$

XBL691-1790

Fig. V-7. Coordination of gold in $[AuCl_4]^-$.

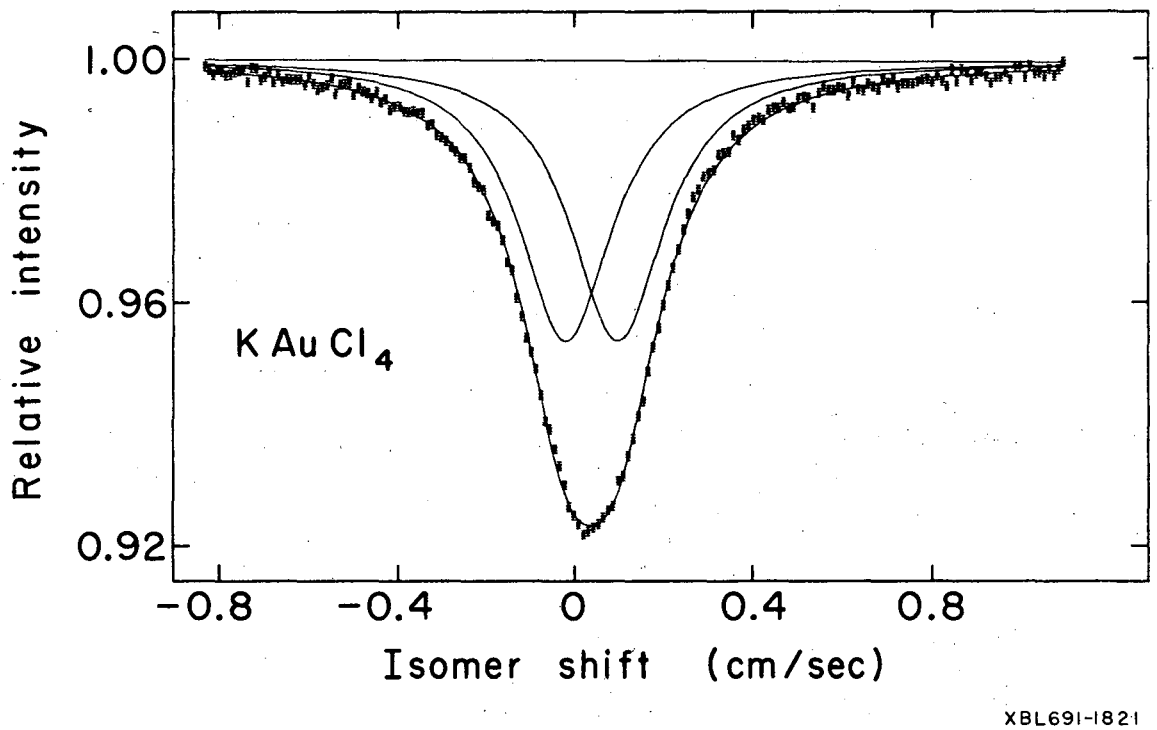

Fig. V-8. Mössbauer spectrum of Au 197 in $KAuCl_4$.

Lorentz lines. Since gold is in a square-planar environment, the two Lorentz lines were constrained to have equal linewidths and absorption intensities. The IS with respect to gold in platinum is +0.044 (0.006) cm/sec and the QS is +0.127 (0.008) cm/sec. The linewidth is 0.254 (0.029) cm/sec. Our IS value is in essential agreement with that of Shirley et al.[3] who report an Au-in-Pt IS value of 0.036 (0.020) cm/sec and no QS for $KAuCl_4$. Roberts et al.[43] obtained an Au-in-Pt IS of 1.3 ± 0.07 mm/sec and no QS. This IS value was not in good agreement with our value. Neither Shirley no Roberts reported the narrow splitting which we have observed.

Both $NaAuCl_4$ and $KAuCl_4$ were used as absorbers. The IS, QS and linewidth values were in agreement. The density of gold for the sodium salt was 302.0 mg/cm^2 and for potassium was 223.8 mg/cm^2. Both of these compounds were purchased from the Alfa Inorganics chemical suppliers.

6. Cesium Aurous Auric Chloride $Cs_2Au(I)Au(III)Cl_6$

This compound, which was discovered by Wells,[29] is of interest because of the presence of gold in its two oxidation states. Its jet-black coloration is ascribed to the existence of both the Au(I) and Au(III) states in the same compound. The compound was found to be diamagnetic, precluding the existence of gold in the +2 state.[53]

The structure was investigated by Elliott and Pauling[47] and was found to have tetragonal symmetry containing complex ions of $[AuCl_2]^-$, which are linear, and $[AuCl_4]^-$, which are square-planar.

The unit cell has the following values: a = 7.49 ± 0.02 Å and c = 10.87 ± 0.02 Å. The space group is D_{4h}^{17}-I4/mmm. The Au-Cl bond lengths in $[AuCl_2]^-$ are 2.31 Å and in $[AuCl_4]^-$ are 2.42 Å. Figure V-9 gives the coordination of the two different gold atoms.

We attempted to fit the Mössbauer spectrum of $Cs_4Au_2(I)Au_2(III)Cl_{12}$ shown in Fig. V-10 with the split lines of AuCl and $[AuCl_4]^-$. The results were in unexpectedly close agreement for the Au(I) chloride. For comparison, the values for the IS and QS of the cesium triple salt and of AuCl and $KAuCl_4$ compounds are given below.

$Cs_4Au_2(I)Au_2(III)Cl_{12}$ Cesium Triple Salt	Separate Gold Chlorides
$[AuCl_2]^-$ portion:	AuCl:
IS = -0.143 (0.028) cm/sec	IS = -0.142 (0.007) cm/sec
QS = 0.410 (0.065) cm/sec	QS = 0.465 (0.001) cm/sec
Γ = 0.216 (0.004) cm/sec	
$[AuCl_4]^-$ portion:	$[AuCl_4]^-$:
IS = -0.009 (0.022) cm/sec	IS = 0.044 (0.008) cm/sec
QS = 0.133 (0.018) cm/sec	QS = 0.127 (0.008) cm/sec
Γ = 0.164 (0.006) cm/sec	

The linewidth for $[AuCl_4]^-$ is smaller than the natural linewidth of 0.194 cm/sec.* Except for the IS of the $[AuCl_4]^-$ portion of the cesium triple salt, the IS and QS values of the triple salt and the double salt are in

* An attempt was made to fit this spectrum with linewidths constrained to equal the natural linewidth, 0.194 cm/sec. It was not successful.

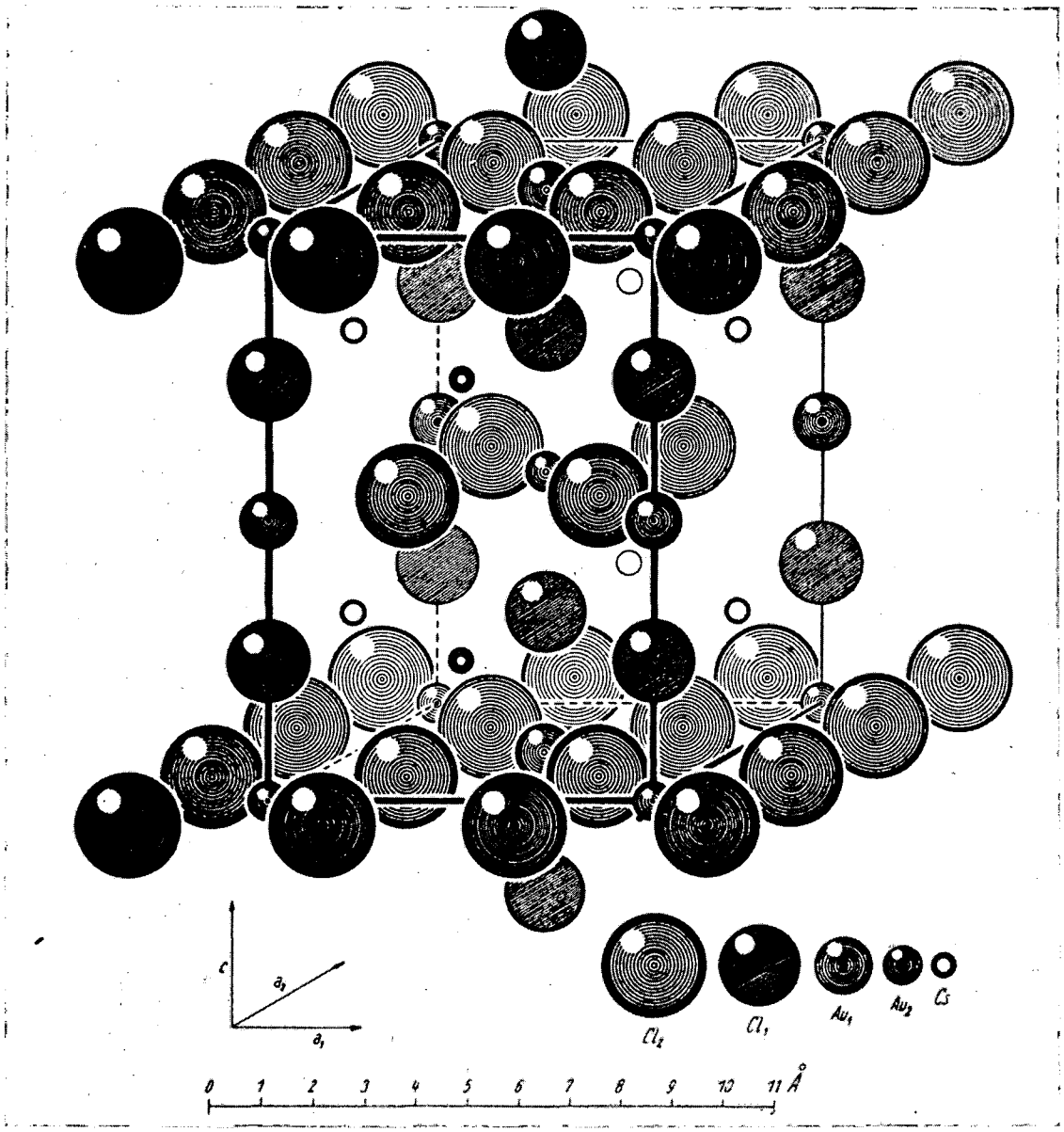

XBB 6811-6957

Fig. V-9. Coordination of gold(I) and gold(III) in $CsAu(I)Au(III)Cl_6$ (Elliott and Pauling[47]).

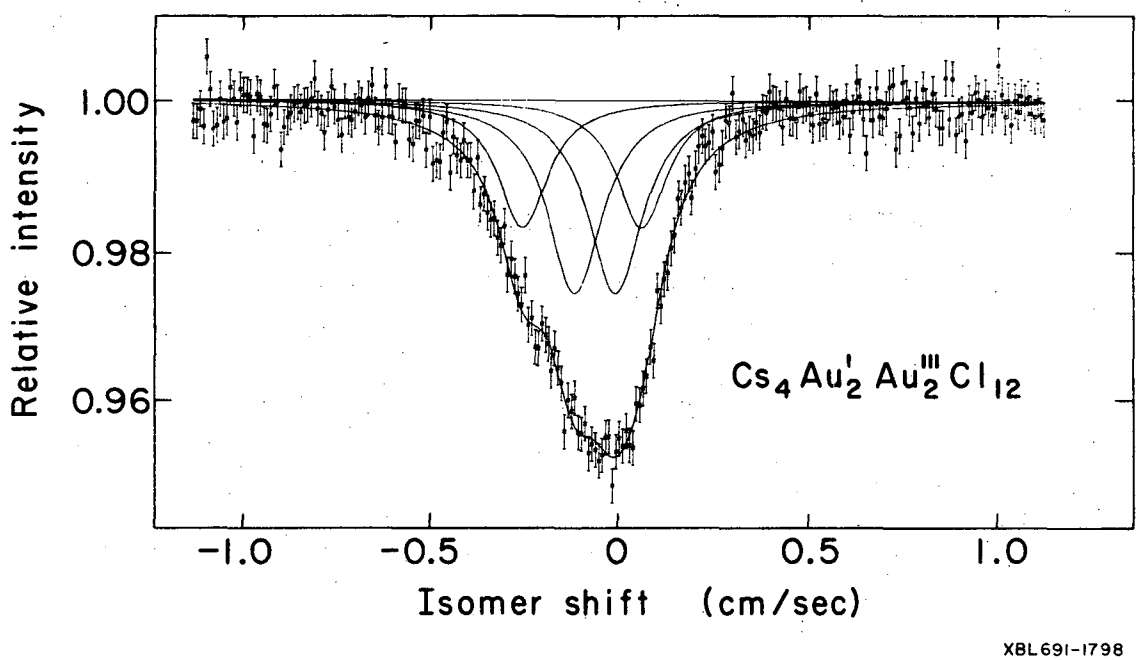

Fig. V-10. Mössbauer spectrum of Au 197 in $Cs_2Au(I)Au(III)Cl_6$.

agreement. Of course, we can at best only guess the origin of the component Lorentz lines. We note, however, that the bond lengths and bond angles of the $[AuCl_4]^-$ portion of the cesium triple salt are essentially the same as those of the sodium and potassium double salts. The $[AuCl_2]^-$ portion of the triple salt was found to be linear. Since only one good run was made of this compound, we hesitate to put great weight on these results.

7. Gold(III) tribromide, $AuBr_3$

This black substance is slightly soluble in water. The three bromide bonds were found to be equivalent by radio-trace chemistry:

$$AuBr + {}^{81}Br_2 \longrightarrow AuBr^{81}Br + Br^{81}Br$$

and molecular weight determination by vaporization yielded the average weight of 910 amu.[54] The theoretical molecular weight for the dimer is 874 amu. The proposed gold coordination is similar to $AuCl_3$ given in Fig. V-4(a). It is a diamagnetic compound with a magnetic susceptability of -0.23×10^{-6} emu.

The Mössbauer spectrum which is shown in Fig. V-11 was least-squares fitted with two Lorentz lines. The resulting linewidth is 0.300 (0.004) cm/sec. The IS with respect to gold in platinum is 0.079 (0.007) cm/sec and the QS is 0.127 (0.002) cm/sec. The component lines were constrained to have equal linewidths and intensities.

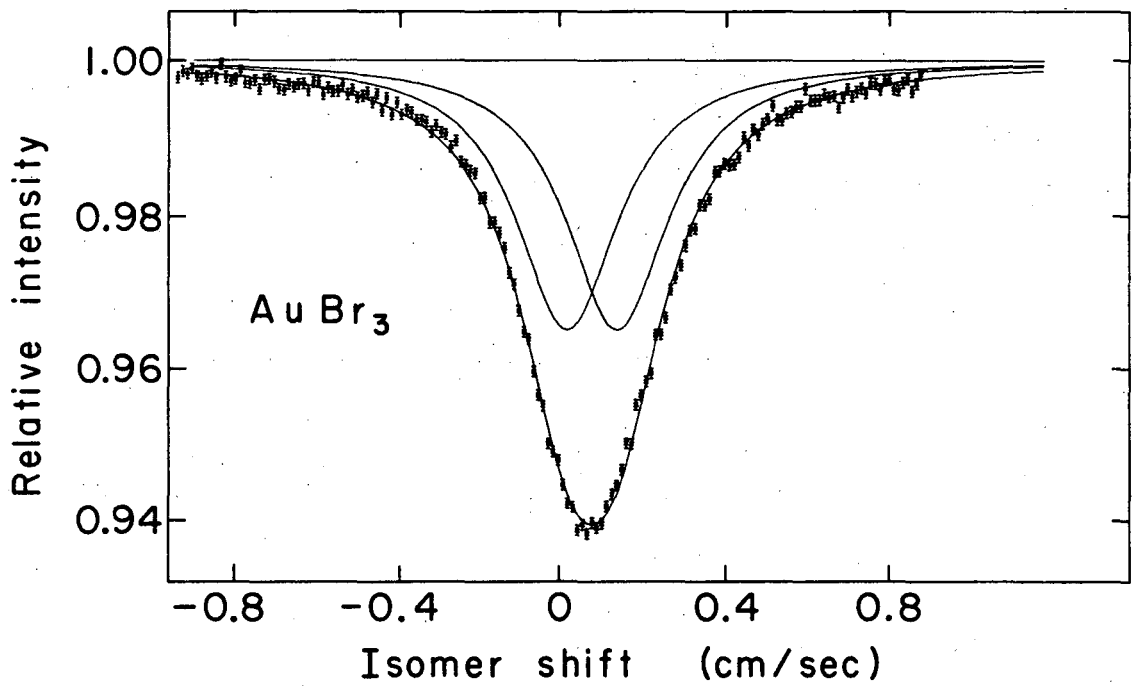

XBL691-1814

Fig. V-11. Mössbauer spectrum of Au 197 in $AuBr_3$.

For the single run performed, we used an absorber with an areal gold density of 186.5 mg/cm^2. The chemical analysis yielded a bromine-to-gold molar ratio of 2.96/1.00.

8. Gold(I) bromide, AuBr

Aurous bromide, a dull grayish-yellow compound, has not been structurally investigated. It is generally assumed that AuBr forms long polymers similar to AuI and that it is probably also linear in the first coordination sphere.

In Fig. V-12, the Mössbauer spectrum for AuBr at 4.2°K is given. The line through the data points represents the least-squares fit of two Lorentz lines. Because of the axial symmetry of AuBr, the two Lorentz lines were constrained to have equal linewidths and absorption intensities. The linewidth determined by the fit is 0.217 (0.008) cm/sec. The IS with respect to gold-in-platinum is -0.147 (0.001) cm/sec, and the QS is 0.423 (0.004) cm/sec. Our values are in good agreement with Shirley *et al.*[3]. They report an Au-in-Pt IS of -0.143 (0.010) cm/sec and a QS of 0.410 (0.020) cm/sec. There were two absorbers of AuBr. One had an areal density of gold of 217.9 mg/cm^2 and the second had 190.3 mg/cm^2. The results of a chemical analysis gave a gold to bromine molar ratio of 1.004.

9. Potassium tetrabromoaurate(III), $KAuBr_4$

The potassium salt of auric tetrabromide is a reasonably stable dark reddish-brown crystalline substance. It is not photosensitive and can be stored for at least a month in a dessicator. It has been

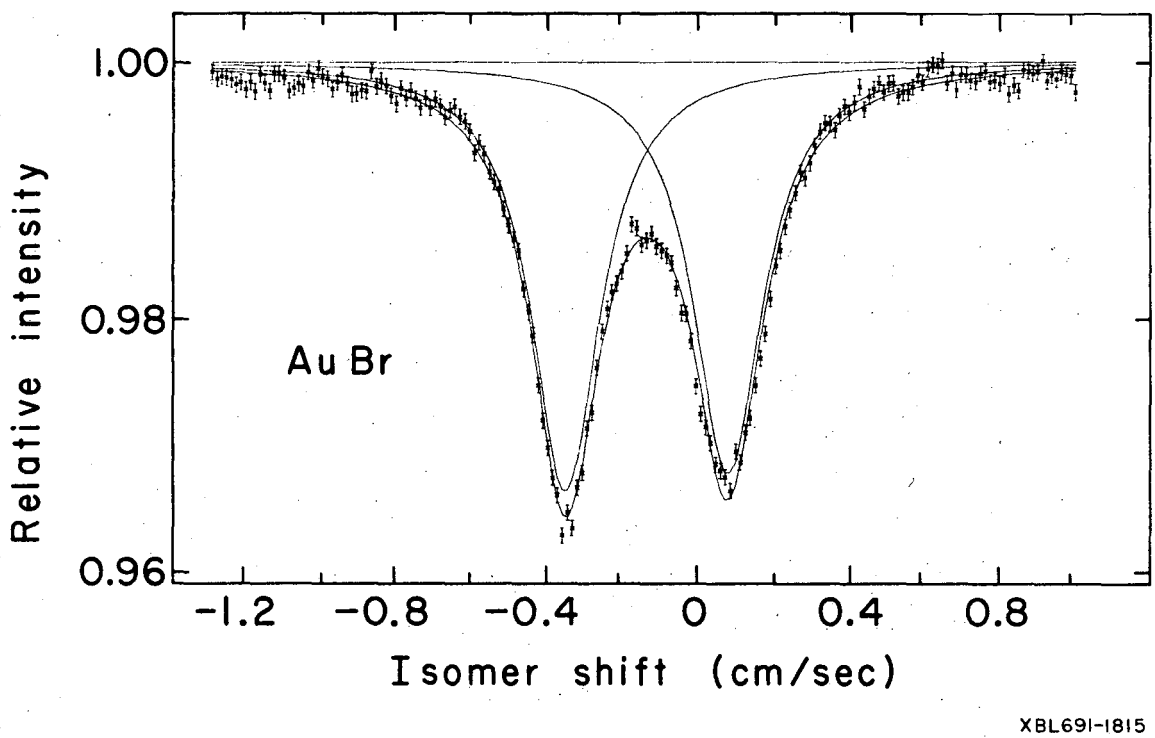

Fig. V-12. Mössbauer spectrum of Au 197 in AuBr.

characterized[52] as having two waters of hydration, $KAuBr_4 \cdot 2H_2O$, and as being monoclinic. It belongs to the $P2_1/n$-C_{2h}^5 space group with the following cell dimensions: a = 9.51, b = 11.93, c = 8.46 Å, with beta = 94°24'. Each unit cell contains four molecules. The two gold-bromine bond lengths are 2.65 and 2.46 Å. The symmetry of the first coordination sphere is square-planar.

Two Lorentz lines were least-squares fitted to the Mössbauer spectrum of $KAuBr_4$. See Fig. V-13. Due to its axial symmetry, the two lines were constrained to have equal linewidths and absorption intensities. The result of the fit gave a linewidth of 0.220 (0.012) cm/sec. The Au-in-Pt IS is +0.067 (0.002) cm/sec and the QS is 0.113 (0.002) cm/sec. Our values for both the IS and QS were slightly larger than the corresponding values reported by Shirley et al.[3]. They observed an Au-in-Pt IS of 0.015 (0.015) cm/sec and no quadrupole splitting.

We used three $[AuBr_4]^-$ absorbers which had gold densities of 177.3 mg/cm^2, 212.1 mg/cm^2, and 156.2 mg/cm^2. The best experiment was done on the sample containing 156.2 mg/cm^2 of gold. The compound was made here in the laboratory and recrystallized in anhydrous ether. A chemical analysis disclosed a potassium to gold to bromine molar ratio, K/Au/Br, of 1.00/1.01/3.97.

10. Gold(I) iodide, AuI

Aurous iodide is a lemon-yellow compound of tetragonal symmetry. It belongs to the C_{4h}^4-$P4_2/n$ space group.[55] There are four molecules per unit cell with cell dimensions of: a = 4.359 ± 0.004 Å, c = 13.711 ± 0.007 Å. The Au-I units connect to each other to form long chains

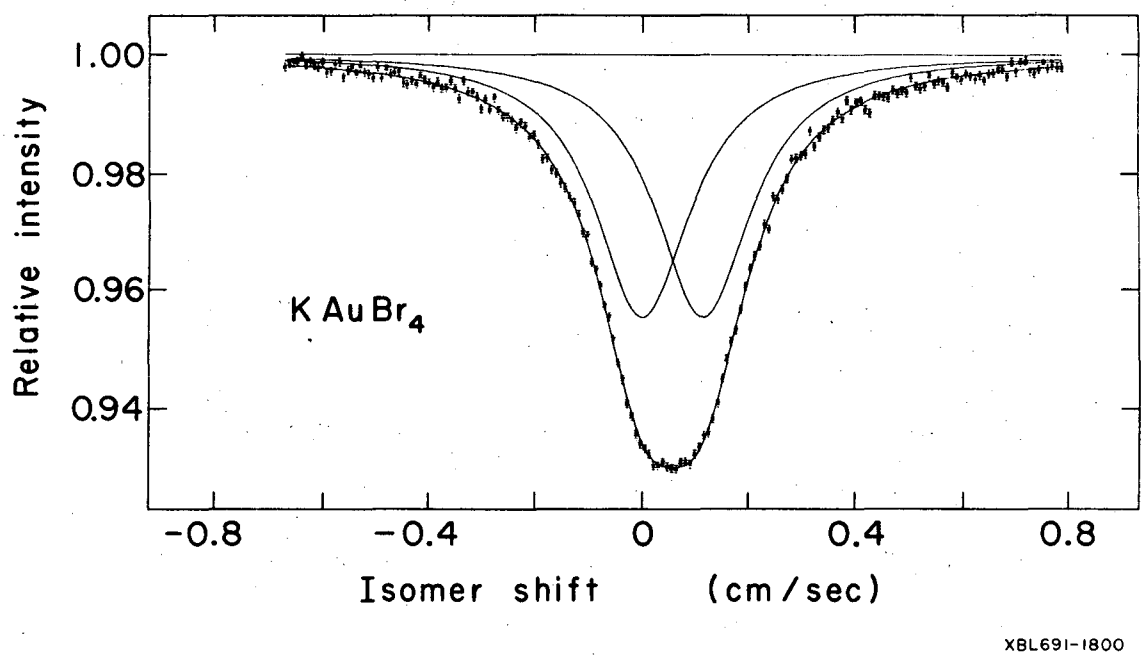

Fig. V-13. Mössbauer spectrum of Au 197 in $KAuBr_4$.

resulting in a coordination number of two and linear symmetry in the first coordination sphere. See Fig. V-14 for a diagram. The gold-iodine bond length has been reported as 2.60 Å[55] and 2.62 Å.[56] Jagodzinski[56] gives the following additional bond distances:

Au has 2 I neighbors at 2.62 Å
Au has 4 Au neighbors at 3.08 Å
Au has 4 Au neighbors at 4.359 Å
Au has 4 I neighbors at 4.02 Å
Au has 2 I neighbors at 5.06 Å

Au-I-Au = 72°

The Mössbauer spectrum illustrated in Fig. V-15 for AuI is the least-squares fit of two Lorentz curves which were constrained to have both equal absorption intensities and linewidths. The best linewidth, as determined by the fit, was 0.242 (0.004) cm/sec. Shirley et al.[3] obtained values in close agreement with our IS and QS values. Machmer[57] observed a pure quadrupole spectrum of Au 197 in AuI at 300°K and 77°K. At the lower temperature, he discovered a triplet. The QS results of Machmer were about 3% larger than ours. The IS and QS values are tabulated in the table which follows.

Quadrupole Splitting in AuI

This work	Shirley et al.[3]	Machmer[57] (0.1% precision)
0.398 (0.001) cm/sec (4.2°K)	0.388 (0.020) cm/sec (4.2°K)	508.296 MH_z=0.40739 cm/sec (300°K)
		512.554 MH_z=0.410799 cm/sec
		516.554 MH_z=0.413898 cm/sec
		516.620 MH_z=0.414058 cm/sec (77°K)

Isomer Shift in AuI

-0.132 (0.003) cm/sec	-0.124 (0.010) cm/sec	-----

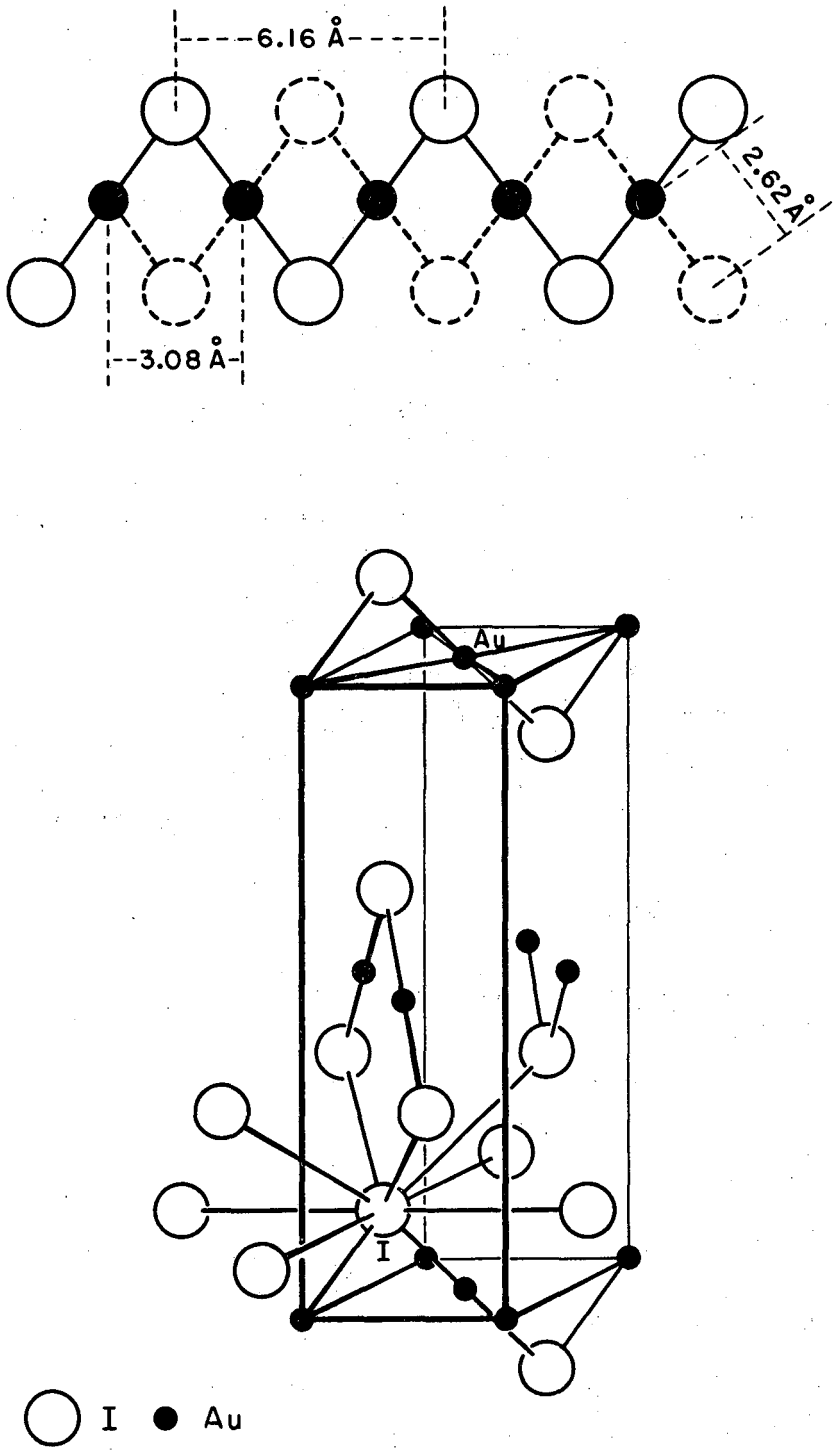

Fig. V-14. Coordination of gold in AuI. (Jagodzinski[56]).

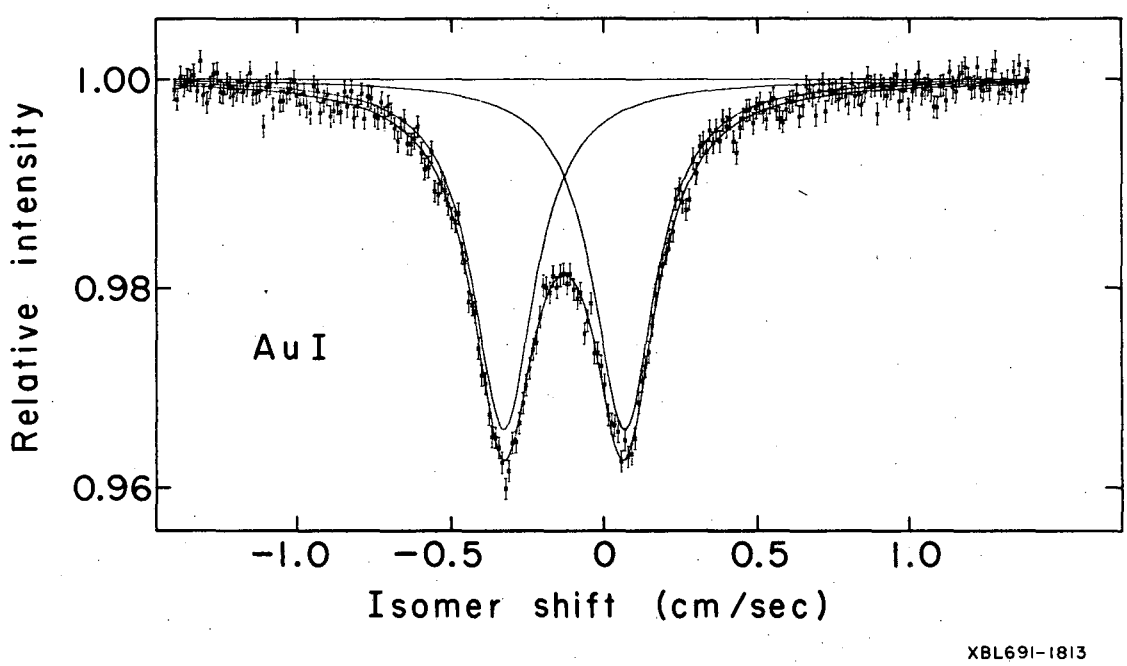

Fig. V-15. Mössbauer spectrum of Au 197 in AuI.

11. Gold(III) iodide, AuI_3

This dark-green finely-divided compound is extremely unstable and has not been structurally characterized. Auric iodide, AuI_3, decomposes into gold metal and aurous iodide, AuI, at 25°C. We have not been able to prepare it in the wet at 0°C. From charge transfer spectra on $[AuCl_4]^-$ and $[AuBr_4]^-$, it was deduced that $[AuI_4]^-$ has a low-energy charge transfer band in the infrared region[21] and hence spontaneously decomposes at room temperature.

The Mössbauer spectrum for AuI_3 at 4.2°K is given in Fig. V-16. The line drawn through the data points is the least-squares fit of two Lorentz curves. Since AuI_3 probably decomposed into AuI before we were able to complete the Mössbauer experiments, we list the results of the two compounds for comparison:

	Linewidth	IS	QS
AuI	0.242 (0.005) cm/sec	-0.132(0.003)cm/sec	0.398(0.001)cm/sec
AuI_3(?)	0.237 (0.041) cm/sec	-0.153(0.037)cm/sec	0.399(0.006)cm/sec

The linewidths are the values determined by the least-squares fit. The corresponding results for AuI and AuI_3(?) are within experimental error. In the section on interpretations, we make a correlation of IS and QS for several gold compounds. From this correlation, the pair of values for AuI_3(?) seem to indicate that they probably belong to the Au(I) oxidation state.

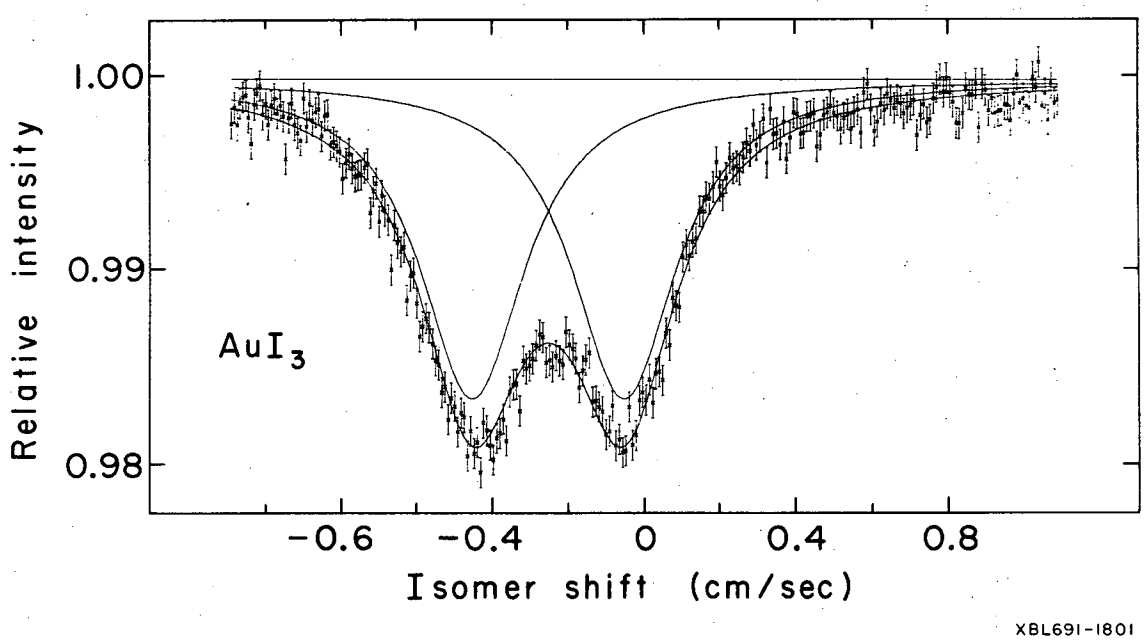

Fig. V-16. Mössbauer spectrum of Au 197 in AuI_3.

We used two AuI samples with areal gold densities of 83.2 mg/cm^2 and 526.9 mg/cm^2. A chemical analysis gave a gold-to-iodine molar ratio of 0.959. The chemical analysis for AuI_3 disclosed an iodine to gold molar ratio of 2.97 and 2.83, but the extra iodine probably existed in elemental form.

12. Gold(I) cyanide, AuCN

Gold cyanide is a stable, finely divided bright yellow substance which has not been thoroughly characterized due to the difficulty of preparing single crystals. AuCN belongs to the C_{6mm}-C^1_{6v} space group[58] and has hexagonal symmetry. It is highly probable that gold cyanide is linear in the first coordination sphere. Most authors report that AuCN forms long (linear) chains of gold atoms connected by CN groups.[58,59] One source[60] reports that AuCN is made up of long continuous zig-zag chains through the crystal lattice. If there is a bend in the structure, it most likely occurs at the nitrogen or carbon atoms. The distance between two gold atoms is 5.09 Å.[58]

```
Au - C = N : Au - C = N
|<------5.09 Å->|
```

The Mössbauer spectrum for AuCN at 4.2°K is shown in Fig. V-17. The data points were least-squares fitted with two Lorentz lines. The linewidth is 0.272 (0.023) cm/sec. The IS with respect to gold in platinum is +0.166 (0.017) cm/sec, and the QS is 0.809 (0.003) cm/sec. We assumed that AuCN has an axially-symmetric environment and constrained

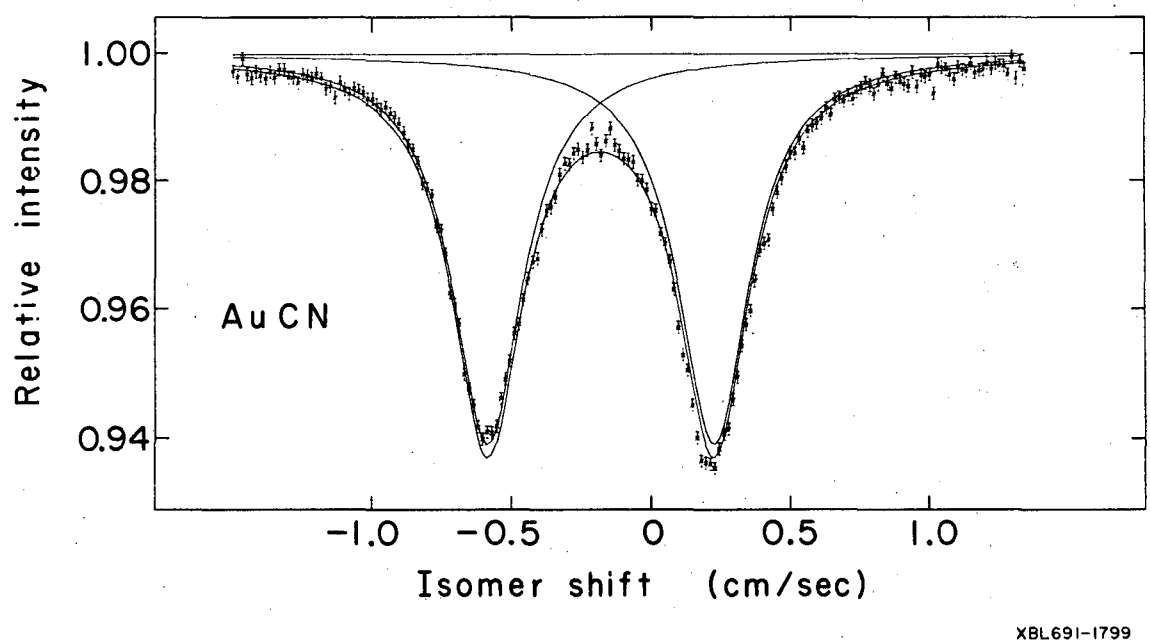

Fig. V-17. Mössbauer spectrum of Au 197 in AuCN.

the two component lines to be of equal linewidth and intensity. AuCN, along with $[Au(CN)_2]^-$, $[Au(S_2O_3)_2]^-$ and $[Au(CN)_4]^-$ manifests the largest QS values observed for gold compounds. For this experiment the absorber sample had a gold density of 289.3 mg/cm^2. No chemical analysis was performed on this insoluble gold cyanide.

13. Potassium dicyanoaurate(I), $KAu(CN)_2$

This colorless complex is one of the most stable complexes of gold. It has a solubility constant $K = 4 \times 10^{28}$,[60] has rhombohedral symmetry, and belongs to the R_3 space group.[61] The cell dimensions are: a = 9.47 Å with $\alpha = 43.9°$. The unit cell contains six $[Au(CN)_2]^-$ complexes. Due to the similarity in the electronic compositions of carbon and nitrogen, an X-ray analysis leaves some ambiguities. However, from infrared spectra[59] of $KAu(CN)_2$, it has been concluded that the carbon is directly bonded to gold. The complex consists of linear layers of $[Au(CN)_2]^-$ ions alternating with K^+ ion layers. See Fig. V-18. The bond lengths and bond angles are:

Au - C = 2.12 ± 0.14 Å
C - N = 1.17 ± 0.20 Å
K - N = 2.78 Å (average distance)
Au- C - N = 172.8 ± 7.5°
C axis-Au-N = 20.4 ± 2.9°
C axis-Au-C = 19.5 ± 4.4°

The sodium congener,[62] which we did not investigate is a colorless crystalline substance with three molecules per unit cell and the following cell dimensions: a = 3.64 Å, c = 27.0 Å and $\alpha = 22°42'$.

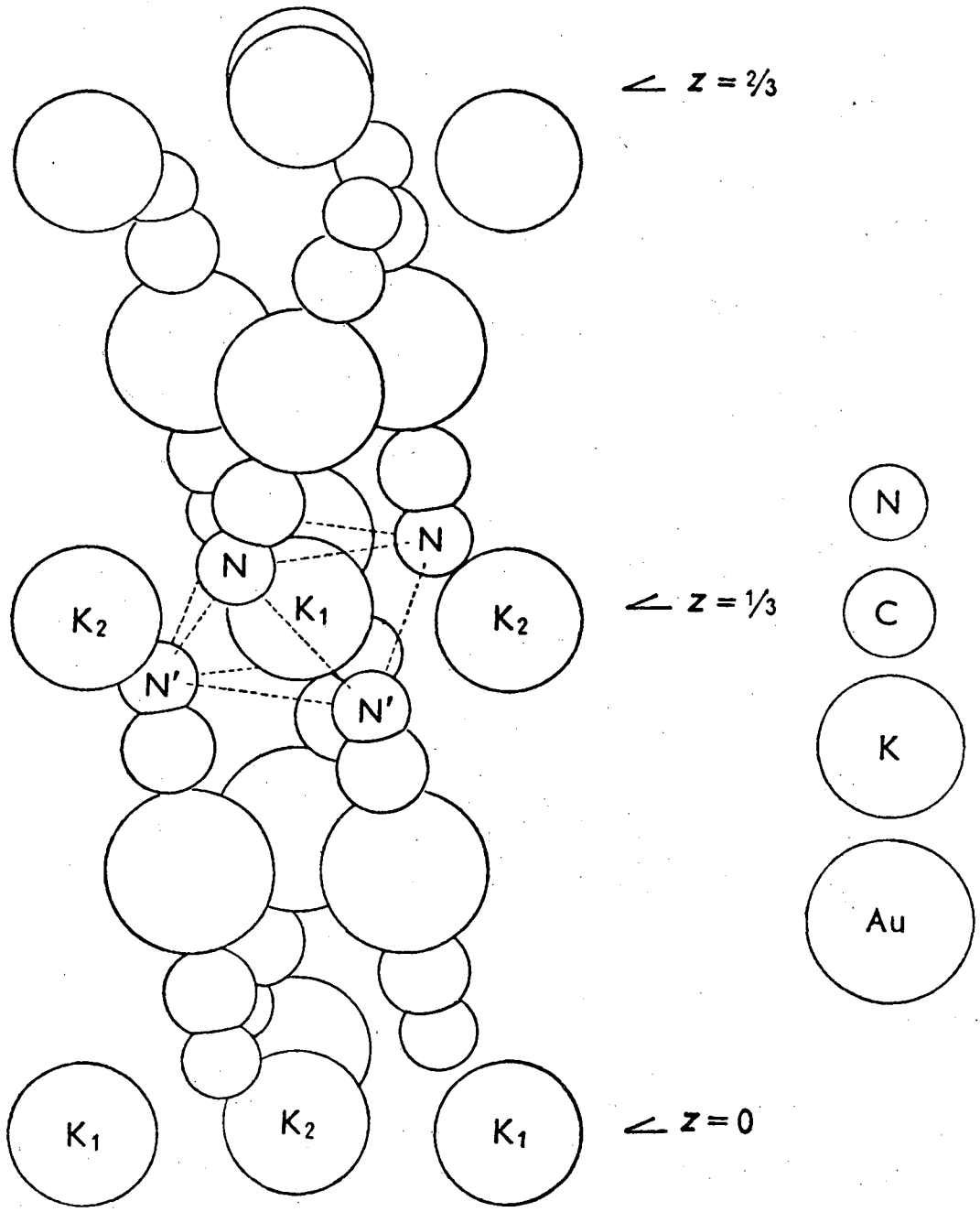

XBL 6811-6161

Fig. V-18. Coordination of gold in $KAu(CN)_2$. (Rosenzweig, et al.[61]).

The IS for $KAu(CN)_2$ is + 0.325 (0.008) cm/sec and the QS is 1.021 (0.006) cm/sec. The Mössbauer spectrum, shown in Fig. V-19, was fitted with two Lorentz lines. The width as determined from the fit was 0.195 (0.014) cm/sec. Since the compound has axial symmetry, the two Lorentz lines were constrained to have equal widths and intensities.

Three of the four samples of $KAu(CN)_2$ contained areal gold densities of 1.005 g/cm^2, 168.2 mg/cm^2, and 271.8 mg/cm^2. The third sample contained some $KAu(CN)_2I_2$ as well as $KAu(CN)_2$. This was the result of an incomplete reaction in the preparation of $KAu(CN)_2I_2$. Although there were two pairs of lines in the spectrum of the mixed absorber, we were able to resolve the two pairs of lines to obtain useful information. (See Fig. V-20).

14. Potassium tetracyanoaurate(III), $K[Au(CN)_4]$

This fairly stable, crystalline substance is colorless, appears to have orthorhombic symmetry[63] and has four complex aggregates in a unit cell. It belongs to the D_{4h} space group and was found not to be perfectly square-planar.[64] Based on infrared spectra, the Au-C-N unit is out of the plane and the C-Au-C unit is deformed. The cell dimensions of $KAu(CN)_4$ are: a = 6.74 ± 0.01, b = 7.18 ± 0.01 and c = 17.48 ± 0.02 Å. The average Au-C bond length is 1.93$_1$Å.

The Mössbauer spectrum for $KAu(CN)_4$ at 4.2°K is shown in Fig. V-21. The line drawn through the data is the least-squares fit of two Lorentz lines with resultant width of 0.218 (0.014) cm/sec. The IS and QS are +0.421 (0.012) cm/sec and 0.699 (0.005) cm/sec, respectively.

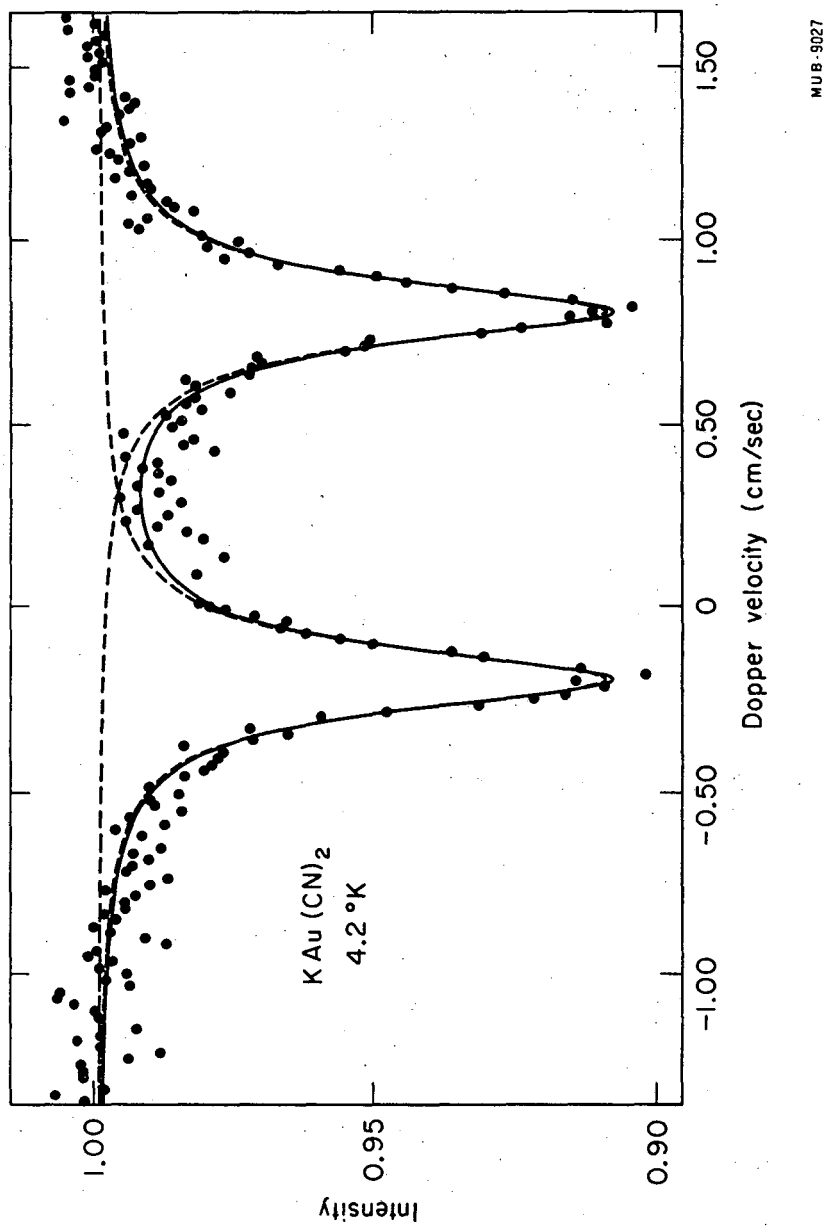

Fig. V-19. Mössbauer spectrum of Au 197 in $KAu(CN)_2$.

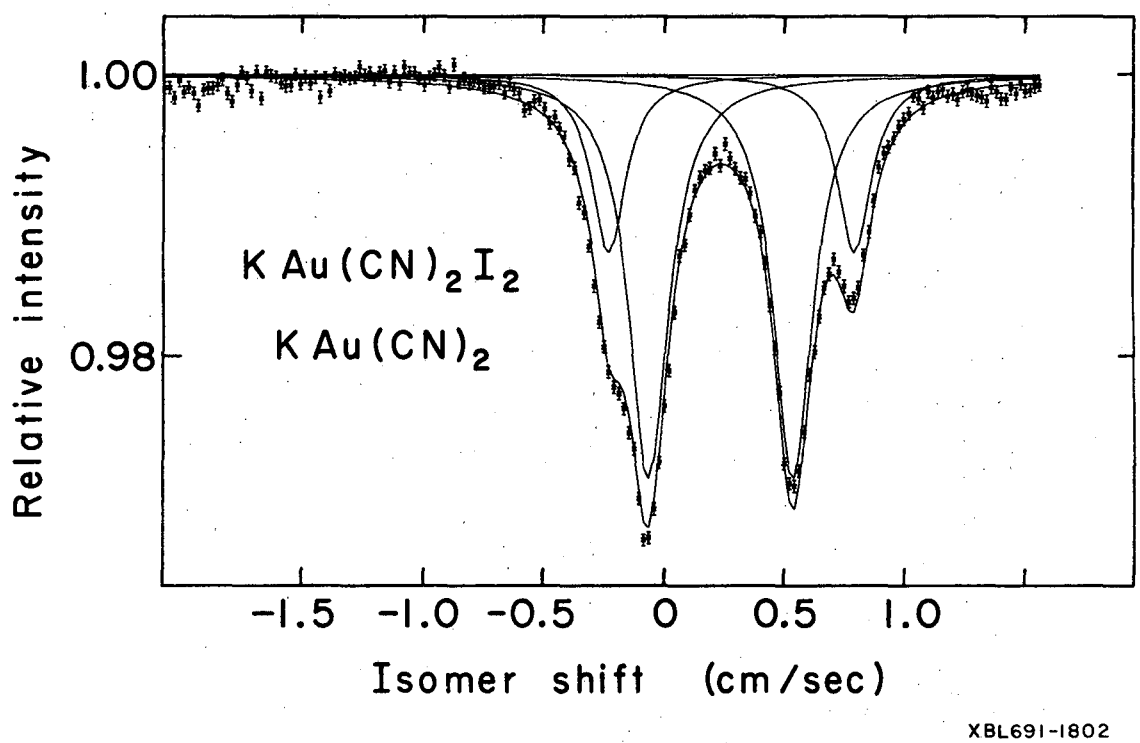

Fig. V-20. Mössbauer spectrum of Au 197 in a mixture $KAu(CN)_2$ and $KAu(CN)_2I_2$.

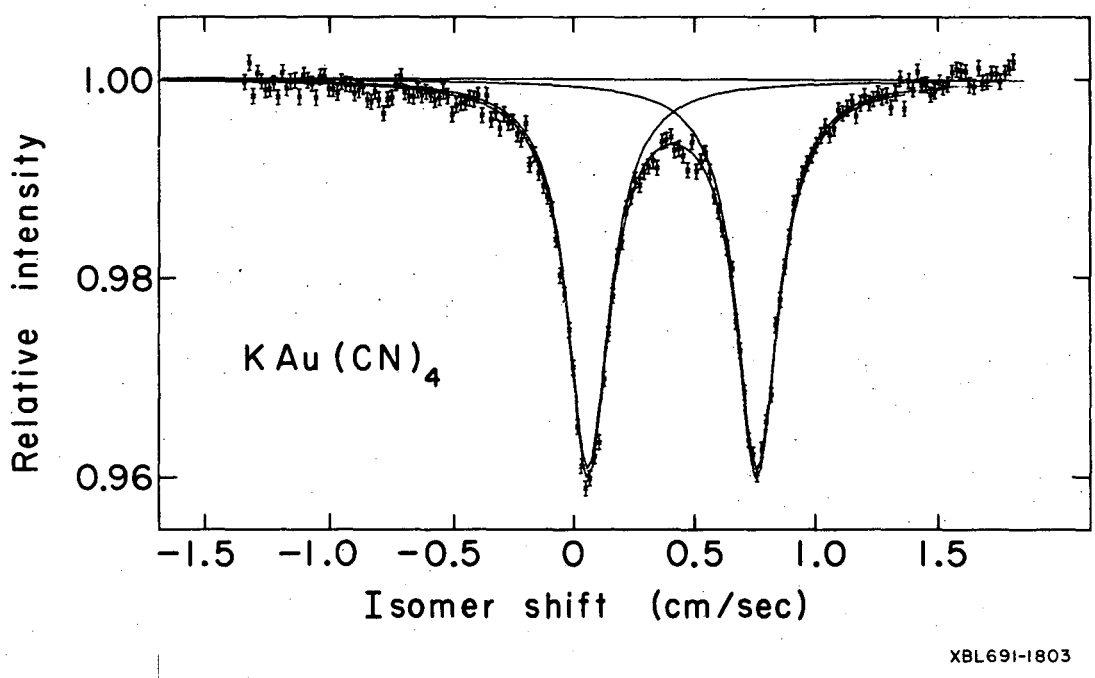

Fig. V-21. Mössbauer spectrum of Au 197 in $KAu(CN)_4$.

Although the symmetry around gold is a slightly-deformed, square-planar configuration, we fitted the results with Lorentz lines of equal linewidths and intensities.

We used four absorber samples with the following areal gold densities: 126.47, 166.6, 170.3, and 206.6 mg/cm^2. One chemical analysis disclosed a potassium to gold to cyanide molar ratio of 1.07/1.00/4.02.

15. Potassium trans-dicyanodihaloaurate(III), $Au(CN)_2X_2$ (X=Cl, Br, I)

From infrared and Raman studies, it was determined that these mixed halogen-cyanide complexes of gold are trans-square-planar isomers,[65] as indicated in Fig. V-22. No extensive X-ray structural determination has yet been reported for these compounds. From an X-ray powder pattern of the bromine-cyanide complex, it has been shown that it is monoclinic.[66] Further structural studies are being conducted.

The potassium salt of the chlorine-cyanide complex is a pale yellow crystalline complex which appears to be reasonably stable. The bromine-cyanide complex is bright yellow and the iodine-cyanide complex is a deep reddish-brown to almost black crystalline substance.

The Mössbauer spectra for $KAu(CN)_2Cl_2$, $KAu(CN)_2Br_2$, and $KAu(CN)_2I_2$ are given in Figs. V-23, 24, 25. The linewidth, IS and QS results are listed below. Although the chemical environment of gold is not symmetric with respect to the ligands, the spectra appeared nearly symmetric so we constrained the two component Lorentz lines to have equal linewidths and intensities.

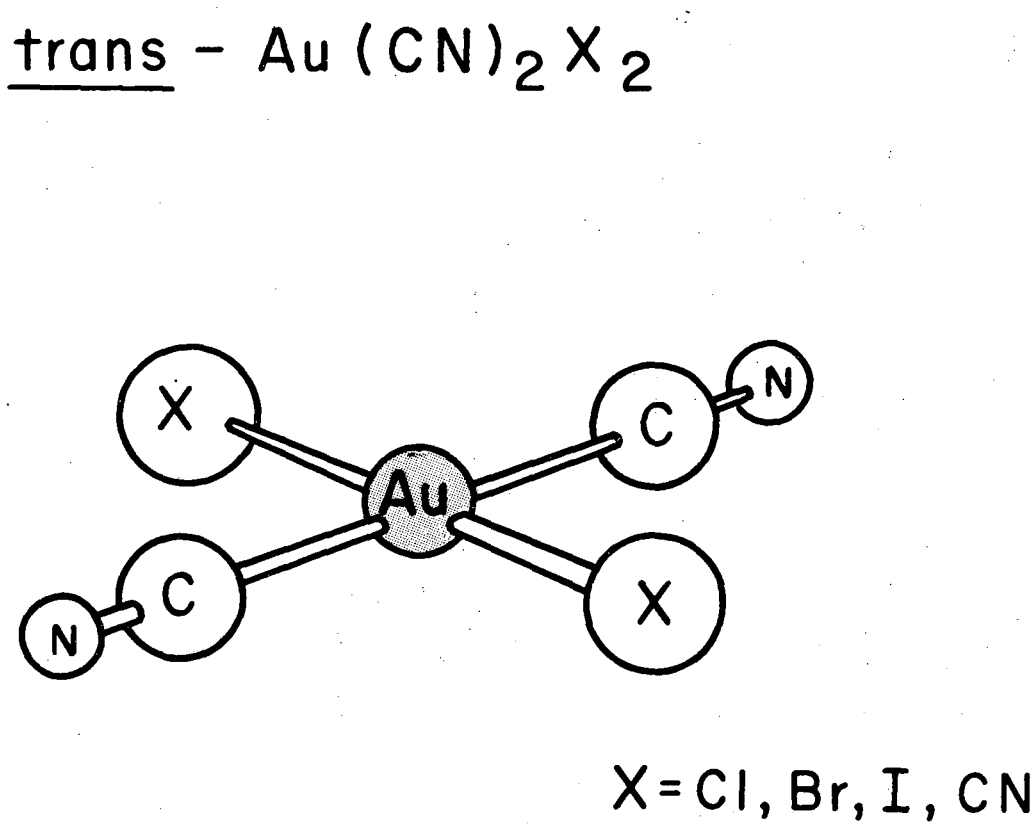

Fig. V-22. Coordination of gold in $Au(CN)_2X_2$, X = Cl, Br, I.

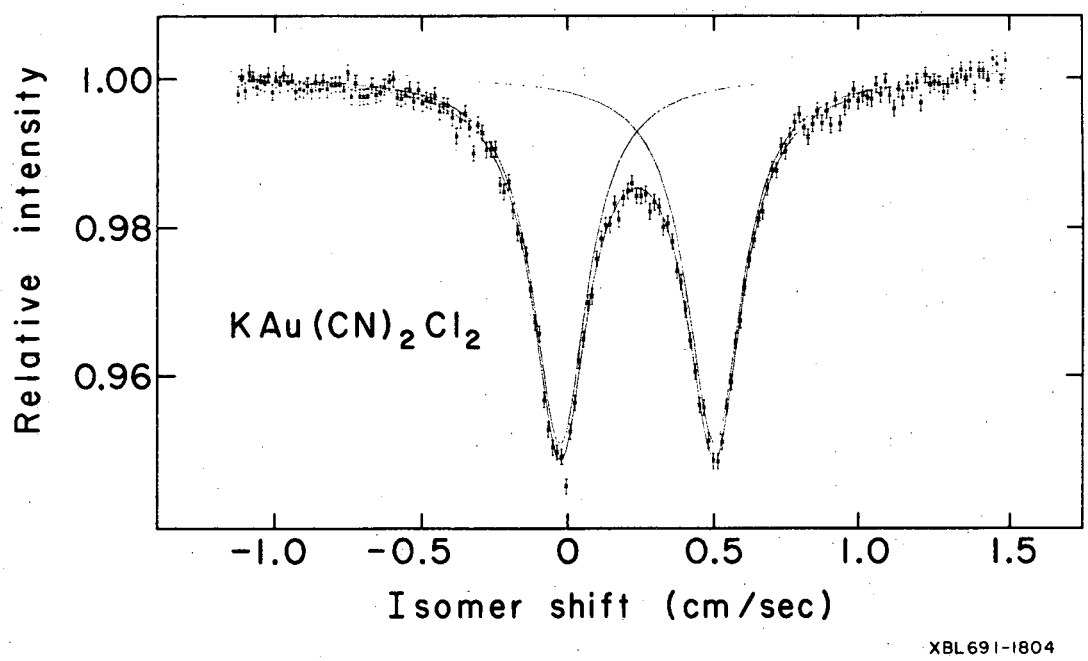

Fig. V-23. Mössbauer spectrum of Au 197 in $KAu(CN)_2Cl_2$.

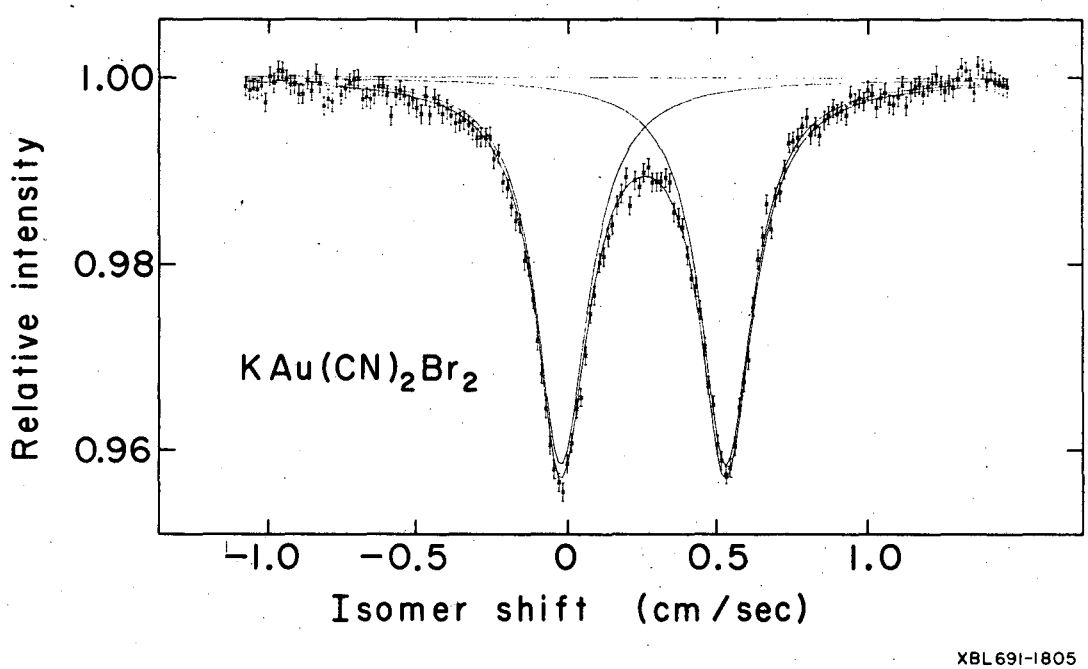

Fig. V-24. Mössbauer spectrum of Au 197 in $KAu(CN)_2Br_2$.

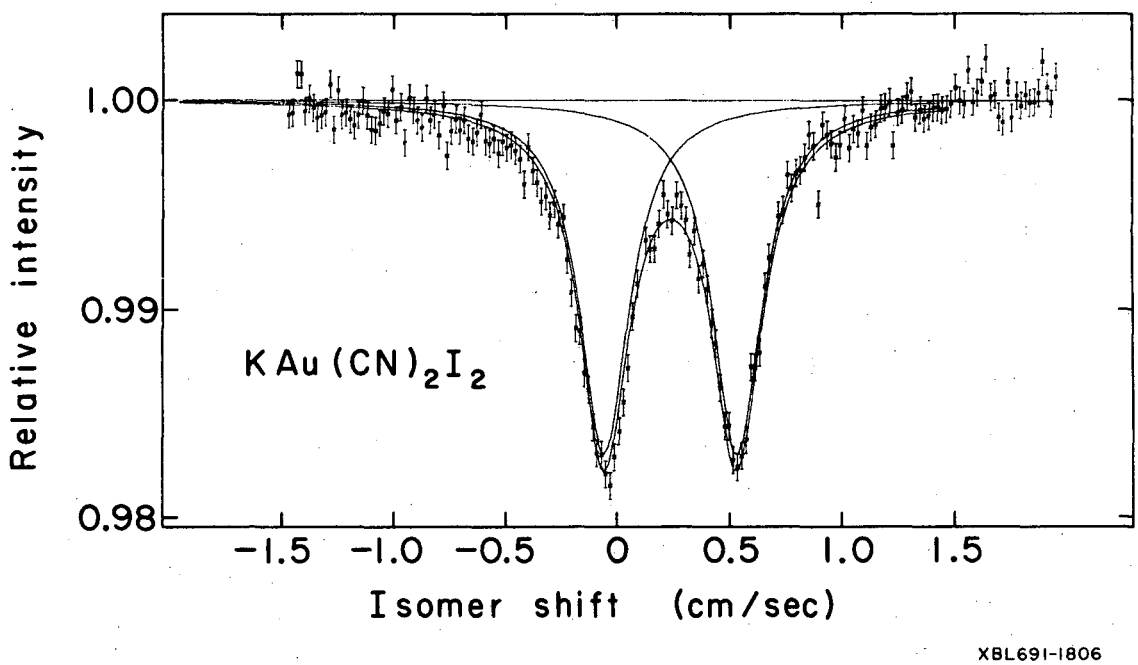

Fig. V-25. Mössbauer spectrum of Au 197 in $KAu(CN)_2I_2$.

	IS	QS	Linewidth
$KAu(CN)_2Cl_2$	+0.256(0.002)cm/sec	+0.526(0.002)cm/sec	0.218(0.004)cm/sec
$KAu(CN)_2Br_2$	+0.272(0.007)cm/sec	+0.546(0.001)cm/sec	0.245(0.025)cm/sec
$KAu(CN)_2I_2$	+0.278(0.006)cm/sec	+0.587(0.003)cm/sec	0.215(.92) cm/sec

The IS and QS values are slightly monotonically increasing from the chlorine complex to the iodine complex, as might be expected from our model which is explained later.

The areal densities of gold in the samples and the results of the chemical analyses are listed in the following table.

	Areal gold density	Chemical Analyses
$KAu(CN)_2Cl_2$	327.6 mg/cm^2	K/Au/Cl/CN = 1.03/1.00/1.99/1.99
$KAu(CN)_2Br_2$	118.9 mg/cm^2	K/Au/Br/CN = 1.03/1.00/1.98/2.05
$KAu(CN)_2I_2$	80.9 mg/cm^2	K/Au/I/CN = 1.02/1.00/2.04/2.05
"sample 2	113.2 mg/cm^2	(no analysis)

16. Sodium dithiosulfatoaurate(I), $Na_2Au(S_2O_3)_2$

This compound, medically known as sanocrycin, has been variously used for attempting to cure tuberculosis, leprosy and arthritis. It is a stable white flocculent compound which has monoclinic symmetry[66] and belongs to the $\underline{P}2_1/a$ space group. There are four molecules per unit cell whose dimensions are: a = 18.206, b = 11.355, and c = 5.44 Å, and β = 97.87°. The S-Au-S bond angle is very nearly 180° and the average Au-S bond distance is 2.28 Å. This compound forms a cyclic structure as shown in Fig. V-26(a).

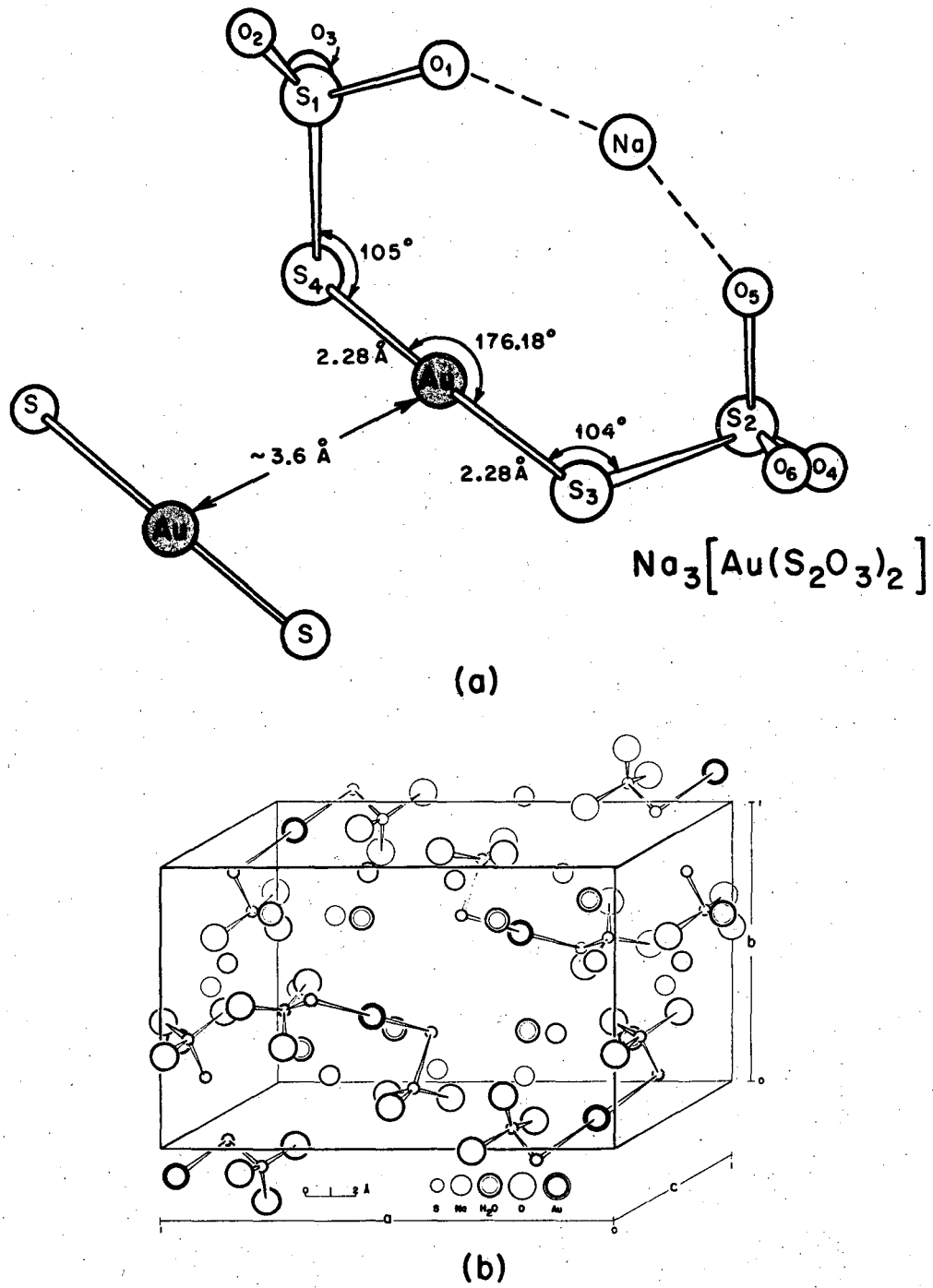

XBL691-1794

Fig. V-26. Coordination of gold in $Na_3Au(S_2O_3)_2$. H. Templeton and H. Rubin, Ref. 66.

This X-ray study is probably the first X-ray structural determination of the thiosulfate anion structure:

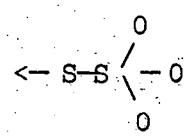

Figure V-26(b) gives the orientation of a unit cell of $Na_3Au(S_2O_3)_2$. A list of the tentative values of the bond lengths and angles are given in Table I.

In Fig. V-27 is given the Mössbauer spectrum of $Na_3(Au(S_2O_3)_2)$. Since the X-ray structural determination of the compound revealed an essentially linear bond at gold, the two Lorentz lines were constrained to have both equal linewidths and line intensities. The linewidth is 0.317(0.020) cm/sec and the IS and QS are +0.072(0.029) cm/sec and 0.708 (0.004) cm/sec respectively.

Since an early chemical analysis showed that there was a large excess of the thiosulfate ligand, we used a larger than average sample. The actual gold content of the sample has not been determined.

17. Au(III) <u>cis</u>-1,2-dicyanoethylene-1,2-dithiolate anion, $[AuS_4C_4(CN)_4]^-$

This medium reddish-brown compound, $[(C_2H_5)_4N]^+[AuS_4C_4(CN)_4]^-$, is diamagnetic and essentially square-planar[67] in the first coordination sphere. It is the only truly bidentate gold complex included in this study. The general structure of this compound is given in Structure I:

Table I. Distances[66] in $Na_3(Au(S_2O_3)_2)2H_2O$*

Atom 1-Atom 2	Bond (A)	Atom 1-Atom 2	Bond (A)
Au - S(4)	2.28	Na(1) - O(6)	2.47
- S(3)	2.28	- W(1)	2.36
		- W(2)	2.39
S(1) - S(4)	2.05		
- O(1)	1.45	Na(2) - O(1)	2.55
- O(2)	1.45	- O(2)	2.43
- O(3)	1.45	- O(3)	2.40
		- O(4)	2.39
S(2) - S(3)	2.06	- O(6)	2.46
- O(4)	1.47	- W(1)	2.34
- O(5)	1.47		
- O(6)	1.47	Na(3) - O(1)	2.55
		- O(2)	2.38
Na(1) - O(1)	2.63	- O(3)	2.39
- O(4)	2.50	- O(4)	2.42
- O(5)	2.46	- W(2)	2.34
		- O(1)	2.91
		- O(6)	2.91

* The standard deviations are Au-S 0.004A, S-S 0.01A, S-O 0.02A, and Na-O 0.02A or less.

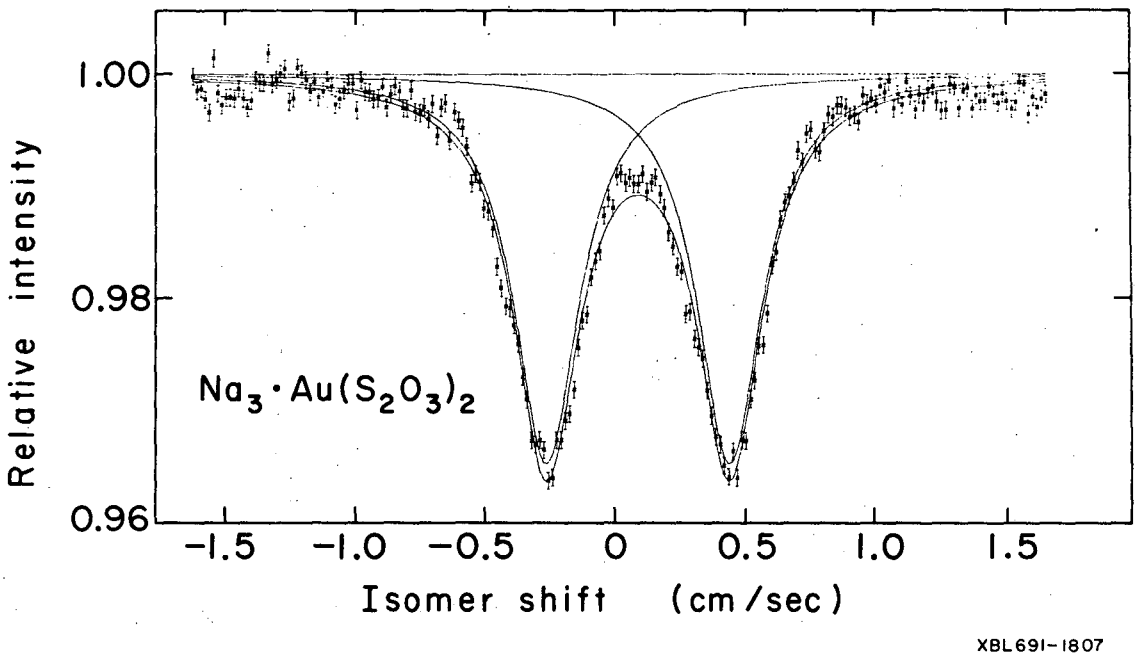

Fig. V-27. Mössbauer spectrum of Au 197 in $Na_3Au(S_2O_3)_2$.

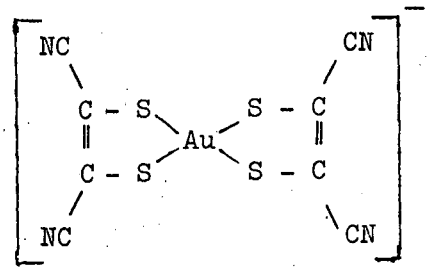

Structure I

The Mössbauer spectrum is not symmetric as seen in Fig. V-28. Since we die not prepare this compound in our laboratory and we are not certain about its stability, it is difficult to evaluate the results. The larger of the two intensities occurs at near zero isomer shift.

We also fitted the spectrum with a single and a double line as shown in Fig. V-28 (b). When the double line was constrained to have equal intensities and linewidths, the resulting linewidth was 0.221 (0.005)cm/sec and the splitting is 0.197 (0.006)cm/sec. The isomer shift with respect to gold in platinum is +0.326 (0.007)cm/sec.

The linewidth of the single line is 0.236 (0.011)cm/sec; it is located at 0.121 (0.008)cm/sec. We have not come to a satisfactory conclusion about this compound. In Sec. II-B-3, we have discussed other possible sources of unequal line intensities.

18. Gold(III) -- sesquioxide, Au_2O_3

This reddish-brown powdery compound has not been characterized. It was purchased from Alfa Inorganics, Inc. If the gold(III) oxide structure is consistent with the other tervalent compounds of golds, it would have coordination number four with square-planar symmetry at the central gold metal.

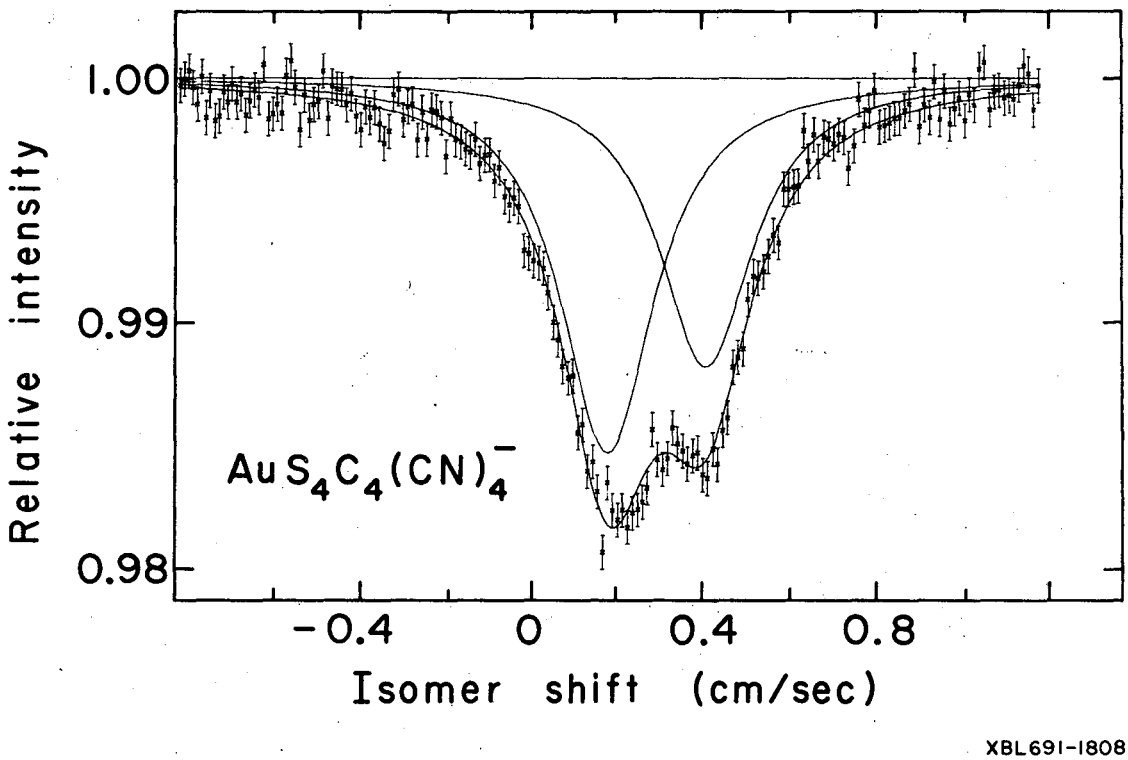

Fig. V-28(a). Mössbauer spectrum of Au 197 in $[AuS_4C_4(CN)_4]^-$.

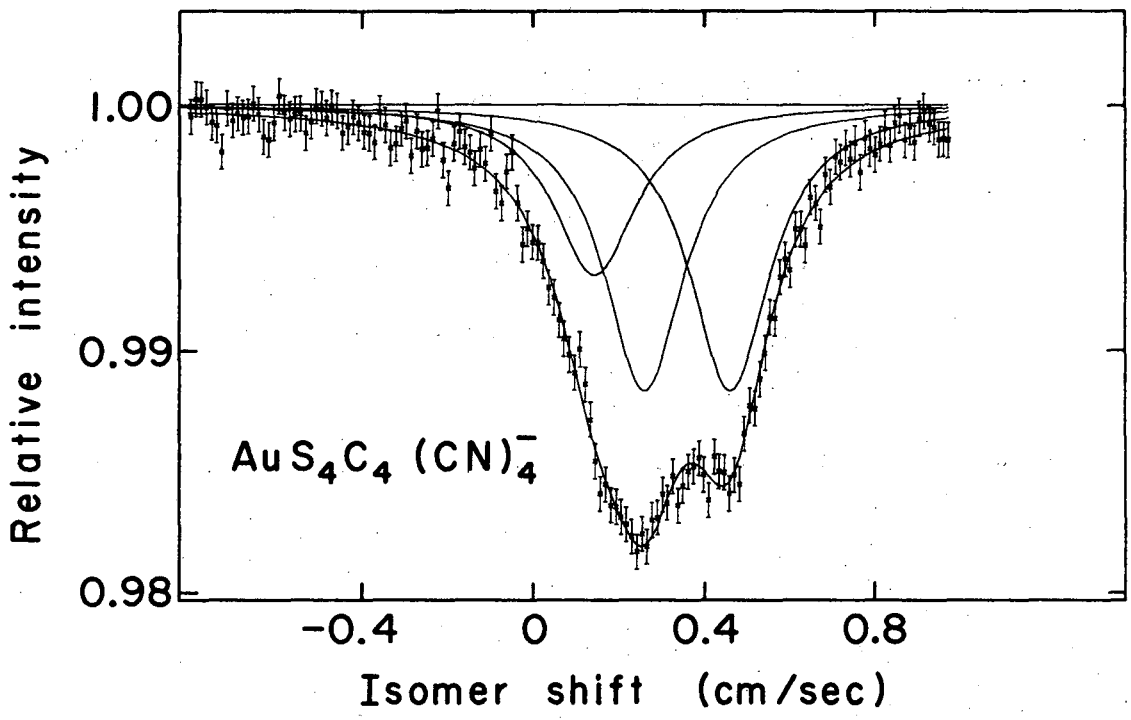

XBL691-1809

Fig. V-28(b). Mössbauer spectrum of Au 197 in $[AuS_4C_4(CN)_4]^-$.

Gold oxide, Au_2O_3, has a slightly asymmetric Mössbauer spectrum as seen in Fig. V-29. This compound is reportedly not very stable, but was investigated as purchased from the Alfa Inorganics, Inc. Chemical Company. The average linewidth is large, 0.350 (0.022)cm/sec, so the Mössbauer spectrum may represent more lines than two. The natural linewidth for the 77 keV γ-ray of Au^{197} is 0.194 cm/sec. We tried fitting the spectrum with three lines, one of which was the line for gold metal at -0.12 cm/sec isomer shift. This did not improve the fit appreciably so we simply approximated the chemical environment of the gold nucleus as being axially symmetric and fitted the spectrum with two lines which were constrained to have equal linewidths and equal line intensities. The IS is +0.094 (0.001)cm/sec and QS is 0.168 (0.004)cm/sec.

The absorber sample contained 232.4 mg/cm^2 of gold. No chemical analysis was performed due to the difficulty of analyzing for oxygen.

19. Gold sulfides: Au_2S, Au_2S_2 and Au_2S_3

The three gold sulfide compounds were reasonably stable, sparingly soluble in water and appeared to be amorphous to X-ray diffraction investigations.[66]

a. Au_2S. Crystalline Au_2S was obtained by some French investigators[68] who had determined that Au_2S belongs to the O_h^4 Pn3m space group of Cu_2O type structure and has cubic symmetry. They report two Au_2S molecules per unit cell and a = 5.020 ± 0.003Å.

The Au_2S Mössbauer spectrum was fitted with two Lorentz lines of unequal intensities but of equal linewidths as shown in Fig. V-30. The

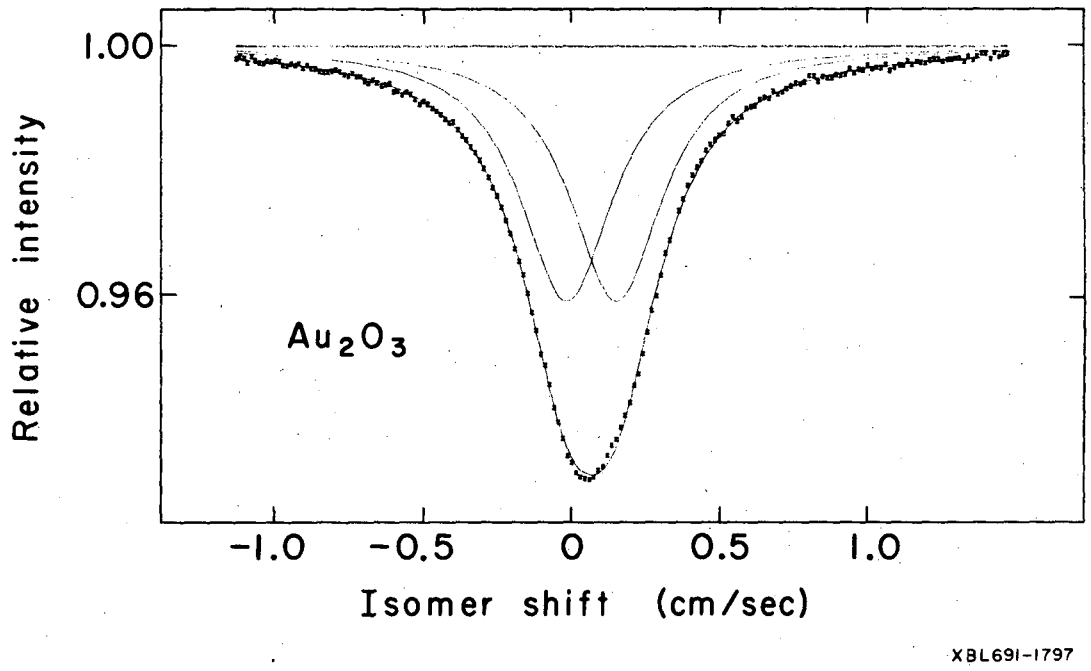

Fig. V-29. Mössbauer spectrum of Au-197 in Au_2O_3.

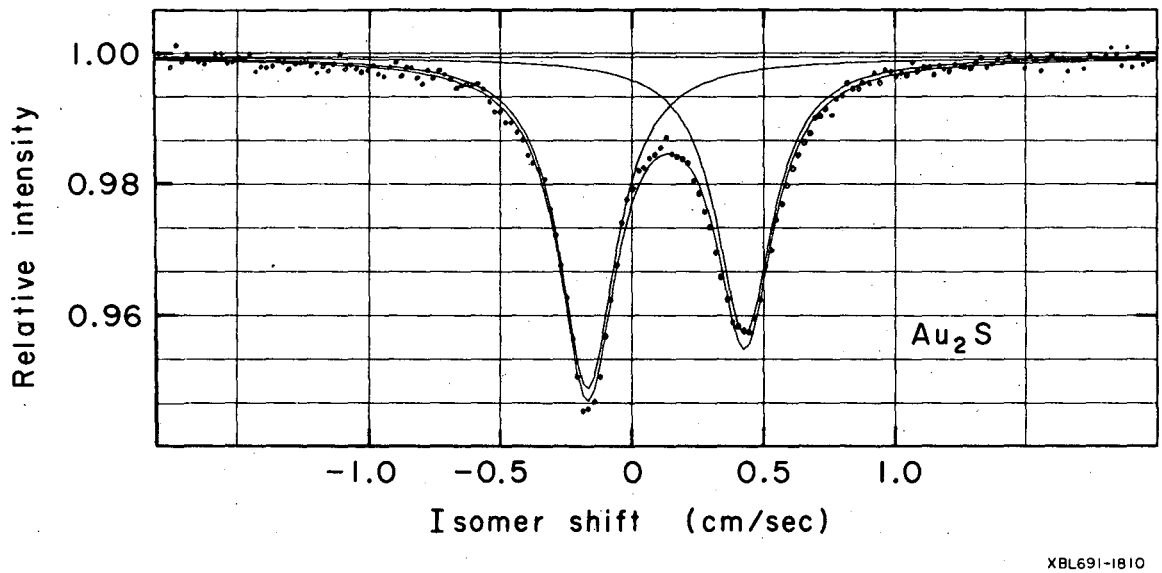

Fig. V-30. Mössbauer spectrum of Au 197 in Au_2S.

linewidth and the two line positions are 0.249 (0.004)cm/sec, and 0.433 (0.007)cm/sec and -0.156 (0.006)cm/sec, respectively. A chemical analysis gave a gold-to-sulfur molar ratio of 2.04.

b. Au_2S_2. Au_2S_2 might be more accurately written as $Au_2S \cdot Au_2S_3$, since it has been amply stated in the literature that many gold compounds with an apparent +2 oxidation state are just gold compounds containing the metal in both the +1 and +3 oxidation states in equivalent amounts. These compounds are invariably black. This gold sulfide was not completely amorphous to X-ray powder studies and had lines similar to those of the gold metal.

The Mössbauer spectrum for Au_2S_2 at 4.2°K is given in Fig. V-31. The spectrum was fitted with four Lorentz lines with no knowledge of the Hamiltonian. The compound may be a combination of several gold sulfides or may even contain some metallic gold. The linewidths were constrained to be equal and the four lines occur at -0.344 (0.011)cm/sec, -0.197 (0.015)cm/sec, +0.021 (0.058)cm/sec and +0.290 (0.011)cm/sec. The linewidth determined by the fit was 0.326 (0.008). The molar ratio of sulfur to gold was determined to be 1.007, which is essentially the theoretical molar ratio.

c. Au_2S_3. Au_2S_3 is a black powder which decomposes into its elements at about 200°C.[34] If this compound is structurally similar to the other gold (III) compounds (square-planar with coordination number four) then the shortest bonds to gold might involve the following structure:

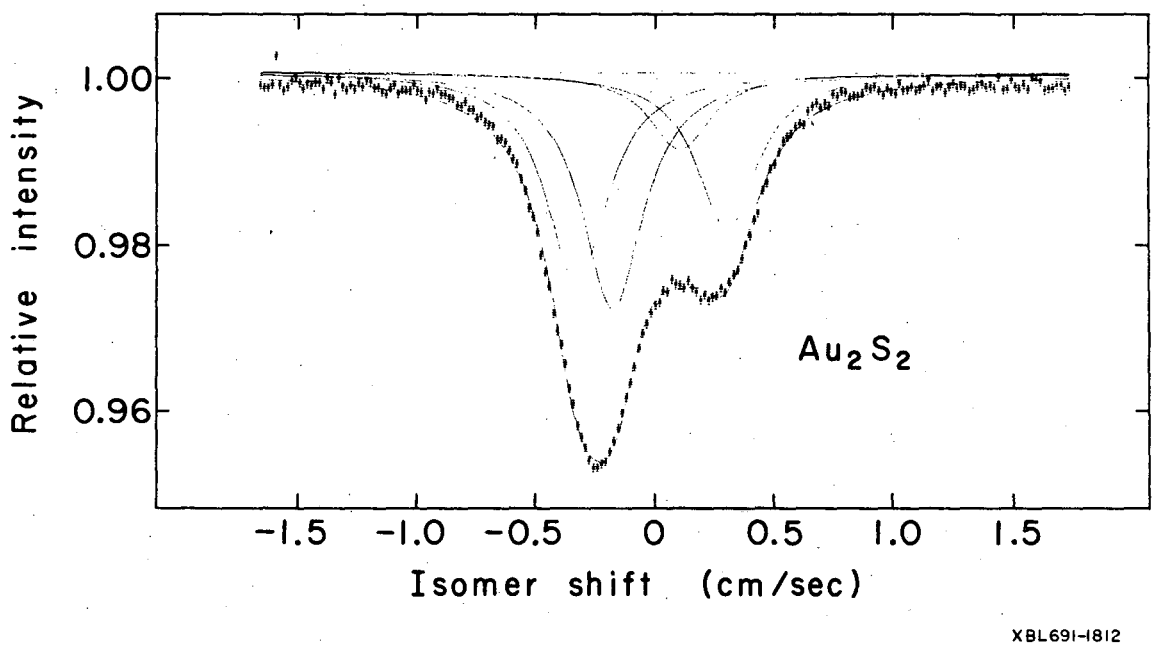

Fig. V-31. Mössbauer spectrum of Au 197 in Au_2S_2.

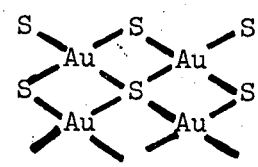

The Mössbauer spectrum for Au_2S_3 is a complicated curve which we attempted to fit with three lines of equal linewidth as shown in Fig. V-32. The line positions are -0.197 (0.009)cm/sec, +0.50 (0.011)cm/sec and +0.348 (0.007)cm/sec. The linewidth determined by the fit was 0.303 (0.016)cm/sec.

Three samples were prepared containing the following areal densities on gold: 81.4 mg/cm^2, 87.2 mg/cm^2 and 77.5 mg/cm^2. The chemical analysis on Au_2S_3 gave a sulfur to gold molar ratio of 1.60, 1.63, and 1.60.

B. General Observations About the Results

The complete results of our Mössbauer effect experiments on gold compounds are given in Table II. In the first column of the table are listed $\Delta\psi(0)^2_{\text{Relativistic}}$ values which were computed from the IS results using Eq. (11) of Sec. II-B-1. For Au 197 we have

$$\text{IS (cm/sec)} \cong 1.618 \times 10^{-27} \cdot \Delta\psi(0)^2_{\text{Relativistic}} \qquad (1)$$

The IS values are relative to a gold-in-platinum source.

In the fourth column are listed the electric field gradients, q_{zz}, which were determined from the following expression

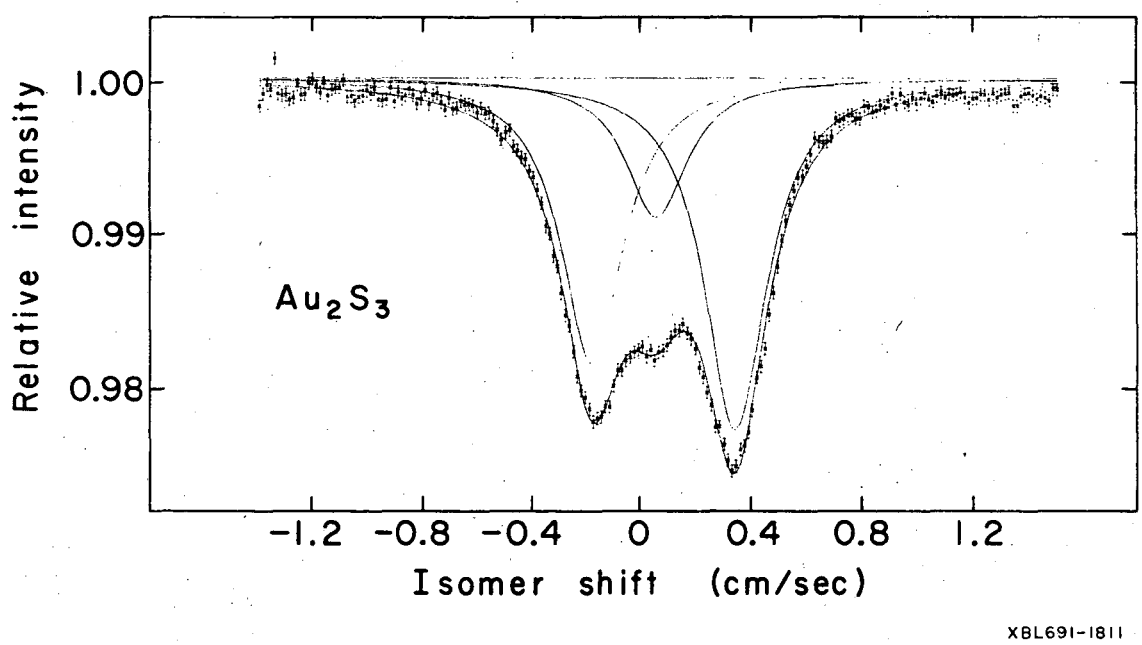

Fig. V-32. Mössbauer spectrum of Au 197 in Au_2S_3.

Table II. Results of the Mössbauer Experiments
(The assumed signs are indicated parenthetically).

Compound	IS cm/sec	$\Delta\psi(0)^2 \times 10^{25}$ Relativistic	QS cm/sec	$\lvert q_{zz} \rvert \times 10^{15}$	Γ cm/sec
AuF_3	-0.107(.001)	-6.611	0.274(.002)	(-) 7.860	0.232(.002)
$[AuF_4]^-$	-0.069(.002)	-4.263	0.182(.002)	(-) 5.221	0.228(.040)
AuCl	-0.142(.001)	-8.774	0.465(.001)	(-)13.339	0.196(.004)
$[AuCl_4]^-$	0.044(.006)	2.7187	0.127(.008)	3.643	0.254(.029)
$AuCl_3$	2.057(.009)	3.521	0.075(.008)	2.151	0.241(.020)
AuBr	-0.147(.001)	-9.083	0.423(.004)	(-)12.134	0.217(.008)
$[AuBr_4]^-$	$.066_6$(.002)	4.115	0.113(.002)	3.2415	0.220(.012)
$AuBr_3$	.079(.007)	4.881	0.127(.002)	3.643	0.300(.004)
AuI	-0.132(.003)	-8.156	0.398(.001)	(-)11.417	0.242(.004)
AuI_3	-0.153(.037)	-9.4537	0.399(.005)	(-)11.446	0.237(.041)
$Cs_4Au^{I}_2AU^{III}_2Cl_{12}$	-0.143(.028)		I 0.410(.005)		0.216(.004)
	-0.009(.022)		III 0.133(.018)		0.164(.006)
AuCN	0.166(.017)	10.257	0.809(.003)	(-)23.207	0.272(.023)
$[Au(CN)_2]^-$	0.325(.008)	20.0815	1.021(.006)	(-)29.288	0.195(.018)
$[Au(CN)_4]^-$	0.421(.012)	26.013	0.699(.005)	20.052	0.218(.014)
$[Au(CN)_2Cl_2]^-$	0.256(.002)	15.818	0.526(.002)	∿ 12.69	0.218(.004)
$[Au(CN)_2Br_2]^-$	0.272(.007)	16.807	0.546(.001)	∿ 13.53	0.245(.025)
$[Au(CN)_2I_2]^-$	0.278(.006)	17.177	0.587(.003)	∿ 13.85	0.215(.012)
$[AuS_4C_4(CN)_4]^-$	0.326(.007)	20.143	0.197(.006)		0.221(.005)
Au_2O_3	0.094(.001)	5.808	0.168(.004)	4.819	0.350(.022)
$[Au(S_2O_3)_2]^{-3}$	0.072(.029)	4.4488	0.708(.004)	(-)20.310	0.317(.020)

$$QS = \frac{1}{2} \quad eq_{zz}Q \quad (1 + \eta^2/3)^{1/2} \qquad (2)$$

This equation was discussed in Sec. II-B-3. Here η, the asymmetry parameter, is taken to be zero. This is valid for most gold(I) and gold(III) compounds, which are considered to have axial symmetry. The known exception is the gold cyano-halides, $KAu(CN)_2X_2$ (X = Cl, Br, I), where $0 < \eta \leq 1$. We do not have the values of η for these compounds. We have approximated the electric field gradients for these three compounds at the end of this section, and have estimated their n values.

The observed linewidths are given in the last column. The quadrupole moment, Q, of Au 197 has the value $+0.594(10) \times 10^{-24} cm^2$ [15] and e is the unit of electronic charge, 4.803×10^{-10} esu. Substituting the above values, we have the following conversion between QS and q_{zz} for Au 197

$$QS \text{ (cm/sec)} \times 28.686 = q_{zz} \times 10^{15} \text{ esu/cm}^3 \qquad (3)$$

Before presenting the detailed calculations for the nuclear electron densities and electric field gradients, we will first make some observations about the results.

1. Isomer Shift

a. The isomer shift and the nuclear electron density. The isomer shift values of gold(I) and gold(III) compounds have been arranged in Fig. V-33 in order of increasingly positive IS values (smaller values

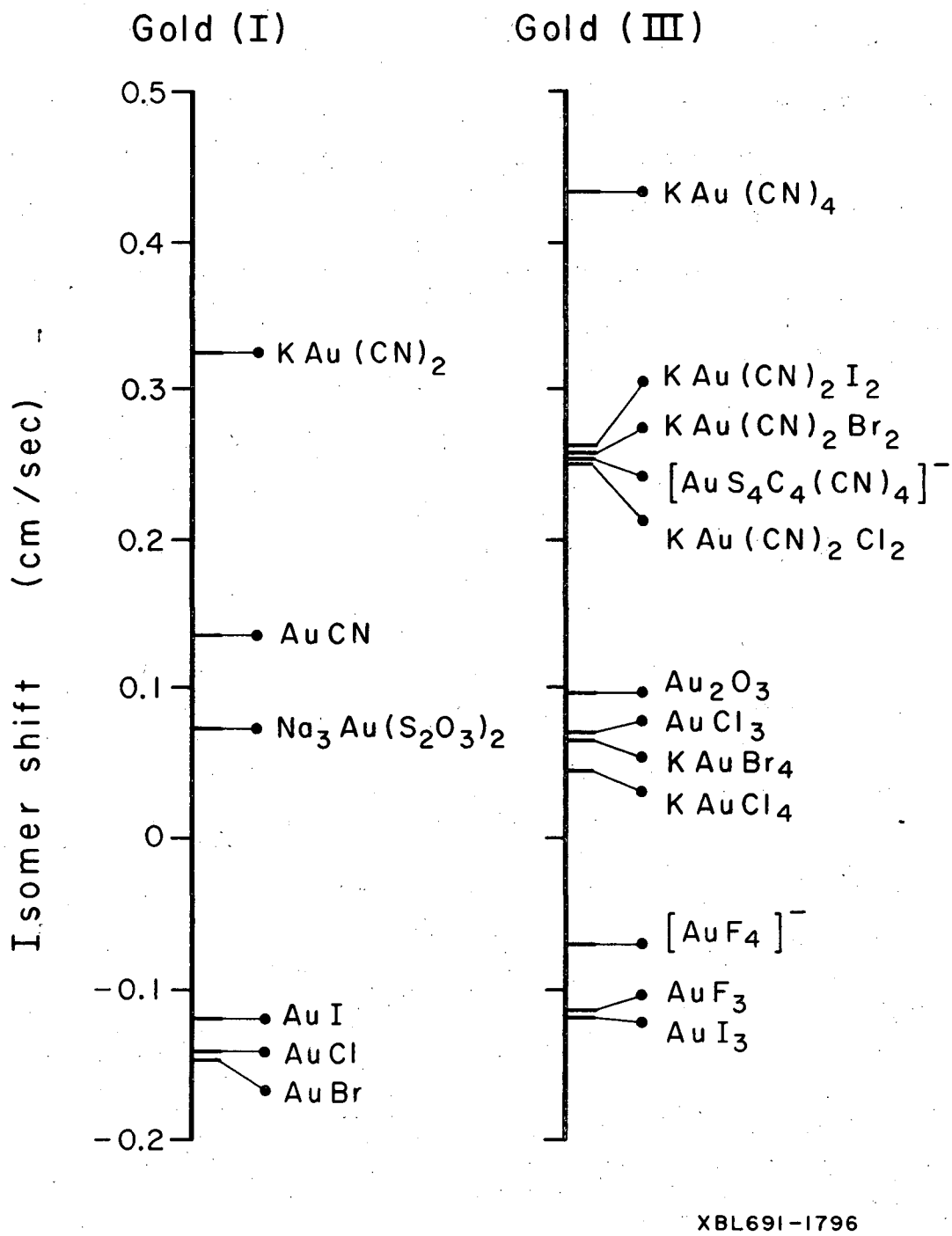

Fig. V-33. Isomer shift results of gold(I) and gold(III) compounds.

at the bottom). In Sec. II-B, we concluded that the gold absorbers with the larger $\psi(0)^2$ values would have the more positive IS values. Gold(I) and gold(III) compounds use 6s6p and $5d6s6p^2$ hybrid orbitals for bonding, respectively. Therefore, in compounds with ligands of lower electronegativities, the gold atoms would be expected to accumulate larger densities of 6s electrons and this have the more positive IS values.

From electronegativity differences between gold and the halides, gold halides are expected to be partially ionic, with the halides having the (slightly) larger portion of the bonding electrons. The cyanide radical is generally considered to be less electron-attracting than the halides. In Fig. V-33, we find the gold halides near the bottom and the cyanides at the top. Therefore, this observed ordering of compounds with respect to IS values helps support the model which proposes an increase in $\psi(0)^2$ from bottom to top of Fig. V-33.

b. Comparison of isomer shift values for gold(I) and gold(III) compounds. In Fig. V-33, we see that for a given ligand, the IS value of the gold(III) compound is more positive than of the corresponding gold(I) compounds. This implies that for a given ligand, the gold(III) compound has a greater nuclear electron density than the corresponding gold(I) compound. Compare, for example, $KAu(CN)_4$ with $KAu(CN)_2$ which have IS values of +0.421 and +0.325 cm/sec, respectively; and $AuCl_3$ with AuCl whose IS values are +0.057 and -0.142 cm/sec, respectively.

In Sec. III-B, we gave the inner electron configurations and hybrid orbitals of the aurous and auric compounds as

$$\text{Gold(I)}; \quad 5d^{10}(6s6p)^{N} \quad 0 \leq N \leq 2 \tag{4}$$

$$\text{Gold(III)}; \quad 5d^{8}(5d6s6p^{2})^{N'} \quad 0 \leq N' \leq 2 \tag{5}$$

To simpify this discussion, consider an hypothetical ligand, L, which forms perfectly covalent bonds with gold ($N = 1$, $N' = 1$): $[AuL_2]^-$ and $[AuL_4]^-$. $[AuL_2]^-$ would have one 6s and one 6p electron. $[AuL_4]^-$ would have one 6s and two 6p electrons and a 5d hole. Although both compounds would have the same number of s electrons, the effective $\psi(0)^2$ for $[AuL_4]^-$ should be more than for $[AuL_2]^-$ due to lower shielding of the 6s electron in the $[AuL_4]^-$ complex by its nine 5d electrons. Therefore, the IS values of the gold(III) would be expected to be more positive than that of the corresponding gold(I) compounds, as observed. The $6p_{1/2}$ electrons, which are more energetic (and therefore farther from the nucleus) than the 6s electrons, are not expected to contribute significantly to the $\psi(0)^2$ value or to effectively shield the 6s electrons.*

---

* $\psi(0)^2_{6p_{1/2}}$ of the $5d^{10}6p_{1/2}$ configuration of gold is about 2% of the $\psi(0)^2_{6s}$ value of the $5d^{10}6s$ configuration. These results are given in Sec. C of this chapter.

2. Quadrupole Splitting

a. Quadrupole splitting results and electric field gradient. In Fig. V-34, the QS results are arranged with the larger values at the top. The sign of the electric field gradient, EFG, whose magnitude is proportional to the QS, cannot be determined by these experimental results. The sign of the EFG of the molecular bond of the gold compounds is accessible from bond symmetry considerations. However, we can only guess the sign of the EFG at the nucleus of gold, which is caused by the bonding electrons. The electronic configuration of gold(I) compounds is depicted in Fig. V-35. The EFG of the sp bonding electrons of gold(I) is negative. However, since the bonding electrons extend a distance from the nucleus of gold, the actual EFG at the nucleus of gold may not directly reflect the symmetry of the bonding electrons. If the repulsive forces of the valence 6p electrons were to distort the inner closed shells of electrons, for instance, the EFG at the nucleus could be oblate and therefore positive.

For gold(III) compounds, the EFG is further complicated by the existence of a $5d_{x^2-y^2}$ electron hole. Figure V-36 gives the geometries of the 5d hole and the dsp^2-hybrid bonding orbitals. Since the two give opposite-sign contributions to the EFG, the sign of the resultant EFG of the valence electrons plus the $5d_{x^2-y^2}$ hole would depend on the relative magnitudes of the 5d and 6p EFG values. With the sign of the EFG of the combined gold(III) bonding and nonbonding electrons themselves in question, it seems speculative to assign a sign to the EFG at the gold nucleus. Although the sign of the EFG at the nucleus may not be the same as that of the bonding and nonbonding electrons, the nuclear EFG is probably proportional to the EFG of the outer electrons.

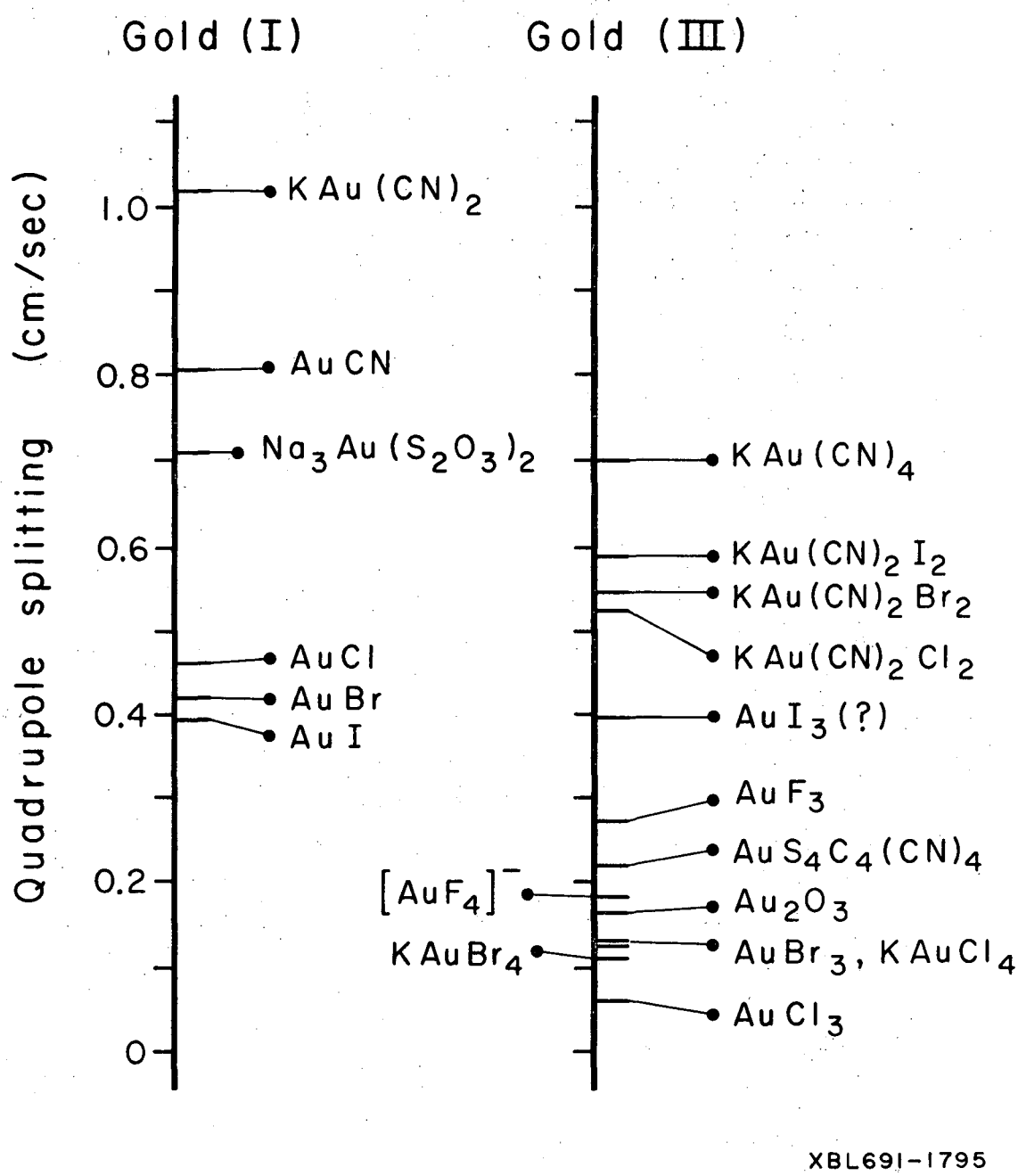

Fig. V-34. Quadrupole splitting results of gold(I) and gold(III) compounds.

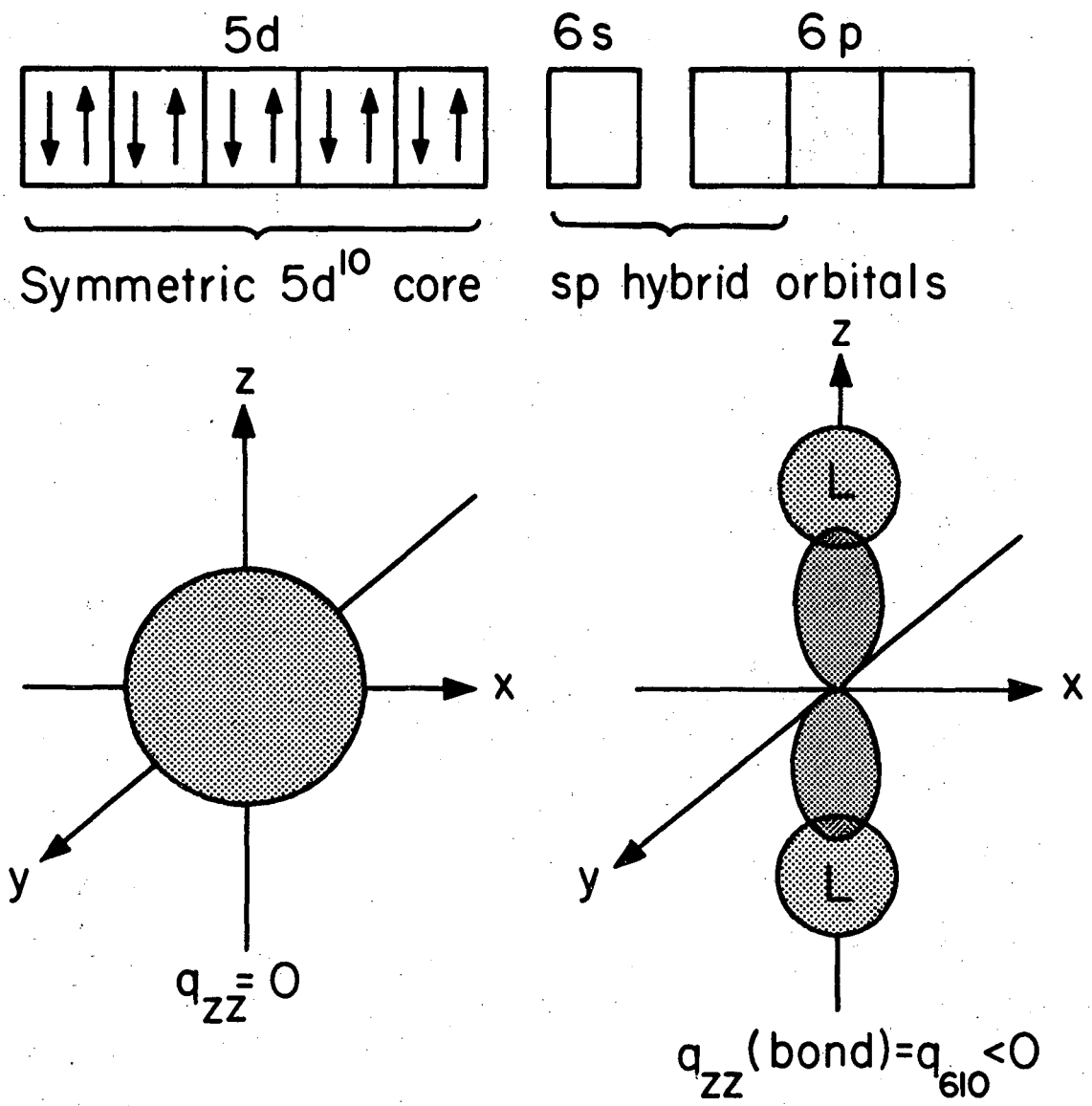

XBL682-1868

Fig. V-35. The electric field gradients of the $5d^{10}$ core and the $6s6p_z$ hybrid orbitals of gold(I).

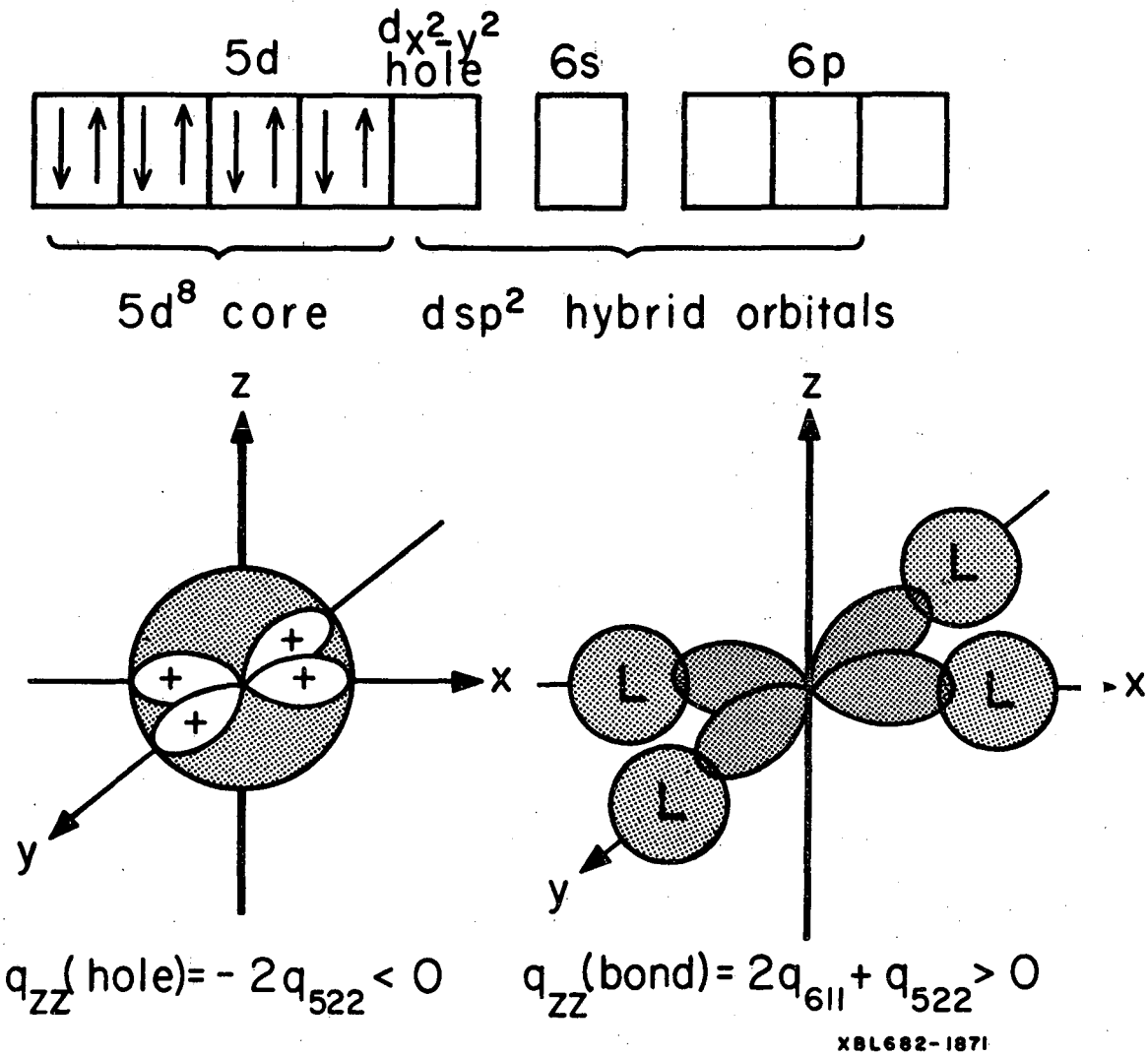

Fig. V-36. The electric field gradients of the $5d^8$ core and the $5d6s6p^2$ hybrid orbitals of gold(III).

b. Comparison of the quadrupole splitting of gold(I) and gold(III) compounds. In the introduction, we explained that the large differences in the QS results of related gold(I) and gold(III) compounds, such as AuCl and $AuCl_3$, aroused our interest in the bonding characteristics of gold compounds. Although our results have raised additional questions, we did arrive at a satisfactory qualitative explanation for the above observation. Earlier workers[4,69,70] on nuclear quadrupole effects considered mainly the p electron contribution to the EFG and essentially neglected the d electrons as a source of EFG. However, from our calculations of the 5d and 6p electron EFG values of various gold ionic and excited states, we find that the EFG of the 5d and 6p electrons are comparable. Therefore, the probable reason for the observed smaller QS values of the gold(III) compounds compared to the corresponding gold(I) compounds is that the $5d_{x^2-y^2}$ hole would decrease the effect of the EFG of the bonding electrons in gold(III) compounds and therefore decrease the QS results.

3. Relationship of the Isomer Shifts and Quadrupole Splittings

a. Gold(I). From the IS and QS results for gold(I) compounds which are given in Figs. V-33 and V-34 respectively, the linear relationship between the IS and QS results is apparent. We have assumed that the electric field gradient, EFG, of the nucleus has the same sign as that of the valence electrons. The alternative assumption would not affect the results of the following discussion. Gold(I) utilizes the two 6s6p hybrid orbitals for bonding. The closed shells of electrons form a symmetric sphere. The bonding electrons, which have a prolate

configuration around gold, have a negative EFG. The electronic distribution around the gold atom is depicted in Fig. V-35. Gold is located at the origin of the coordinates and the ligands, L, are located along the z axis.

We have plotted the IS against a quantity which is proportional to the quadrupole coupling constant, $\frac{1}{2} eq_{zz}Q(1 + \eta^2/3)^{1/2}$, in Fig. V-37. The QS is equal to the magnitude of this quantity. The best straight line through all the data points, determined by the least-squares method, is

$$IS(Au(I)) = 0.7815\ (eqQ/2) - 0.4744\ \text{cm/sec} \qquad (6)$$

The IS and (eqQ/2) are in units of cm/sec.

b. Gold(III). For Gold(III) compounds, a linear relationship between the shift and the quadrupole coupling constant would also exist if there were a difference in the sign of the EFG between the gold fluorides and the remaining gold compounds. This is not unreasonable since a sign difference does exist between the $5d^8(5d6s6p_x6p_y)^0$ and the $5d^8(5d6s6p_x6p_y)^2$ electronic configurations. The first electronic configuration represents the ionic extreme where gold has the $5d^8(+3)$ configuration, having none of the bonding electrons. In the second electronic configuration, gold has all of the eight bonding electrons. The first case would have a prolate charge distribution and thus a negative EFG: the second has an

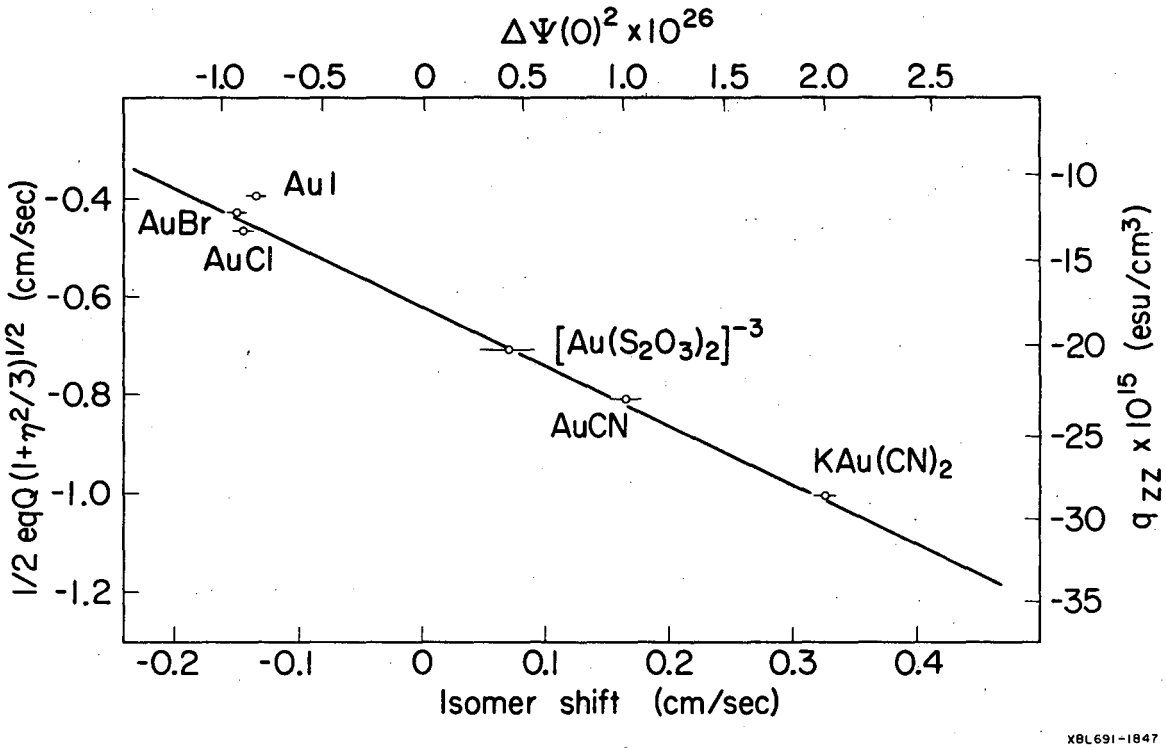

Fig. V-37. Linear relationship of isomer shift and 1/2(eqQ) for Gold(I) compounds.

oblate distribution and a positive EFG. The assumption is that in the gold fluoride compounds, the highly electronegative fluorine atom retains a major share of the bonding electrons and that the resulting EFG on gold is negative. As the gold atom receives a greater and greater protion of the bonding electrons, the sign of the outer-electron EFG changes from negative to positive. The electronic configuration of the outer electrons in gold(III) compounds is given in Fig. V-36. The gold atom is located at the origin of the coordinates and the ligands, L, along the x and y axes.

The linear relationship between the IS and the quadrupole coupling constant is shown in Fig. V-38. Here, as for gold(I) compounds, we have assumed that the nuclear EFG has the same sign as that of the outer electrons. The equation of the best straight line through the axially symmetric gold compounds, determined by the least-squares method, is

$$IS(Au(III)) = 0.5422\ (eqQ/2) + 0.0162\ \text{cm/sec} \qquad (7)$$

The data used in determining this equation were taken from the following compounds

Compound	1/2(eqQ) cm/sec	IS cm/sec
$[AuF_4]^-$	(-) 0.182	-0.069
$[AuCl_4]^-$	0.127	0.044
$[AuBr_4]^-$	0.113	0.067
$[Au(CN)_4]^-$	0.699	0.421

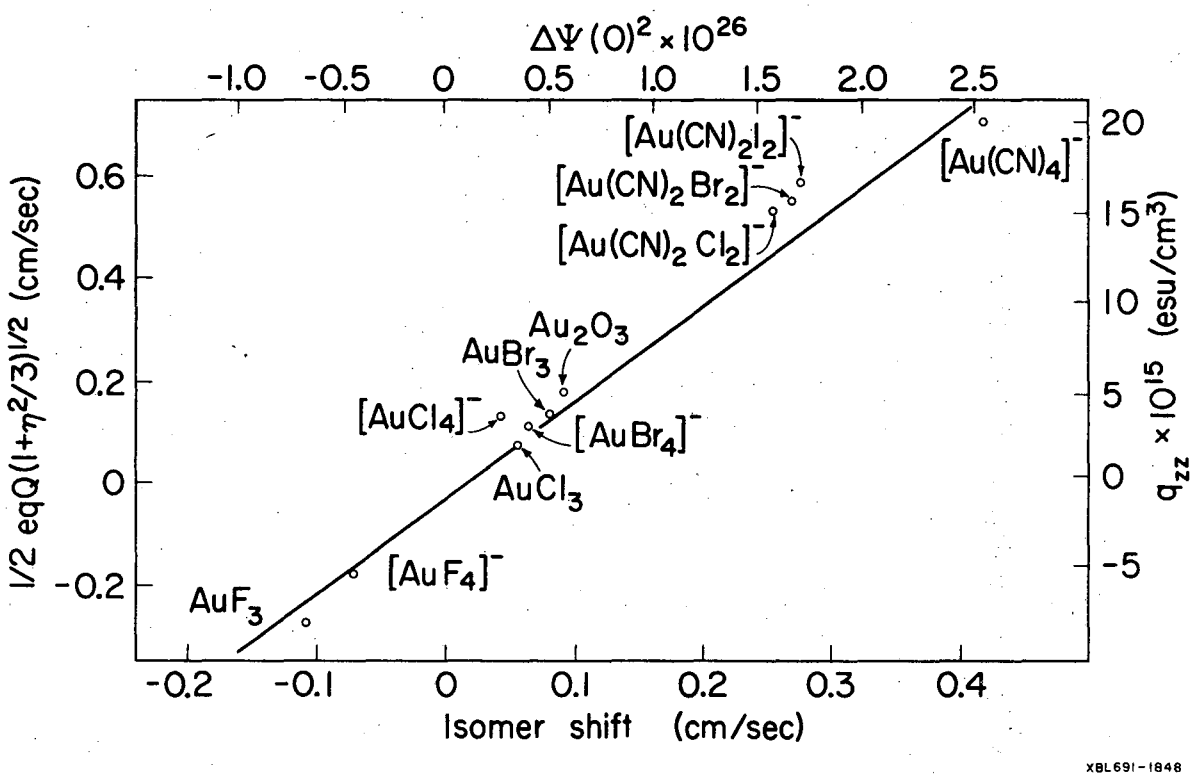

Fig. V-38. Linear relationship of isomer shift and quadrupole splitting of gold(III) compounds.

If we include the following nearly axially symmetric compounds

Compound	1/2 (Eq. Q)	IS
AuF_3	(-) 0.274	- 0.107
$AuCl_3$	0.075	0.057

the best straight line is

$$IS(Au(III))' = 0.5704\ (eqQ/2) + 0.0078\ cm/sec \qquad (8)$$

The assumed signs for the 1/2(eqQ) values are indicated parenthetically.

The linear relationship between the isomer shift and quadrupole coupling constant shows that the gain in nuclear electron density (mainly from the 6s electrons) is approximately proportional to the gain in the 5d and 6p electron unbalance. This suggests that the hybridization of the sp and dsp^2 orbitals remains constant and that the change in the IS and QS from one gold compound to another is caused by the change in the number of bonding electrons at the gold atom. The proportion of the bonding electrons which reside at the gold atom is governed by the electronegativity of the ligands.

From the graph in Fig. V-38, we can now estimate the asymmetry parameter, η, for the gold(III) cyano-halides. Since the QS values for gold(I) halides and gold(I) cyanides lie at opposite extremes of the scale in Fig. V-34 , large values of η^2 are expected for the gold(III) cyano-halides. We determined η^2 to be 1.1, 1.0, and 1.2 for $KAu(CN)_2Cl_2$, $KAu(CN)_2Br_2$, and $KAu(CN)_2I_2$ respectively. However, η^2 should be between zero and one. The fact that these values were determined to be about 10% high may indicate that the line which was determined from the QS

and IS relationship should be steeper or the intercept should be a little larger. The q_{zz} values of these compounds were computed from Eq. (18) of Sec. II and are listed in Table III.

C. Calculation of Nuclear Electron Density

The $\psi(0)^2$ calculations were made with parameters generated by Mann[71] in Dirac-Fock atomic structure calculations for excited states of gold. The major component of the radial wave function, P, is given by

$$P = PA \cdot r^{l+1} \left[1 - \alpha r^2 + \beta r^4 + \ldots \right] \tag{9}$$

The minor component, Q, is

$$Q = PA \cdot r^{l} \left[q_o + q_1 r^2 + q_2 r^4 + \ldots \right] \tag{10}$$

where q_o is zero for $s_{1/2}$, $p_{3/2}$, and $d_{5/2}$ electrons. PA, q_o, q_1, q_2, α, and β are available in Mann's program.

The normalization condition is:

$$\int_0^\infty (P_i P_j + Q_i Q_j)^2 \, dr = \delta_{ij} \tag{11}$$

Near the origin, the charge density for a $s_{1/2}$ or $p_{1/2}$ electron is:

$$\frac{\omega_i}{4\pi r^2} (P_i^{\,2} + Q_i^{\,2}) \tag{12}$$

Table III. Determination of η^2 for the potassium dicyanodihaloaurates.

Compound	IS (cm/sec)	QS(calc) n=0 (cm/sec)	q_{zz}(calc) 10^{15}esu/cm^3	QS observed cm/sec	η^2 calculated
$KAu(CN)_2Cl_2$	0.256	0.4423	12.69	0.526	1.114
$KAu(CN)_2Br_2$	0.272	0.4718	13.53	0.546	1.007
$KAu(CN)_2I_2$	0.278	0.4828	13.85	0.587	1.196

Both IS and QS values are the observed values. QS(calc) are the values which were determined from Eq. (7) and q_{zz}(calc) was computed from Eq. (3). η^2, the asymmetry parameter, was determined from Eq. (2).

where ω_i is the occupation number of the shell.

For the $s_{1/2}$ shell,

$$\left|\psi(r)^2_s\right| = \frac{\omega_i (PA)^2}{4\pi} \left[1 - (2\alpha - q_1)r^2 + (2\beta + \alpha^2 + 2q_1q_2)r^4 + \ldots \right] \tag{13}$$

and for the $p_{1/2}$ shell,

$$\left|\psi(r)^2_{p_{1/2}}\right| = \frac{\omega_i (q_o \cdot PA)^2}{4\pi} \left[1 + (2q_1/q_2 + 1/q_o^2)r^2 + [2q_2/q_o + (q_1/q_o)^2 - 2\alpha/q_o^2]r^4 + \ldots\ldots \right] \tag{14}$$

The units are in a_o^{-3}. The electron density at the nucleus is,

$$|\psi(0)^2| = \int_0^R \psi^2(r) r^2 \, dr / \int_0^R r^2 \, dr \tag{15}$$

where $R(= 2.0219 \times 10^{-5} A^{1/3})$ is the nuclear radius.[71] This yields the following explicit expressions

$$\left|\psi(0)^2_{s_{1/2}}\right| = \frac{\omega_i (PA)^2}{4\pi (R^3/3)} \left[\frac{R^3}{3} - \frac{R^5}{5}(2\alpha^2 - q_i) + \frac{R^7}{7}(2\beta + \alpha^2 + 2q_1q_2) + \frac{R^9}{9}(2q_2 - 2\alpha\beta) + \ldots \right] \tag{16}$$

$$\left|\psi(0)^2_{p_{1/2}}\right| = \frac{\omega_i (q_o PA)^2}{4\pi(R^3/3)} \left[\frac{R^3}{3} + \frac{R^5}{5}\left(\frac{1}{q_o^2} + \frac{2q_1}{q_o} \right) + \frac{R^7}{7}\left(\frac{2q_2}{q_o} + \left(\frac{q_1}{q_o} \right)^2 - \frac{2\alpha}{q_o^2} \right) + \ldots \right] \quad . \tag{17}$$

Multiplying the above expressions by 0.067486×10^{26} converts the units from a_o^{-3} to cm^{-3}.

The values of $\psi(0)^2_{ns}$ for the individual shells (n = 1, 2, 3, 4, 5, 6) are given in Table IV for comparison between the different ionic states. The total nuclear electron density, $\Sigma\psi(0)^2_s$, is also indicated. A few values of $\psi(0)^2_{np_{1/2}}$ are given in Table V. We find that $\Sigma\psi(0)^2_{p_{1/2}}$ is approximately 5% of the s electron nuclear density, $\Sigma\psi(0)^2_s$.

D. Calculation of the Electric Field Gradient

The electric field gradient, q, of an electron is given by the following expression*

$$q_{nll} = e \frac{(2l)}{(2l + 3)} \langle 1/r^3 \rangle_{nl} \tag{18}$$

where e is the electron charge, equal to 4.803 10^{-10} esu, and l is the azimutal quantum number. The determination of q_{nll} of a particular electron requires its $\langle 1/r^3 \rangle$ value, which can be calculated from the

*See Eq. (10), Appendix C for consideration of spin and relativistic correction.

Table IV. Nuclear electron densities for ns electrons, $\psi(0)^2_{ns}$, for gold.

State	$\psi(0)^2_{1s^2}$ $\times 10^{31}$	$\psi(0)^2_{2s^2}$ $\times 10^{30}$	$\psi(0)^2_{3s^2}$ $\times 10^{29}$	$\psi(0)^2_{4s^2}$ $\times 10^{28}$	$\psi(0)^2_{5s^2}$ $\times 10^{28}$	$\psi(0)^2_{6s^n}$ $\times 10^{26}$	$\sum_{n=1}^{5,6} \psi(0)^2_{ns}$ $\times 10^{31}$
$5d^{10}6s$	1.0811351	1.6181933	3.7074950	9.2513488	1.7240657	6.4876425 n=1	1.291068257
$5d^{9}6s$	1.08113463	1.6181935	3.707404	9.2519601	1.7327180	8.9125445 n=1	1.29110182
$5d^{8}6s$	1.0811339	1.61819598	3.707491	9.2527926	1.7448536	11.1568264 n=1	1.29113758
$5d^{9}6s^2$	1.08113399	1.61819893	3.7074957	9.25316815	1.7387135	14.6529252 n=2	1.29116725
$5d^{9}6p$	1.08113444	1.61818562	3.70729750	9.25044562	1.728676	----	1.29100509
$5d^{10}$	1.08113533	1.61821324	3.70725501	9.25010076	1.71813546	----	1.29099743
Mercury $5d^{10}6s^2$	1.13463355	1.71599995	3.9414777	9.8927001	1.8956166	16.0490299 n=2	1.35759712

Table V. Nuclear electron densities for $np_{1/2}$ electrons, $\psi(0)^2_{np_{1/2}}$, for gold.

State	$\psi(0)^2_{2p^6}$ $\times 10^{29}$	$\psi(0)^2_{3p^6}$ $\times 10^{28}$	$\psi(0)^2_{4p^6}$ $\times 10^{27}$	$\psi(0)^2_{5p^6}$ $\times 10^{27}$	$\psi(0)^2_{6p^1}$ $\times 10^{25}$	$\sum_{n=2}^{5,6} \psi(0)^2_{np}$ $\times 10^{31}$
$5d^{10}6s$	3.6570099	9.3985819	23.1275442	3.79192177	----	0.0486606
$5d^{10}6p_{1/2}$	1.23705252	3.17923915	7.82373819	1.28323049_9	1.63742407	0.04938630
$5d^{10}$	1.23705170	3.17921018	7.82340609	1.28086806	----	0.04938046
$5d^9 6p_{1/2}$	3.6569434	9.3986248	23.13267997	3.8222755	3.92364908	0.04866752

appropriate electronic wavefunction. This task has proven to be our greatest problem. In this section we discuss how we arrived at the q_{nll} values which we finally selected.

Relativistic $\langle 1/r^3 \rangle$ values for free ions were obtained from Mann,[71] where

$$\langle 1/r^3 \rangle_i = \int_0^\infty 1/r^3 (P_l^2 + Q_l^2)\, dr \tag{19}$$

P and Q are the major and minor components respectively of the relativistic wavefunctions and are given in Sec. V-C.

1. Electric Field Gradient for 5d Electrons

For the 5d electrons, we calculated the average $\langle 1/r^3 \rangle_{5d}$ values of several ionic states from the occupation numbers of the $5d_{3/2}$ and $5d_{5/2}$ states and the $\langle 1/r^3 \rangle_{5d_{3/2}}$ and $\langle 1/r^3 \rangle_{5d_{5/2}}$ values supplied by Mann.[71] These values are listed in Table VI and are plotted in Fig. V-39. Unfortunately, we are interested in bonding configurations that are not found in the free ions, thus precluding direct calculation. By connecting the points (solid lines) of the states of equal numbers of 5d electrons and varying numbers of 6s and 6p electrons, we find that the lines formed have nearly the same curvatures. Therefore, we have estimated the $\langle 1/r^3 \rangle_{5d}$ dependence on charge for the $5d^9 6s 6p^2$ state by drawing a dashed line with a curvature similar to the other existing curves but occurring midway between the points for the $5d^9 6p$ and $5d^9 6s$ states. This results in the following expression for $\langle 1/r^3 \rangle_{5d}$ as a function of charge

Table VI. Determination of $\langle 1/r^3 \rangle_{5d}$ values from $\langle 1/r^3 \rangle_{5d_{3/2}}$ and $\langle 1/r^3 \rangle_{5d_{5/2}}$ values. (Mann[71])

State	J	electron occupation number	$\langle 1/r^3 \rangle_J$	$\langle 1/r^3 \rangle_{5d}$
$5d^{10}6s$	$^5D_{5/2}$	6	15.6964	14.1861
	$^5D_{3/2}$	4	11.9206	
$5d^{10}6p$	$^5D_{5/2}$	6	12.2721	13.6826
	$^5D_{3/2}$	4	15.7984	
$5d^9 6s^2$	$^5D_{5/2}$	5	12.7303	14.4079
	$^5D_{3/2}$	4	16.5048	
$5d^{10}$	$^5D_{5/2}$	6	15.9915	14.4938
	$^5D_{3/2}$	4	12.2474	
$5d^9$	$^5D_{5/2}$	5	13.4185	15.0836
	$^5D_{3/2}$	4	17.1650	
$5d^8$	$^5D_{5/2}$	4	14.5384	16.4632
	$^5D_{3/2}$	4	18.3880	
$5d^9 6s$	$^5D_{5/2}$	5	13.0329	14.7014
	$^5D_{3/2}$	4	16.7870	
$5d^8 6s$	$^5D_{5/2}$	4	14.1190	16.0361
	$^5D_{3/2}$	4	17.9532	
$5d^9 6p$	$^5D_{5/2}$	5	13.279	14.8603
	$^5D_{3/2}$	4	16.837	
$5d^8 6s6p$	$^5D_{5/2}$	4	13.9782	15.7983
	$^5D_{3/2}$	4	17.6186	

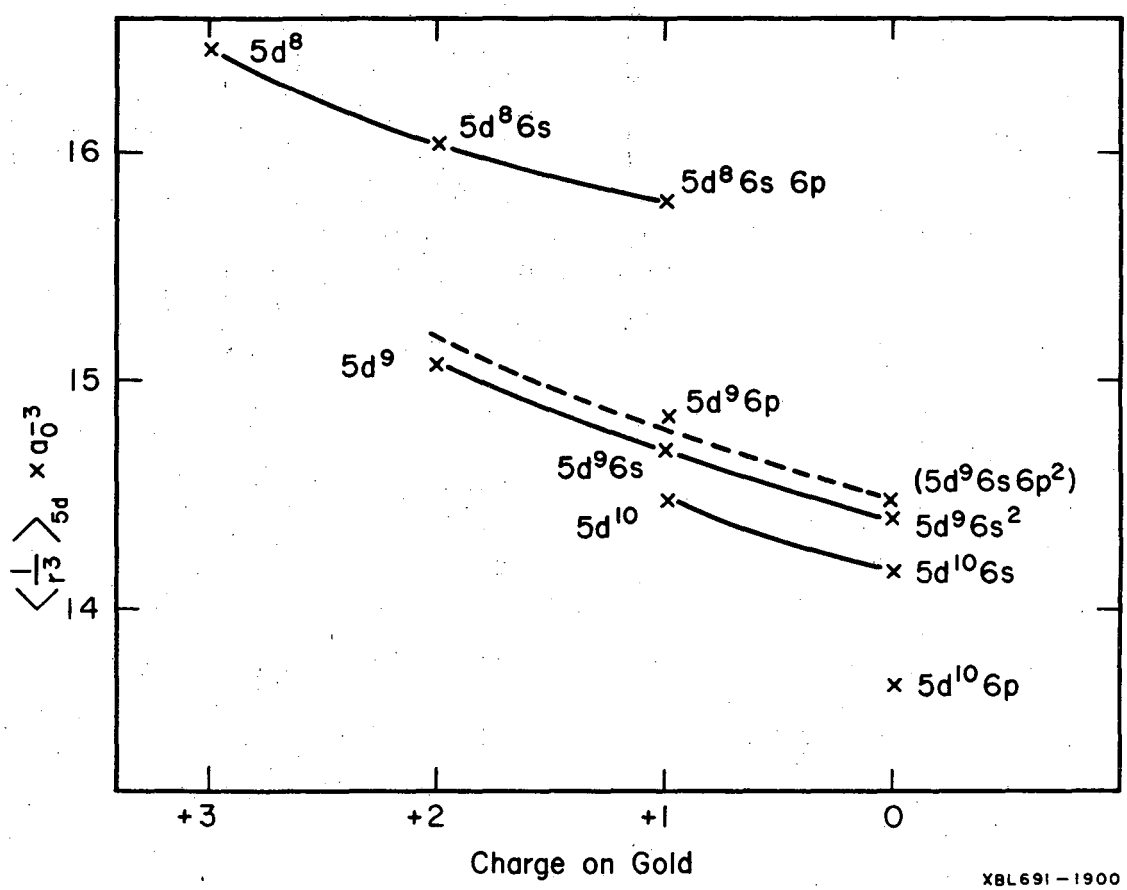

Fig. V-39. The Dirac-Fock $\langle 1/r^3 \rangle_{5d}$ results of free-atom states of gold.

$$\langle 1/r^3 \rangle_{5d} = 0.0443\ X^2 + 0.249\ X + 14.49 \tag{20}$$

where X is the charge on the gold atom and the expression is in units of a_o^{-3}. The $\langle 1/r^3 \rangle_{5d}$ of the above equation is not a very sensitive function of charge for small X. This is as one might have expected, since the ionic charges on gold arises from differing numbers of 5d, 6s, and 6p electrons. The mutual shielding of the 5d electrons is probably not very effective and the shielding of the 5d electrons by the 6s and 6p electrons would be even less so. The value of $\langle 1/r^3 \rangle_{5d}$ obtained in this way for neutral gold (X = 0), is reasonable when compared with the values of 12.3 a_o^{-3} and 11.8 a_o^{-3} which were obtained from magnetic hyperfine structure and atomic fine structure determination, respectively.[72]

For the calculations made in Sec. E of this chapter, we used $\langle 1/r^3 \rangle_{5d}$ value for neutral gold of 14.49 a_o^{-3}. Due to the approximate nature of the calculations in Sec. E, this simplification is probably justified. Using Eq. (18) of this section, we get the following EFG

$$q_{522} = 26.86 \times 10^{15}\ \text{esu/cm}^3 \tag{21}$$

2. <u>Electric Field Gradient for 6p Electrons</u>.

The determination of $\langle 1/r^3 \rangle_{6p}$ for gold was considerably more difficult and the results are less certain. The difficulty arises partly because the 6p electron of gold is loosely bound and close in energy to the continuum. Therefore, the directly calculated $\langle 1/r^3 \rangle_{6p}$ values for

free-atom gold has been substantially smaller than we had expected and are surely not a good estimation for molecular configurations. From the value of $\langle 1/r^3 \rangle_{6p}$ of $8.8_7\ a_o^{-3}$ for Hg 201,[73] we would expect a comparable value for $\langle 1/r^3 \rangle_{6p}$ for gold.*

We considered several sources of $\langle 1/r^3 \rangle_{6p}$ calculations and attempted to extrapolate a value which would be appropriate for gold. The sources of $\langle 1/r^3 \rangle_{6p}$ calculations are discussed and evaluated in Appendix B. These calculations are described below and the results are tabulated in Table VII. The results of cases B through E include a relativistic correction factor, R_r,[74] which was applied to the Hartree-Fock non-relativistic results.

Case A. Mann[71] made Dirac-Fock calculations of $\langle 1/r^3 \rangle_{6p_{3/2}}$ for the following excited ionic states of gold: $5d^5 6p(+3)$, $5d^8 6p(+2)$, and $5d^9 6p(+1)$. This is probably the best set of calculations among the five cases that we considered (cases A through E). The $\langle 1/r^3 \rangle$ values are given in Table VII. The equation of the best straight line, determined by the least-squares method is

$$\langle 1/r^3 \rangle_{6p} = (5.775\ X + 3.9833)\ a_o^{-3} \tag{22}$$

Here X is the ionic charge on gold. Using Eq. (16) and doubling the value to obtain the EFG along the z axis, we have

---

* This value corresponds to 23×10^{15} esu/cm^3 for the electric field gradient.

Table VII. $\langle 1/r^3 \rangle_{6p}$ values of gold and related elements (in units of a_o^{-3}).

Au excited states	Case A: Dirac-Fock (Mann)[71]
$5d^7 6p$ (+3)	21.30
$5d^8 6p$ (+2)	15.55
$5d^9 6p$ (+1)	9.72

Element	R_r[74]	Case B ground states Hartree-Fock (Mann)[75]	Case C ground states Slater-Hartree-Fock (Herman&Skillman)[76]	Case D $5d^{10}6p$ isoelectronic states Hartree-Fock (minimal basis set)	Case E $5d^{10}6s^2 6p$ isoelectronic states Hartree-Fock (minimal basis set)
Au	1.3172				
Hg	1.3268			7.52	
Tl	1.3369	10.09	15.963	13.89	8.48
Pb	1.3470	14.80	21.565	18.47	13.75
Bi	1.3574	19.63	26.55	24.84	20.10
Po	1.3681	25.09		33.42	25.73

$$q_{610} = (14.874\ X + 10.258) \times 10^{15}\ \text{esu/cm}^3 \tag{23}$$

Case B. Case B consists of $\langle 1/r^3 \rangle_{6p}$ values obtained from the Hartree-Fock atomic structure calculations for the ground states of Tl, Pb, Bi, and Po, which were published by Mann.[75] The equation of the best straight line, as determined by the least-squares method, is

$$\langle 1/r^3 \rangle_{6p} = (4.981\ X_Z - 0.031)\ \ a_o^{-3} \tag{24}$$

where X_Z is the increase in nuclear charge over that of gold (Z = 79). The corresponding electric field gradient expression is

$$q_{610} = (12.83\ X_Z - 0.081) \times 10^{15}\ \text{esu/cm}^3 \tag{25}$$

Case C. From the Slater-Hartree-Fock atomic structure calculations of Herman and Skillman,[76] we computed the $\langle 1/r^3 \rangle_{6p}$ values for the ground states of Tl, Bi, and Po. The result gave

$$\langle 1/r^3 \rangle_{6p} = (5.293\ X_Z + 5.480)\ \ a_o^{-3} \tag{26}$$

where X_Z is the increase in nuclear charge over that of gold (Z = 79). The corresponding electric field gradient is

$$q_{610} = (13.632\ X_Z + 14.114) \times 10^{15}\ \text{esu/cm}^3 \tag{27}$$

Case D. Using a minimal basis set, we made atomic structure calculations on a program written and developed by Roothaan,[77,78] for the $5d^{10}6p$ isoelectronic states of the following atoms: Au, Hg, Tl, Pb, Bi, and Po. The resulting $\langle 1/r^3 \rangle_{6p}$ function is

$$\langle 1/r^3 \rangle_{6p} = (6.275\ X + 0.804)\ a_o^{-3} \tag{28}$$

which corresponds to

$$q_{610} = (16.160\ X + 2.071) \times 10^{15}\ \text{esu/cm}^3 \tag{29}$$

There, X corresponds to the ionic charge on the atoms.

Case E. A set of calculations similar to case D above was made for the $5d^{10}6s^2 6p$ isoelectronic states of Au, Hg, Tl, Pb, Bi, and Po. The equation of the best straight line determined by the results is

$$\langle 1/r^3 \rangle_{6p} = (5.810\ X - 3.322)\ a_o^{-3} \tag{30}$$

where we have that

$$q_{610} = (14.964\ X - 8.555) \times 10^{15}\ \text{esu/cm}^3 \tag{31}$$

Compared to the $\langle 1/r^3 \rangle_{5d}$ functions, the $\langle 1/r^3 \rangle_{6p}$ functions are much more sensitive to the ionic or nuclear charge. The shielding coefficient of the outer 6p electrons should reflect the number of inner

5d and 6s electrons. However, it is not evident that the $\langle 1/r^3 \rangle_{6p}$ values should vary so greatly with the charge.

If we wish to estimate the valence-electron occupation number on the gold atom in the various gold compounds, we are faced with the selection of some value for $\langle 1/r^3 \rangle_{6p}$ for gold which is reasonable. We feel that the $\langle 1/r^3 \rangle_{6p}$ values which were extrapolated to gold in cases A through E are too small. These calculations were made for gold free-atom states. The maximum radii (as determined by Mann[71]) of some of these states are

$$5d^9 6p_{3/2}\ (+1): \qquad r_{6p} = 3.195\ a_o = 1.69\ \text{Å}$$
$$5d^8 6p_{3/2}\ (+2): \qquad r_{6p} = 2.825\ a_o = 1.49\ \text{Å}$$
$$5d^7 6p_{3/2}\ (+3): \qquad r_{6p} = 2.603\ a_o = 1.37_5\ \text{Å}$$

Molecularly bonded gold, on the other hand, would have somewhat more confined wave functions due to the electrons on the ligands. Some of the measured interatomic distances in gold compounds are given in Table VIII. In the third column of Table VIII are listed the covalent radii of the ligands. This radius should represent a lower limit in the ligand radius. If we take the sum of the gold 6p maximum radius ($r = 1.69$ Å) for the $5d^9 6p$ (+1) excited state and the covalent radius of the ligand, it should give the approximate interatomic distance required for no interaction to exist between the gold 6p electron and those electrons of the ligand. For interatomic distances shorter than this, the electron should experience some confinement of its wavefunctions. In the fifth

Table VIII. Comparison of interatomic distances with those determined from covalent radii and the maximum extension of the 6p electron of the $5d^9 6p(+1)$ excited state of the gold ion.

Compound	Interatomic distance, Å	Ligand covalent radius	Ligand ionic radius	Ligand covalent radius plus 1.69Å
AuF_3	2.00	0.72	(F^-) 1.36	2.41
$[AuCl_4]^{-1}$	2.29	0.99	(Cl^-)1.81	2.68
$[AuBr_4]^{-1}$	2.56	1.14	(Br^-)1.95	2.83
$[AuCl_2]^{-1}$	2.30	0.99	(Cl^-)1.81	2.68
$[Au(S_2O_3)_2]^{-3}$	2.28	1.02	(S_2^-)1.84	2.71
$[Au(CN)_2]^{-1}$	2.12	0.77	(C^{-4})2.60	2.46
AuI	2.62	1.33	(I^-) 2.16	3.02

column of Table VIII, these values are, without exception, larger than the measured interatomic distance (column two). Therefore, the 6p wave-functions for molecular gold should have less radial extension than the 6p free-atom wave functions. This would result in a larger $\langle 1/r^3 \rangle_{6p}$ value for molecular gold. The ionic radii of the ligands are given in the fourth column to indicate the upper limit of the calculated inter-atomic distance, below which gold-ligand electron interaction will occur.

The electric field gradient of gold should probably be close to that of mercury[73] which has a q_{610} value of about 23×10^{15} esu/cm^3. This corresponds to a $\langle 1/r^3 \rangle_{6p}$ value of 8.87 a_o^{-3}. We estimate $\langle 1/r^3 \rangle_{6p}$ for gold as that calculated for the 6p electron in the $5d^9 6p$ gold ion. Due to the approximate nature of this aspect of the calculation, we shall not consider $\langle 1/r^3 \rangle_{6p}$ as a function of charge but as

$$\langle 1/r^3 \rangle_{6p} = 9.71 \ a_o^{-3} \tag{32}$$

which gives an electric field gradient value of

$$q_{610} = 25.01 \times 10^{15} \text{ esu/cm}^3 \tag{33}$$

In the next section, we have made a second estimation of q_{610} by an indirect method involving the expressions for the nuclear factor, $\delta R/R$ (in the isomer shift equation), and Eqs. (V-52) and (V-53).

E. Discussion

In Sec. III-B, we discussed the hybrid orbitals of gold as well as the molecular orbitals of gold with a ligand, L. The molecular orbitals were approximated as

$$\psi_{AuL} = \alpha\psi_{Au} \pm \beta\psi_L \tag{34}$$

where α and β are positive real numbers. This approximation is reasonably good in the region close to the nucleus. Fortunately, we are interested in the electric field gradients at the nucleus where Eq. (31) probably best describes the true molecular orbitals. The normalization condition would require that

$$\int_0^\infty \psi_{AuL}{}^2 d\tau = \alpha^2 + \beta^2 + 2\alpha\beta \int \psi_{Au}\, \psi_L \; d\tau \tag{35}$$

We know from studies on (diatomic) molecules that the overlap term can be non-negligible.[79] However, in keeping with the already approximate nature of the present treatment, we will neglect the overlap term in the normalization and make the further simplification that

$$\alpha^2 + \beta^2 = 1 \tag{36}$$

The EFG at gold due to a bond with a ligand, L, is

$$q_{zz}(\mathrm{Au,bond}) = e \int \psi_{AuL} \left(\frac{3\cos^2\theta - 1}{r^3} \right) \psi^*_{AuL} \, d\tau \tag{37}$$

where ψ_{AuL} is given by Eqs. III-(4), (5), and (7). Due to the $1/r^3$ factor, where r is the distance from the gold nucleus, the only significant term in the expansion of the above expression is

$$q_{zz}(\mathrm{Au,bond}) = e\alpha^2 \int \psi_{Au} \left(\frac{3\cos^2\theta - 1}{r^3} \right) \psi^*_{Au} \, d\tau \tag{38}$$

The gold wavefunctions, ψ_{Au}, have been given in Chapter III for the two linear gold(I) hybrid orbitals as

$$\psi_{Au(I)} = 1\sqrt{2}\ (6s \pm 6p_z) \tag{39}$$

and the four square-planar gold(III) hybrid orbitals as

$$\psi Au(III) = \begin{matrix} 1/2 6s \pm 1\sqrt{2}\ 6p_x - 1/2\ 5d_{x^2-y^2} \\ 1/2 6s \pm 1\sqrt{2}\ 6p_y + 1/2\ 5d_{x^2-y^2} \end{matrix} \tag{40}$$

The upper signs designate one hybrid orbital and the lower signs designate the other.

Combining Eqs. (35) and (36), we have the EFG for gold(I) compounds

$$q_{zz}(\mathrm{Au(I),bond}) = \alpha^2/2\ [q_{6s} + q_{6p_z} + q_{6s,6p_z}] \tag{41}$$

From the symmetry rules which are outlines in Appendix C, only the second term in square brackets is non-zero. After transforming to spherical harmonics,* we have that

$$q_{zz}(\mathrm{Au(I)},\mathrm{bond}) = \alpha^2/2\ [q_{610}] \tag{42}$$

In a gold(I) molecule or complex, there are two hybrid orbitals which can accomodate two spin-paired electrons each, resulting in a total of four bonding electrons.** Therefore, the EFG in a gold(I) molecule is given by

$$q_{zz}(\mathrm{Au(I)},\mathrm{molecule}) = 4(\alpha^2/2)\ q_{610} = 2\alpha^2\ q_{610} \tag{43}$$

where α was defined in Eq. (34).

Due to possibly large Sternheimer antishielding factors, the lattice contribution to the EFG cannot be categorically disregarded. For gold(I) compounds, the observable EFG, $q_{zz}(\mathrm{Au(I)})$, which includes the Sternheimer[80,81] antishielding factors and the lattice contributions, is

$$q_{zz}(\mathrm{Au(I)}) = (1 - \gamma_\infty)q^{\mathrm{latt}} + 2\alpha^2(1 - R_{6p})q_{610} \tag{44}$$

---

* See Appendix C.

** The bonding electron count is made in Sec. III-B.

Here, q^{latt} is the lattice EFG, γ_∞ the lattice Sternheimer antishielding factor, and R_{6p} the Sternheimer antishielding factor for the gold 6p electrons. From the γ_∞ value calculated for Bi(+3),[82] γ_∞ for Au(+1) can be approximated as -40. In Appendix D we have estimated the average q^{latt} for gold(I) compounds as between zero and -0.06×10^{15} esu/cm^3. Since this would result in an average lattice contribution of less than -2.5×10^{15} esu/cm^3 as compared to the q_{610} value of about -25×10^{15} esu/cm^3,* the lattice correction has not been applied to the q_{zz} calculations of this section. We will also have to disregard the R_{6p} correction since that value has not been calculated for gold(I). We thus have

$$q_{zz}(\mathrm{Au(I)}) = 2\alpha^2\, q_{610} \tag{45}$$

The EFG for gold(III) compounds is

$$q_{zz}(\mathrm{Au(III),bond}) = [\tfrac{1}{4}q_{600} + \tfrac{1}{4}q_{522} + \tfrac{1}{2}q_{611} + \tfrac{1}{2}q_{600,522} + \tfrac{1}{\sqrt{2}}q_{610,611} + \tfrac{1}{\sqrt{2}}q_{522,611} \tag{46}$$

From the symmetry rules given in Appendix C, we have that the second, third and fourth terms in the square brackets are non-zero. The fourth term is probably small. We will regard the orbital EFG to be

$$q_{zz}(\mathrm{Au(III),bond}) = \alpha^2(\tfrac{1}{4}\, q_{522} + \tfrac{1}{2}\, q_{611}) \tag{47}$$

---

* q_{610} is determined to be even larger (-44×10^{15} esu/cm^3) at the end of this section by a second method of computation.

As explained in Chapter III, there are a total of eight spin-paired bonding electrons. In addition to these eight bonding electrons, there are eight non-bonding 5d electrons with an EFG of $-2q_{522}$. The molecular EFG is therefore

$$q_{zz}(\mathrm{Au(III)},\mathrm{molecule}) = -2q_{522} + 2\alpha^2[q_{522} + 2q_{611}] \qquad (48)$$

Since no Sternheimer antishielding factors have been calculated for the gold(III) lattice, 6s or 6p EFG and as the average q^{latt} is small (0 to $\sim 0.03\times10^{15}$ esu/cm^3)* compared to the q_{522} and q_{611} values, we will approximate q_{zz}(Au(III)) by Eq. (48).

From the results in this chapter, one can solve for the nuclear factor $\delta R/R$, from the expression for the isomer shift (Eq. (II-2)). The equation for the isomer shift can be modified to give the difference in the IS values of two different absorbers (when using a chemically equivalent source):

$$\Delta IS = IS_{abs(I)} - IS_{abs(III)} = 5.39\cdot10^{-24}(\delta R/R)\left[\sum_{abs(I)} \psi(0)^2 - \sum_{abs(II)} \psi(0)^2\right] \qquad (49)$$

The nuclear electron densities can be approximated from the free-atom Dirac-Fock wavefunctions. We will take the first absorber, abs(I), to be the completely ionic gold ion ($\alpha^2 = 0$) and the second absorber, abs(II),

---

* Appendix D.

to be a 100% covalent gold compound ($\alpha^2 = 1/2$). The two states of interest for gold(I) compounds are

$$5d^{10}(+1) \quad \text{and} \quad 5d^{10}[6s6p](-1) \tag{50}$$

and the gold(III) compounds are

$$5d^8(+3) \quad \text{and} \quad 5d^8[5d6s6p^2]^1 = 5d^9 6s6p^2(-1) \tag{51}$$

The approximate nuclear electron densities are given in Table IX where the free-atom states from which the $\psi(0)^2$ values were taken are indicated. For gold(I) compounds of $\alpha^2 = 0$ and $\alpha^2 = 1/2, \Delta\psi(0)^2$ is -7.08×10^{26} and for gold(III) compounds for $\alpha^2 = 0$ and $\alpha^2 = 1/2, \Delta\psi(0)^2$ is -7.91×10^{26}.

No corrections have been applied for $\sum_{n=1}^{5} \psi(0)^2_{ns}$ due to shielding by the additional 6s electrons. We found this shielding effect, which was suggested by Crawford and Schawlow,[83] to be negligible. In Appendix E, we discuss this effect.

The values of IS($\alpha^2 = 0$) and IS($\alpha^2 = 1/2$) are obtained from the values of the molecular EFG, q_{zz}, which are computed from Eqs. V-(45) and V-(48) and are subsequently converted to quadrupole splitting values by Eq. V-(3) and to the IS values by Eqs. V-(6) and V-(7):

$$\Delta IS(\text{gold-I}) = -0.7815\ q_{610}/28.686\times10^{15} \tag{52}$$

Table IX. Determination of $\Delta\psi(0)^2$ for gold(I) and gold(III) states where $\alpha^2 = 0$ and 1/2.

α	State Required	State	$\Sigma\psi(0)^2 \times 10^{26}$
	gold(I)		
0	$5d^{10}$	$5d^{10}$	$\sum_{n=1}^{5} \psi(0)^2_{ns} = 129099.743$
1/2	$5d^{10}6s6p$	$5d^{10}6s$	$\sum_{n=1}^{6} \psi(0)^2_{ns} = 129106.825$
			$\Delta\psi(0)^2_{ns}$ Au(I) $= -7.08_2$
	Au(III)		
0	$5d^8$	$5d^8 6s$	$\sum_{n=1}^{5} \psi(0)^2_{ns} = 129102.601$
1/2	$5d^9 6s6p^2$	$5d^9 6s$	$\sum_{n=1}^{6} \psi(0)^2_{ns} = 129110.182^*$
		$5d^9 6p$	$\psi(0)^2_{6p^2} = 0.327^{**}$
			$\Delta\psi(0)^2$ Au(III) $= -7.908$

*,** The difference of shielding of $\sum_{n=1}^{5} \psi(0)^2_{ns}$ by the 6s and 6p electrons is only about 5 parts in 10^6. Therefore we approximated $\psi(0)^2_{total}$ of $\alpha = 1/2$ by summing the two $\psi(0)^2$ values.

and

$$\Delta IS(\text{gold-III}) = 0.5422\ (q_{610} - q_{522})/28.686 \times 10^{15} \qquad (53)$$

Assuming that Eqs. V-(42) and V-(45) are good approximations of the molecular EFG for the aurous and auric compounds respectively, one can solve for the nuclear factor, $\delta R/R$. The equations for the nuclear factor, from gold(I) and gold(III) compound results respectively, are:

$$\delta R/R(\text{gold-I}) = 5.06 \cdot 10^{6}\ q_{610}/\Delta\psi(0)^{2} \qquad (54)$$

$$\delta R/R(\text{gold-III}) = 3.51 \cdot 10^{6}\ (q_{610} - q_{522})/\Delta\psi^{2}(0) \qquad (55)$$

If the values of q_{522} and q_{610} are taken as 26.86×10^{15} esu/cm^3 and -25×10^{15} esu/cm^3 respectively [Eqs. V-(22) and V-(20)], and the $\Delta\psi(0)^2$ ($\alpha = 0$, $\alpha = 1/2$) is approximated by those values in Table IX, then $\delta R/R$ (gold-I) and $\delta R/R$(gold-III) are 1.78×10^{-4} and 2.30×10^{-4} respectively.

The nuclear factors should be the same from both the gold(I) and gold(III) data; therefore, an alternative method is suggested by first considering $\delta R/R$ to be constant and solving for q_{610} from Eqs. (54) and (55). This results in a q_{610} value of -44.04×10^{15} esu/cm^3 and a $\delta R/R$ value of 3.1×10^{-4}. The $\delta R/R$ value is very close to that estimated by Shirley[13] ($\delta R/R = 3\times10^{-4}$).

Because of the q_{610} value for Hg of 23×10^{15} esu/cm^3 which was determined by Dehmelt et al.,[73] we expected a similar value for gold.

However, if q_{610} is -25×10^{15} esu/cm^3, the charges on gold are somewhat more negative than one might expect. The values of q_{zz}, α^2 and X are given in Table X from Eqs. (45) and (48). The charge, X, for gold(I) and gold(III) compounds was determined from the following equations

$$X(\text{Au-I}) = 1 = 4\alpha^2 \tag{56}$$

$$X(\text{Au-III}) = 3 - 8\alpha^2 \tag{57}$$

where α^2 is computed from Eqs. (45) or (48). The charge on gold for q_{610} equals -25×10^{15} esu/cm^3, ranges from -0.5 in AuF_3 to -2.6 in $KAu(CN)_4$.

The much larger q_{610} value of -44×10^{15} esu/cm^3 which was determined in this section gives an internally more consistent set of results. Not only is $\delta R/R$ a constant, but the calculated charges on the gold atom are more neutral.

From electronegativity considerations, we expect the charge on gold to be positive for (at least) the gold chlorides, bromides and iodides. This means that according to our model, q_{610} should be larger in magnitude for gold(III) compounds. For gold(I) compounds, q_{610} of -44×10^{15} esu/cm^3 results in positive charges on gold in AuCl, AuBr, and AuI. For gold(III) however, a value of q_{610} equal about -50×10^{15} esu/cm^3 is required for the gold atom to be positively charged in the gold(III) halides. This is approximately a 12% difference between these values for $|q_{610}|$. Since q_{610} values for gold(I) and gold(III) need not be the same value and indeed are probably not identical, this difference may not be unreasonable. The values of α^2 and charges X for gold in the individual compounds are listed in Table X for q_{610} values of -25×10^{15}, -35×10^{15}, -40×10^{15}, -44×10^{15} and -50×10^{15} esu/cm^3.

Table X. Bonding results of gold compounds.

Compound	q_{zz}	$q_{610}=-25$		$q_{610}=-35$		$q_{610}=-40$		$q_{610}=-44$		$q_{610}=-50$	
		α^2	X	α^2	X	α^2	X	α^2	X	α^2	X
Gold(I)											
AuCl	13.339	0.27	-0.07	0.19	+0.24	0.17	+0.33	0.15	0.41	0.13	0.47
AuBr	12.134	0.24	0.03	0.17	0.31	0.15	0.39	0.13_5	0.46	0.12	0.51
AuI	11.417	0.23	0.09	0.16	0.35	0.14	0.43	0.12_6	0.49	0.11	0.54
$Au(S_2O_3)_2^{-3}$	20.310	0.41	-0.62	0.29	-0.16	0.25	-0.02	0.23	0.10	0.20	0.19
AuCN	23.207	0.46	-0.86	0.33	-0.32	0.29	-0.16	0.26	-0.03	0.23	+0.07
$KAu(CN)_2$	29.288	0.59	-1.34	0.42	-0.67	0.37	-0.46	0.33	-0.30	0.29	-0.17
Gold(III)											
AuF_3	-7.860	0.44	-0.54	0.37	0.04	0.34	0.26	0.32	0.41	0.29	+0.61
$[AuF_4]^-$	-5.221	0.47	-0.74	0.39	0.14	0.36	0.10	0.34	0.26	0.32	0.48
$KAuCl_4$	3.643	0.55	-1.42	0.46	-0.70	0.43	-0.43	0.40	-0.24	0.37	0.01
$AuCl_3$	2.151	0.54	-1.31	0.45	-0.61	0.42	-0.34	0.39	-0.15	0.36	0.09
$KAuBr_4$	3.242	0.55	-1.39	0.46	-0.68	0.43	-0.41	0.40	-0.21	0.37	0.04
$AuBr_3$	3.643	0.55	-1.42	0.46	-0.70	0.43	-0.43	0.40	-0.24	0.37	0.01
$KAu(CN)_4$	20.052	0.71	-2.69	0.60	-1.77	0.55	-1.41	0.52	-1.16	0.48	-0.84
$KAu(CN)_2Cl_2$	~12.69	0.64	-2.12	0.54	-1.29	0.50	-0.97	0.47	-0.75	0.43	-0.46
$KAu(CN)_2Br_2$	~13.53	0.65	-2.19	0.54	-1.35	0.50	-1.02	0.47	-0.80	0.44	-0.50
$KAu(CN)_2I_2$	~13.85	0.65	-2.21	0.55	-1.37	0.51	-1.04	0.48	-0.81	0.44	-0.52
$[AuS_4C_4(CN)_4]^-$	5.651	0.57	-1.58	0.48	-0.84	0.44	-0.55	0.42	-0.35	0.39	-0.09
Au_2O_3	4.819	0.56	-1.52	0.47	-0.78	0.44	-0.50	0.41	-0.30	0.38	-0.05

q_{zz}, q_{610} are in units of 10^{15} esu/cm^3.

VI. SUMMARY

From the Mössbauer experiment results of the linear gold(I) and square-planar gold(III) compounds, a direct relationship was established between the isomer shifts and quardupole splittings for both oxidation states of gold. This relationship was explained in terms of the hybridization of the bonds and the number of bonding electrons on gold. The results suggest that the hybridizations of the compounds remain essentially constant, sp for the gold(I) and dsp^2 for the gold(III) compounds, and that the changes in the isomer shift and quadrupole splittings are due to the differences in the ionic character of the various compounds.

We attempted to determine the values of q_{522} and q_{610} from Dirac-Fock free-atom wavefunctions of gold which were calculated by Mann.[71] For q_{522}, we deduced a value of 26.86×10^{15} esu/cm^3. q_{522} was not a sensitive function of charge. Unfortunately, the q_{610} value was much more difficult to determine and was found to be a very sensitive function of charge. From the free-atom wavefunctions, we estimated q_{610} to be about -25×10^{15} esu/cm^3. However, from the results of the linear relationship of the isomer shift and quadrupole splitting for gold(I) and gold(III) compounds, and the nuclear electron density calculations, we arrived at a q_{610} value of -44×10^{15} esu/cm^3. This corresponds to a nuclear factor, $\delta R/R$, of $+3.1\times10^{-4}$. The charges on gold in the compounds were determined for several q_{610} values between -25×10^{15} and -50×10^{15} esu/cm^3. From electronegativity considerations, the charge on gold is expected to be positive for gold halides. This implies a minimum value of $|q_{610}|$ for gold(I) compounds of about -37×10^{15} esu/cm^3 and a minimum value of $|q_{610}|$ for gold(III) compounds of about

-50×10^{15} esu/cm^3. This difference may not be unreasonable since the q_{610} value which is applicable for the gold(I) compounds is most likely not identical to that which is applicable for the gold(III) compounds.

It appears that the free-atom wavefunction calculations are not adequate for estimating the electric field gradient for loosely bound electrons such as the 6p electrons of gold. Further insight into the bonding characteristics of these gold compounds must await molecular structure calculations which are not available at this time for heavy atoms.

APPENDIX A

Error Analysis[85]

We give brief definitions for the standard deviation and probable error, and a detailed discussion of the computation of the errors reported in this work.

For a function, F, of several variables x, y, ..., its standard deviation, σ_F, is defined as:

$$\sigma_F = \sqrt{\left(\frac{\partial F}{\partial x}\,\sigma_x\right)^2 + \left(\frac{\partial F}{\partial x}\,\sigma_y\right)^2 + \ldots} \qquad (1)$$

where σ_x, σ_y,... are the standard deviations of x, y, ... σ_x, σ_y, are not always known and cannot always be readily determined.

The standard deviation, σ, for a collection of N measurements is

$$\sigma = \sqrt{\sum_{i=1}^{N} \frac{(\bar{x} - x_i)^2}{N}} \qquad (2)$$

where $\bar{x}$ is the average value of the measured x_i's. From the standard deviation, we can compute the probable error, pe, of the collection of measurements:

$$pe = 0.6745\sigma \qquad (3)$$

The pe is the 50%-confidence limit as explained in Sec. IV-D.

For the results of an experiment as complex as that of the Mössbauer effect, it is difficult to find a simple probability model for the computed measurements: isomer shift IS, quadrupole splitting QS and

linewidth Γ. In this work we have given the more limited statistical precision indices. A detailed error analysis follows for AuF_3.

Table I includes a tabulation of the $v_o(1)$ and $v_o(2)$ values which are the line positions of the two component lines for the three AuF_3 experiments: runs 184a, 184 and 185. The IS and QS are computed from the expressions below for diamagnetic compounds in axially symmetric environments and are tabulated in columns III and V respectively:

$$IS = \frac{v_o(1) + v_o(2)}{2} \tag{4}$$

$$|QS| = |v_o(1) - v_o(2)| \tag{5}$$

For AuF_3 the IS and QS are +0.107 (.006) and 0.274(.002) cm/sec respectively. The linewidth is 0.232 (.002) cm/sec. The pe, given in parentheses, are determined by applying Eqs. (2) and (3). In Sec. IV-D, it was explained that the mirror-image IS values should be averaged, and not treated as independent results. This averaging is done in column IV which yields the same IS value but a smaller (and more accurate) pe of 0.001 cm/sec (which was actually computed as 0.0005 cm/sec). The pe for all the compounds were computed in this manner. To give an indication of the statistics for each run, the values of the baselines of each run are listed in column VII. Chi-squares are given in the eighth column. The value of chi-square, χ^2, equal to one is the ideal lower limit. The Chi-square increases with poorer fits.

Table I. Computation of probable error, pe, as reported in the results.

Run	I $v_o(1)$ cm/sec	II $v_o(2)$ cm/sec	III IS cm/sec	IV IS cm/sec	V QS cm/sec	VI Γ cm/sec	VII Baseline counts	VIII χ^2
184a	-.253070	.026410	-.113330	-0.107591	.279480	.237019	2.54×10^6	1.9287
	-.238533	.0348272	-0.101853		.273360	.230792		1.5851
184	-.252539	.0192205	-.116609	-0.107731	.271760	.235090	1.32×10^6	1.2396
	-.235279	.0375700	-.098854		.272849	.230300		0.97819
185	-.255759	.0181634	-.1182978	-0.1068019	.2739225	.231904	5.22×10^5	1.0537
	-.232544	.0419315	-.095306		.274476	.229290		1.1830
			Ave=-0.107_4	Ave=0.107_4	Ave=0.274_3	Ave=0.232_4		
			Pe = $.006_1$	pe =$.00_{48}$	pe =$.001_{66}$	pe = $.0018_6$		

An alternative method of determining a pe for the isomer shift, IS, and the quadrupole splitting, QS, would be to use the RMSU values of $v_o(1)$ and $v_o(2)$ which are computed by FLOR*. Table II has a tabulation of these RMSU values for AuF_3. If these RMSU values are taken to be the errors in $v_o(1)$ and $v_o(2)$, then the σ_{IS} and σ_{QS} can be calculated from Eq. (1) where F would be given by Eqs. (4) and (5),

$$\sigma_{IS} = \frac{1}{2} \sqrt{\text{RMSU } v_o(1)^2 + \text{RMSU } v_o(2)^2} \tag{6}$$

$$\sigma_{QS} = \sqrt{\text{RMSU } v_o(1)^2 + \text{RMSU } v_o(2)^2} \tag{7}$$

From these standard deviations, the probable errors can be computed as above in Table I. This method yields a pe of $(.000_2)$ and $(.000_4)$ cm/sec for the IS and QS respectively. The pe for the IS computed in Table I is approximately 2-1/2 times larger than computed in Table II. That for the QS is more than 4 times larger.

The pe for the gold compounds in general, as computed in Table I, has been between two and six times larger than the corresponding pe values computed by the method of Table II. We have a few instances were the former pe is more than an order of magnitude larger than the latter pe for the IS. Table I-type pe values are consistently closer than the Table II-type pe values to the value of the velocity interval between successive channels, which is an index of the precision limit. The most frequent value of the velocity interval between successive channels is 0.012 cm/sec. Therefore, we have given the Table I-type errors.

---

*FLOR is the computer program to fit Lorentz curves to the Mössbauer spectra.

Table II. Computation of probable error, pe, from RMSU values.

Run	I RMSU-$v_o(1)$	II RMSU-$v_o(2)$	III σ(IS)	IV pe$(IS)_i$	V σ(QS)	VI pe(QS_i)	VII RMSU Γ
184a	2.18868×10^{-4}	2.20659×10^{-4}	1.55397×10^{-4}	1.04815×10^{-4}	3.10795×10^{-4}	2.09631×10^{-4}	5.44693×10^{-4}
	2.16905×10^{-4}	2.13252×10^{-4}	1.52089×10^{-4}	1.02584×10^{-4}	3.04178×10^{-4}	2.05168×10^{-4}	5.19611×10^{-4}
184	-3.42478-4	3.37090-4	2.421204-4	1.633102-4	4.842409-4	3.266205-4	8.01626-4
	-3.42342-4	3.63835-4	2.497869-4	1.6848126-4	4.995738-4	3.369625-4	9.24460-4
185	-5.84786×10^{-4}	5.65212×10^{-4}	4.0664458-4	2.74281769-4	8.1328917-4	5.4856355-4	1.2996×10^{-3}
	-5.74241-4	5.80842-4	4.083902-4	2.754592-4	8.167804-4	5.509184-4	1.33841×10^{-3}

σ_T =	σ =
2.8880139-4	5.7760288E-4
pe =	pe =
1.94797-4 IS	3.895931-4 QS

APPENDIX B

Evaluation of $\langle 1/r^3 \rangle$ Calculations

To calculate $\langle 1/r^3 \rangle$ for gold, we initially made Hartree-Fock atomic structure calculations of various excited states of gold with a program devised by Roothaan.[77,78] This program uses Slater orbitals and treats exchange exactly. We started by using a minimal basis set for these calculations. However, we soon realized the serious extent of the limitations of the program for heavy atoms. The maximum total number of vector components allowed in the program is 150. This number could adequately treat configurations up to about $[Kr]5s^2$ and probably could not accommodate elements with 4d electrons.

As an alternative, we calculated $\langle 1/r^3 \rangle$ values from the Slater-Hartree-Fock atomic structure calculations published by Herman and Skillman.[76] These calculations, like those with the Roothaan's program are nonrelativistic. Also, Herman and Skillman use the Slater approximation for exchange. We find that the use of this approximation is not always justified by comparing some $\langle 1/r^3 \rangle$ values with those of Mann,[71] who has published Hartree-Fock atomic structure calculations where he has treated exchange exactly. We see from Table I, that the $\langle 1/r^3 \rangle_{5d^n}$ values for Ir, Pt and Au ground states which were calculated from the Herman and Skillman results and by Mann agree to about 10%. The former values being larger. However, we get much less agreement when comparing $\langle 1/r^3 \rangle_{6p^n}$ values in Table II. Here, the Herman and Skillman method yields much larger $\langle 1/r^3 \rangle$ values than does Mann's. Table I also

Table I. Non-relativistic $\langle \frac{1}{r^3} \rangle_{5d}$ values for Ir, Pt and Au in units of a_o^{-3}.

Element \ Method of Calcs.	Mann Hartree-Fock	Hermann & Skillman Slater-Hartree Fock	Roothaan Hartree-Fock (minimum basis set)
Ir	$5d^7 6s^2$	$5d^7 6s^2$	$5d^8(+1)$
	$\langle \frac{1}{r^3} \rangle_{5d^7}=10.542$	$\langle \frac{1}{r^3} \rangle_{5d^7}=12.49$	$\langle \frac{1}{r^3} \rangle_{5d^8}=4.776$
Pt	$5d^9 6s$	$5d^9 6s$	$5d^9(+1)$
	$\langle \frac{1}{r^3} \rangle_{5d^9}=11.116$	$\langle \frac{1}{r^3} \rangle_{5d^9}=13.145$	$\langle \frac{1}{r^3} \rangle_{5d^9}=6.017$
Au	$5d^{10} 6s$	$5d^{10} 6s$	$5d^{10} 6p(+0)$
	$\langle \frac{1}{r^3} \rangle_{5d^{10}}=12.43$	$\langle \frac{1}{r^3} \rangle_{5d^{10}}=13.624$	$\langle \frac{1}{r^3} \rangle_{5d^{10}}=6.874$

Table II. Non-relativistic $\langle 1/r^3 \rangle_{6p}$ values for Tl, Pb and Bi in units of a_o^{-3}.

Method of calcs. / Element	Mann Hartree-Fock	Hermann & Skillman Slater-Hartree-Fock	Roothaan Hartree-Fock minimal basis set
Tl	$5d^{10}6s^2 6p(+0)$	$5d^{10}6s^2 6p(+0)$	$5d^{10}6s^2 6p(+0)$
	$\langle 1/r^3 \rangle = 7.55$	$\langle 1/r^3 \rangle_{6p} = 11.94$	$\langle 1/r^3 \rangle_{6p} = 6.34$
Pb	$5d^{10}6s^2 6p^2(+0)$	$5d^{10}6s^2 6p^2(+0)$	$5d^{10}6s^2 6p(+1)$
	$\langle 1/r^3 \rangle_{6p^2} = 10.99$	$\langle 1/r^3 \rangle_{6p^2} = 16.02$	$\langle 1/r^3 \rangle_{6p} = 10.21$
Bi	$5d^{10}6s^2 6p^3(+0)$	$5d^{10}6s^2 6p^3(+0)$	$5d^{10}6s^2 6p(+2)$
	$\langle 1/r^3 \rangle_{6p^3} = 14.57$	$\langle 1/r^3 \rangle_{6p^3} = 19.71$	$\langle 1/r^3 \rangle_{6p} = 14.924$

illustrates the inadequacy of the minimal basis set calculations which we made with Roothaan's program. One strong indication that Mann's Hartree-Fock calculations are probably reliable is the good agreement of the $\langle 1/r^3 \rangle_{5d}$ value for gold between his calculations ($12.43\ a_o^{-3}$) and experimental results. $\langle 1/r^3 \rangle_{5d}$[9] for gold has been determined as 12.3 and 11.8 a_o^{-3} from magnetic hyperfine interaction and atomic fine-structure splitting.[72]

In Table III, we tested the agreement between calculations made with Roothaan's program and those made by Mann by calculating the wave functions and $\langle 1/r^3 \rangle_{4p}$ values for bromine by using Clementi's[87] expanded basis set. The Roothaan-Clementi result ($\langle 1/r^3 \rangle_{4p} = 11.186\ a_o^{-3}$) was in excellent agreement with that of Mann ($\langle 1/r^3 \rangle_{4p} = 11.996\ a_o^{-3}$). We feel that Mann's atomic structure calculations are the best available. As was evident in Section V-D, the problem of calculating electric field gradients lies largely in determining which free-atom states are applicable to the given molecular situation.

Table III. Non-relativistic $\langle 1/r^3 \rangle_{4p^5}$ values for the ground state of bromine.

Mann[75] Hartree-Fock	Herman & Skillman[76] Slater-Hartree-Fock	Roothaan† Hartree-Fock
		Expanded basis set: $11.186\ a_o^{-3}$
$11.996\ a_o^{-3}$	$14.857\ a_o^{-3}$	
		Minimal basis set: $7.322\ a_o^{-3}$

† The expanded basis set consisted of 76 basis vectors as determined by Clementi.[86] The minimal basis set consisted of only 26 vectors.

APPENDIX C

Electric Field Gradients

1. The Main Sources of Electric Field Gradients

The quadrupole splitting, QS, obtained with the Mössbauer effect is a sensitive indication of the electric field gradient, EFG, of the nuclear electronic environment. Care is required in interpreting these results as several factors affect the EFG: the hybridization of the bonds, their ionic character, the effective lattice field gradient and its effect on the closed electron shells, and the extent of multiple bonding, to name a few. With Sternheimer's calculations, we find that the distortions of the inner closed shells by the valence electrons and the lattice charges cannot always be disregarded. The Sternheimer[80-82] shielding (antishielding) factors are often large enough to make the lattice contributions to the EFG significant. These contributions to the EFG are related as follows:

$$q_{zz} = (1 - \gamma_\infty)q^{latt} + \sum_{nlm} (1 - R_{nl})a_{nlm} \langle q_{nlm} \rangle_i \qquad (1)$$

The q_{zz} is the observed field gradient oriented about the z axis and q^{latt} is the field gradient due to lattice charges in the limit of zero polarizability of the closed shells. $(1 - \gamma_\infty)$ is the lattice Sternheimer shielding factor. If γ_∞ is negative, the factor is said to be antishielding. $(1 - R_{nl})$ is the atomic Sternheimer shielding (antishielding) factor for the nl electrons. $\langle q_{nlm} \rangle$ is the expectation value of the field gradient for the nlm electron with its coefficient, a_{nlm}, which gives its fractional

contribution to the molecular wavefunction. The atomic contributions are summed over all the orbitals used in bonding. Neither γ_∞ nor R_{nl} has been theoretically calculated for gold.

If it were not for large lattice Sternheimer antishielding factors, the penetrating valence electrons would be the most significant source of EFG at the nucleus. Townes and Dailey[4] had predicted that of the valence electrons, the p electrons were probably the most important. They based this assumption largely on available experimental evidence. For example, the ratio of the EFG for the cesium 5d and 6p electrons is[4]

$$\langle q_{5d}(\mathrm{Cs})\rangle / \langle q_{6p}(\mathrm{Cs})\rangle \cong 1/11 \tag{2}$$

However, we have determined that the values of $\langle q_{5d}\rangle$ and $\langle q_{6p}\rangle$ are more comparable for gold

$$\langle q_{5d}(\mathrm{Au})\rangle / \langle q_{6p}(\mathrm{Au})\rangle \cong 1 \tag{3}$$

From our calculations in Sec. V-D, it appears that the EFG of the 5d electrons can be even larger than that of the 6p electrons. Therefore, it would be incorrect to categorically disregard all non-p electron contributions to the EFG.

We offer the following explanation for the increase in the ratio of $\langle q_{5d}\rangle / \langle q_{6p}\rangle$ in going from cesium to gold. For cesium, both the excited 5d and 6p electrons are subjected to approximately the same amount of screening from the (xenon-configuration) closed shell. Due to the r^2

dependence of the electron density of 6p electrons near the nucleus as compared to the r^4 dependence of the 5d electrons, there would be a larger EFG at the cesium nucleus caused by the 6p electrons.

For gold, however, the mutual screening of the 5d electrons in the nearly filled shell is less than their collective screening of the valence 6p electrons. Therefore, the 5d electrons in gold are held more tightly by the larger effective nuclear charge than are the 6p electrons, and thus have a larger EFG.

2. Calculation of Electric Field Gradients

The calculation of atomic and molecular electric field gradients has been treated in the literature,[4,5,69] therefore we will develop here only that portion which is necessary for understanding our results. The molecular electric field gradients, q, cannot be caluclated exactly even neglecting antishielding factors. They can, however, be estimated for atoms and molecules by using hydrogenic wave functions, ψ_{nlm}

$$\psi = \sum_{nlm} a_{nlm} \psi_{nlm} \tag{4}$$

where n, l, and m are the principal, azimuthal and magnetic quantum numbers respectively and a_{nlm} is the coefficient of ψ_{nlm}.

The molecular electric field gradient, q_{zz}, is discussed in Sec. V-E. There, we estimated the dominating term of the q_{zz} of a gold atom which is bonded to a ligand, L, as

$$q_{zz}(Au) = \alpha^2 \int \psi_{Au} \frac{(3\cos^2\theta - 1)}{r^3} \psi_{Au} \, d\tau \tag{5}$$

where α is defined in Eq. (3) of Sec. V-E by

$$\psi_{AuL} = \alpha\psi_{Au} \pm \beta\psi_L \tag{6}$$

and overlap is neglected in normalization, i.e.,

$$\alpha^2 + \beta^2 = 1 \tag{7}$$

The EFG arising from a given pair of atomic orbitals, ψ_{nlm} and $\psi_{n'l'm'}$ is designated as $q_{nlm,n'l'm'}$ where

$$\langle q_{nlm,n'l'm'} \rangle = -e \int \psi_{nlm} \left(\frac{3\cos^2\theta - 1}{r^3} \right) \psi_{n'l'm'} \, d\tau \tag{8}$$

and the total EFG of the molecule is

$$q_{zz}(\text{molecule}) = \sum_{nlm,n'l'm'} | a_{nlm} a^*_{n'l'm'} | \, q_{nlm,n'l'm'} \tag{9}$$

The value of $q_{nlm,n'l'm'}$ is non-zero if $m = m'$ and either $l = l'$ $(l \neq 0)$ or $l = l' \pm 2$, a consequence of the behavior of spherical harmonics and the second order Legendre polynomial factor, $(3\cos^2\theta - 1)$. For clarity, if $n = n'$ and $l = l'$, $q_{nlm,nlm}$ is given as q_{nlm}. The q_{nlm} terms make the largest contribution to q_{zz}(molecule).

The EFG due to a single hydrogenic orbital electron is given in closed form as

$$q_j = e \frac{(2j - 1)}{(2j + 2)} \langle 1/r^3 \rangle_{nl} R_r \tag{10}$$

where j is the sum of the electron spin and the orbital momentum, l. z is that direction in space in which l has the maximum projection (m = l). R_r[74] is the relativistic correction factor. The problem of obtaining the orbital EFG is reduced to determining the average value of $1/r^3$, $\langle 1/r^3 \rangle$, for the electrons of interest.

For the non-relativistic hydrogenic case,

$$\langle 1/r^3 \rangle = \frac{Z^3}{n^3\, l(l+1/2)(l+1)a_o^{\,3}} \tag{11}$$

where Z is the nuclear charge, and a_o is the Bohr radius, $h/2\pi me^2$. When screening effects become important, as with heavy nuclei, the values of z and n must be modified to reflect the effective nuclear charge and the effective total quantum number. This necessarily introduces uncertainties.

Fortunately, there are two experimental methods of obtaining more reliable values of $\langle 1/r^3 \rangle$. $\langle 1/r^3 \rangle$ can be calculated from the magnetic hyperfine structure constant, a, if the value of the nuclear magnetic moment, μ_I, is known,

$$a = \frac{2\mu_I \mu_o}{I} \langle 1/r^3 \rangle \frac{l(l + 1)}{j(j + 1)} F_r \tag{12}$$

where μ_o is the Bohr magneton, I the nuclear spin, and F_r is a relativistic correction. These relativistic corrections approach unity for small Z. Their values are tabulated in Refs. 5 and 74.

The second experimental method of determining $\langle 1/r^3 \rangle$ is from the separation between two fine structure levels, $\Delta\nu$:

$$\Delta\nu = Z_i(l + 1/2) \langle 1/r^3 \rangle R\, \alpha^2\, Hr\, dn^*/dn \tag{13}$$

Z_i is the effective Z for a penetrating orbit, R is the Rydberg constant, α is the fine structure constant and H_r is a relativistic correction. The change in the effective principal quantum number, with respect to the principal quantum number is dn^*/dn, and is usually taken as unity.

We obtained our $\langle 1/r^3 \rangle$ values from Dirac-Fock atomic structure calculations which were supplied by Mann.[71] These results are discussed in Sec. V-D and Appendix B.

Given a value for $\langle 1/r^3 \rangle$, q_{nll} can be calculated from Eq. (10). If the electron orbital of interest lies along the symmetry axis (as in a diatomic molecule) the required field gradient, q_{nl0}, is given by

$$q_{nl0} = -\frac{(l + 1)}{(2l - 1)}\, q_{n\,ll} \tag{14}$$

and q_{nlm} is non-zero for $l > 0$. For s electrons ($l = 0$), the charge distribution is symmetric and does not contribute to the field gradient.

For p electrons ($l = 1$), which have zero probability of being in the nucleus (except for relativistic $p_{1/2}$ electrons), we have from

Laplace's equation, $\nabla^2\phi = 0$, that

$$q_{611} + q_{61\bar{1}} + q_{610} = 0 \tag{15}$$

and from symmetry,

$$q_{611} = q_{61\bar{1}} \tag{16}$$

Therefore, as we also have from Eq. (11) for l = 1, we have

$$-q_{611} = 1/2\ q_{610} \tag{17}$$

For convenience, we have been using hydrogenic wavefunctions, ψ_{nlm}, in discussing field gradients. However, when treating bonds, such as in Sec. III, we used the more descriptive atomic orbitals (e.g., p_x, p_y, ect.). Therefore we now give the unitary transformation matrix which maps the p orbitals into the equivalent hydrogenic wavefunctions:

$$\begin{bmatrix} 6p_x \\ 6p_y \\ 6p_z \end{bmatrix} = 1/\sqrt{2} \begin{bmatrix} 1 & 1 & 0 \\ 1 & -1 & 0 \\ 0 & 0 & 1 \end{bmatrix} \begin{bmatrix} 611 \\ 61\bar{1} \\ 610 \end{bmatrix} \tag{18}$$

Thus, if $\hat{q}$ is the field gradient operator,

$$q_{6p_x} = \langle 6p_x|\hat{q}|6p_x\rangle = 1/2(q_{611} + q_{61\bar{1}}) = q_{611} \tag{19}$$

Similarly,

$$q_{6p_y} = q_{611} \tag{20}$$

and

$$q_{6p_z} = q_{610}$$

For the d electrons (l = 2), we get the following relationships by using the same reasoning as for the p electrons:

$$q_{522} + q_{52\bar{2}} + q_{521} + q_{52\bar{1}} + q_{520} = 0 \tag{21}$$

where

$$q_{522} = q_{52\bar{2}} \tag{22}$$

and

$$q_{521} = q_{52\bar{1}} \tag{23}$$

From Eq. (14) we have;

$$q_{520} = -q_{522} \tag{24}$$

therefore,

$$q_{521} = -1/2 q_{522} \tag{25}$$

The unitary transformation between the d orbitals and the hydrogenic wavefunctions is

$$\begin{bmatrix} \psi_{d_{x^2-y^2}} \\ \psi_{d_{xy}} \\ \psi_{d_{xz}} \\ \psi_{d_{yz}} \\ \psi_{d_{z^2}} \end{bmatrix} = 1/\sqrt{2} \begin{bmatrix} 1 & 1 & 0 & 0 & 0 \\ 1 & -1 & 0 & 0 & 0 \\ 0 & 0 & 1 & 1 & 0 \\ 0 & 0 & 1 & -1 & 0 \\ 0 & 0 & 0 & 0 & 1 \end{bmatrix} \begin{bmatrix} \psi_{522} \\ \psi_{52\bar{2}} \\ \psi_{521} \\ \psi_{52\bar{1}} \\ \psi_{520} \end{bmatrix} \tag{26}$$

This gives the following relationships

$$q_{d_{z^2}} = q_{520} \tag{27}$$

$$q_{d_{xz}} = q_{d_{yz}} = 1/2\ q_{521} + 1/2 q_{52\bar{1}} = q_{521}$$

$$q_{d_{x^2-y^2}} = q_{d_{xy}} = 1/2 q_{52\bar{2}} + 1/2 q_{52\bar{2}} = q_{522}$$

APPENDIX D

The Calculation of q^{latt} Values

For the purpose of calculating q^{latt} values, we will treat the charges of the ligands, X_L, as point charges which are located a distance r (the interatomic distance) from the gold atom. The expression for the electric field gradient due to the point charges is

$$q_{zz} = \sum_i X_{L(i)} \cdot e\,(3\cos^2\theta - 1)/r^3 \qquad (1)$$

where e is the electronic charge 4.803×10^{-10} esu/cm^3 and θ is the angle measured from the z axis. The charge X_L is related to α, the contribution of the gold atomic orbitals to the molecular wavefunction, by the following equation

$$X_L = 2\alpha^2 - 1 \qquad (2)$$

The nearest-neighbor lattice contribution to the electric field gradient at the gold nucleus is

$$q^{latt}(Au(I)) = 4(2\alpha^2 - 1)e/r^3 \qquad (3)$$

for the linear gold(I) compounds and

$$q^{latt}(Au(III)) = -4(2\alpha^2 - 1)e/r^3 \qquad (4)$$

for the square-planar gold(III) compounds.

In Table I, several values of q^{latt} are given. In the third column, the maximum possible q^{latt} is listed which was determined by assuming that the ligands had a full charge of -1. The fifth column has q^{latt} values which reflects the α^2 values which were determined by taking q_{610} to be -25.01×10^{15} esu/cm^3. The sixth and seventh columns have α^2 and q^{latt} values respectively which correspond to a q_{610} of -37.48×10^{15} esu/cm^3. See Secs. V-C and V-E.

The interatomic distances are in angstroms and the q^{latt} values are in units of 10^{15} esu/cm^3.

Table I. q^{latt} values for gold compounds of known interatomic distances.

Compounds	Interatomic distances Å	q^{latt} for $\alpha^2=0$	α_I^2	q^{latt}	α_2^2	q^{latt}
AuF_3 [41]	2.00	+0.240	0.44	+0.029	0.36	+0.067
$KAuCl_4$ [45]	2.29	+0.160	0.55	-0.016	0.45	+0.016
$KAuBr_4$ [52]	2.56	+0.115	0.55	-0.011	0.44	+0.014
		Average =+0.17		Average = 0.00		Average =+0.032
$[AuCl_2]^-$ [47]	2.30	-0.158	0.27	-0.073	0.18	-0.101
$Na_3Au(S_2O_3)_2$ [66]	2.28	-0.180	0.41	-0.029	0.27	-0.075
$KAu(CN)_2$ [62]	2.12	-0.202	0.59	+0.036	0.39	-0.044
AuI [56]	2.62	-0.107	0.23	-0.058	0.15	-0.075
		Average =-0.16		Average = 0.00		Average =-0.06

APPENDIX E

Evaluation of Crawford-Schawlow Effect

The Crawford-Schawlow[83] effect has been of interest where the density of the electrons in the nucleus is of importance. Crawford and Schawlow had predicted that the shielding of the inner s electrons by the valence s electrons would be significant at the nucleus where the inner electrons have a high density. For the isotope effect in Hg, they estimated a 16% correction due to such shielding.

Since the isomer shift is a function of $\psi(0)^2$, such an effect would be important if it were large enough to warrant subsequent corrections. To test for this shielding effect, we compared the $\psi(0)^2$ values for the $5d^9 6s$ and $5d^9 6s^2$ states of gold which differ by one 6s electron. We found, however, that the $\psi(0)^2_{ns}$ values for corresponding n values were very close and that where they differed, the $5d^9 6s^2$ state usually had the larger electron density. This is in the unexpected direction and it is difficult to understand since the $5d^9 6s$ state of gold has a residual +1 charge in addition to having one less 6s electron. Table IV of Sec. V-C gives a complete list of the $\psi(0)^2_{ns}$ values of interest.

We further compared the $5d^{10} 6s$ gold ground state with the ground state of mercury, $5d^{10} 6s^2$. Here, we found that without exception, mercury had higher $\psi(0)^2_{ns}$ values than the corresponding gold orbitals. This is understandable since mercury has a higher nuclear charge (Z = 80) than has gold (Z = 79). Mercury, therefore, has a greater attraction for its electrons.

The third pair of cases was chosen to have the following properties:

1. The same element so that Z would be of equal value
2. The same ionic charge
3. One less valence s electron in one case of the pair
4. Equal numbers of 5d electrons to eliminate differences in the shielding therefrom.

The $5d^9 6s$ (+1) and $5d^9 6p$ (+1) states fulfilled these requirements. Here, we observed the predicted shielding effects. Table I facilitates the comparison of the corresponding $\psi(0)^2_{ns}$ values of the two states, giving both their algebraic differences and the percentage differences. As expected, the percentage shielding effect increases with principal quantum number n. The shielding effect, however, is very small (a few tenths of a percent to less than 10^{-4} percent) and a correction due to shielding differences is not warranted in our calculations.

Crawford and Schawlow estimated the importance of the screening effect of the valence s electrons on the inner s electrons by evaluating the ratio of $\psi(0)^2_{ns}/\psi(0)^2_{6s}$, using Hartree wavefunctions. In Table II we list their Hartree-$\psi(0)^2_{ns}$ values along with the $\psi(0)^2_{ns}/\psi(0)^2_{6s}$ ratios. For comparison, we have tabulated the Dirac-Fock-$\psi(0)^2_{ns}$ values and the corresponding $\psi(0)^2_{ns}/\psi(0)^2_{6s}$ ratios. From the Table II, it is evident that the magnitude of the screening effect appeared larger using the less accurate Hartree wavefunctions, but is greatly reduced when Dirac-Fock wavefunctions are considered instead.

Table I. Screening correction due to 6s electrons in $5d^9 6s$ and $5d^9 6p$ states of gold.

ns	$5d^9 6s$ $\lvert\psi(0)^2_{ns}\rvert$	$5d^9 6p$ $\lvert\psi(0)^2_{ns}\rvert$	Δ	$\Delta\%$
1s	1.081135×10^{31}	1.081134×10^{31}	1.913×10^{24}	1.76×10^{-5}
2s	1.618193×10^{30}	1.618186×10^{30}	7.889×10^{23}	4.88×10^{-5}
3s	3.707404×10^{29}	3.707298×10^{29}	1.068×10^{25}	2.78×10^{-3}
4s	9.251960×10^{28}	9.250446×10^{28}	$1.514_5\times10^{25}$	1.68×10^{-2}
5s	1.732718×10^{28}	1.728676×10^{28}	4.042×10^{25}	2.34×10^{-1}

Table II. $|\psi(0)^2_{ns}|$ values of Hg and the ratios, $|\psi(0)^2_{ns}|/|\psi(0)^2_{6s}|$.

ns orbital	Mann Dirac-Fock $\lvert\psi(0)^2_s\rvert$	$\frac{\lvert\psi(0)^2_{ns}\rvert}{\lvert\psi(0)^2_{6s}\rvert}$	Crawford-Schawlow Hartree[83] $\lvert\psi(0)^2_s\rvert \cdot \pi a H^3$	$\frac{\lvert\psi(0)^2_{ns}\rvert}{\lvert\psi(0)^2_{6s}\rvert}$
1s	1.1346×10^{31}	7050	5.06×10^{5}	15850
2s	1.715999×10^{30}	1070	5.56×10^{4}	1740
3s	3.94148×10^{29}	246	1.23×10^{4}	385
4s	9.89270×10^{28}	61.6	3.06×10^{3}	95.5
5s	1.89562×10^{28}	11.8	6.10×10^{2}	19.1
6s	1.60490×10^{27}	1	3.2×10	1

ACKNOWLEDGMENTS

It is with pleasure that I acknowledge those who contributed to this work:

Professor D. A. Shirley for his tireless assistance and guidance through all phases of this research, and the members of his group who have been helpful and informative;

My husband, Andris, whose understanding encouragement and aid have been invaluable;

Mr. D. Voronin, Mr. R. Zane, Mr. L. Crowder, and Mr. C. Ward for their able technical assistance;

Mrs. Winifred Heppler and Mrs. Gertrude Boltz whose willing aid and cheerfulness helped make these years a pleasant experience;

Mr. R. Giauque who analyzed the gold compounds and Mr. R. Dod for his help in the preparation of the unstable gold fluoride compounds;

Mr. H. Anderson and Mrs. E. Potter who helped in many ways;

Mrs. R. Fink (nee Collom) and Mr. L. Wilson who wrote the program for refining experimental data;

Dr. B. Mann and Mr. C. Fadley for their part in the atomic structure calculations;

Dr. Leo Brewer and Dr. J. Rasmussen with whom I had several profitable discussions:

I wish to thank Mrs. James Huntzicker for her timely help with the typing while the thesis was in progress.

This work was performed under the auspices of the United States Atomic Energy Commission.

REFERENCES

1. V. I. Gol'danskii and R. H. Harber, Chemical Application of Mössbauer Spectroscopy (Academic Press, New York, 1968).
2. D. A. Shirley, Science 161, 745 (1968).
3. D. A. Shirley, R. W. Grant, and D. A. Keller, Rev. Mod. Phys. 36, 352 (1964).
4. C. H. Townes and B. P. Dailey, J. Chem. Phys. 17, 782 (1949).
5. C. H. Townes and A. L. Schawlow, Microwave Spectroscopy, (McGraw-Hill Book Company, Inc., New York, 1955).
6. C. H. Townes, Handbuch der Physik (Springer-Verlad, Berlin, 1957), Vol. 38, part 1, p. 443.
7. J. F. Boyle and H. E. Hall, Mössbauer Effect. Rept. progr. Phys. 25, 441 (1962).
8. H. Frauenfelder, The Mössbauer Effect, (W. A. Benjamin, New York, 1962).
9. G. K. Wertheim, Mössbauer Effect: Principles and Applications, (Academic Press, New York, 1964).
10. W. B. Newford, W. K. Robinson, J. O. Thomson, R. E. Obenshain, and L. D. Roberts, Bull. Am. Phys. Soc., 10, 252 (1965).
11. D. A. Shirley, M. Kaplan, and P. Axel, Phys. Rev. 123, 816 (1961).
12. D. O. Patterson, L. D. Roberts, J. O. Thomson, and R. P. Levey, Oak Ridge National Laboratory Report, ORNL-TM-1685, 1967.
13. D. A. Shirley, Rev. Mod. Phys. 36, 339 (1964).
14. A. Abragram and F. Boutron, C. R. Aca. Sci., 252, 2404 (1961).

15. A. G. Blachman, D. A. Landman and A. Lurio, Phys. Rev. 161 161 (1967).

16. S. V. Karyagin, Doklady Akad. Nauk SSSR 148, 1102 (1963).

17. V. I. Gol'danshii, E. F. Makarov, and V. V. Khrapov, Phys. Letters, 3, 344 (1963).

18. V. I. Gol'danshii, The Mössbauer Effect and its Application to Chemistry (D. Van Nostrand Co., Inc., New York, 1966).

19. V. I. Gol'danshii, S. V. Karyagin, E. F. Makarov, and V. V. Khrapov, Transactions of the Conference on the Mössbauer Effect (Dubna, July 1962).

20. T. C. Waddington, Trans. Faraday Soc., 55, 1531 (1959).

21. A. K. Gangopodhyay and A. Chakravorty, J. Chem. Phys. 35, 2206 (1961).

22. L. Pauling, The Nature of the Chemical Bond (Cornell University Press, New York, 1960).

23. B. E. Douglas and D. H. McDaniel, Concepts and Models of Inorganic Chemistry, (Blaisdell Publishing Company, New York, 1965).

24. S. Akerstrom, Arkiv für Kemi, 14, 403 (1959).

26. R. P. Rao, New Fluorides of the Noble Metals (Ph.D. thesis), University of British Columbia, 1965.

27. I. Markland and B. Lindstrom, Arkiv Fysik 22, 422 (1962).

28. C. M. Lederer, J. M. Hollander and I. Perlman, Table of Isotopes (John Wiley and Sons, Inc., New York, 1967), sixth edition.

29. H. L. Wells, Am. J. Sci., 3, 315 (1922).

30. J. C. Bailar, Jr., Inorganic Synthesis (McGraw-Hill Book Co., 19), Vol. IV. p. 14.

31. A. B. Prescott and O. C. Johnson, Quantitative Chemical Analysis (D. Van Nostrand Co., New York, 1933), p. 234.

32. J. M. Smith, L. H. Jones, I. Kressen, and R. A. Penneman, Inorg. Chem. 4, 369 (1965).

33. H. Brown, J. Am. Chem. Soc., 49, 958 (1927).

34. N. V. Sidgwick, The Chemical Elements and Their Compounds (Clarendon Press, Oxford, 1950).

35. M. C. Sneed, J. L. Maynard, and R. C. Brasted, Comprehensive Inorganic Chemistry (D. Van Nostrand Co., Inc., New York, 1954), Vol. 2.

36. R. Zane, Mössbauer Effect Velocity Drive Linearized by Shape Correction, UCRL-16401, 1965.

37. H. Hollis Wickman, Nuclear and Magnetic Resonance Studies in S-State Ions (Ph.D. thesis), UCRL-11538, 1964.

38. M. Klein and R. Zane, Absolute Velocity Calibrations Employing Doppler Shifted Laser Radiation, Laboratory of Chemical Biodynamics, Quarterly, 1964.

39. R. S. Preston, S. S. Hanna, and J. Heberle, Phys. Rev., 128, 511 (1962).

40. W. C. Davidon, Variable Metric Minimization, Argonne National Laboratory Report ANL 5990 Rev., 1959.

41. W. B. Einstein, P. R. Rao, James Trotter, and Neil Bartlett, J. Chem. Soc., 478 (1967).

42. L. B. Asprey, F. H. Kruse, K. H. Jack, and R. Maitland, Inorg. Chem. 3, 602 (1964).

43. L. D. Roberts, H. Pomerace, J. O. Thomson, and E. F. Dam, Am. Phys. Soc., 7, 565 (1962).

44. A. G. Sharpe, Chem. Soc. (London) pt. 4, 2901 (1949).

45. E. S. Clark, D. H. Templeton, Acta Cryst. 11, 284 (1958).

46. L. Capella and C. Schwab, Compt. Rend. 206, (16) (Group 8), 4337 (1965).

47. N. Elliott and L. Pauling, J. Am. Chem. Soc., 60, 1846 (1938).

48. W. Blitz, B. Fisher, and R. Juza, A. Anorg. Chem. 176, 125 (1928).

49. W. Blitz and B. Fisher, A. Anorg. Chem., 176, 81 (1928).

50. P. Machmer, M. Read, and P. Cornil, Compt. Rend., Ser. A, B 262B, (9), 650 (1966).

51. M. Bonamico, G. Dessy, and A. Vaciago, Atti Accad. Nazl. Lincei, Rend., Classe Sci. Fis. Mat. Nat. 39 (6), 504 (1965).

52. E. G. Cox and K. C. Webster, J. Chem. Soc. 1635 (1936).

53. N. Elliott, J. Chem. Phys. 2, 419 (1934).

54. A. Burawoy and C. S. Gibson, J. Chem. Soc., 217, (1935).

55. V. A. Weiss and A. Weiss, Z. Naturforsch, 116, 604 (1956).

56. H. Jagodzinski, Z. für Krist. 112, 80 (1959).

57. P. Machmer, Z. Naturforsch, 21 (11), 1025 (1966).

58. G. S. Zhdanov and E. A. Sugam, Acta Physicochim, URSS 20, 253 (1945).

59. L. H. Jones, J. Chem. Phys. 27, 468 (1957).

60. F. A. Cotton and G. Wilkinson, Advanced Inorganic Chemistry, (Interscience Publishers, New York, 1962), p. 867.

61. A. Rosenzweig and D. T. Cromer, Acta Cryst. 12, 709 (1959).

62. R. A. Penneman and E. Staristzky, Inorg. Nucl. Chem. 17, 45 (1958).

63. C. Weyl, C. R. Acad. Sc. Paris, t. 258, p. 3713 (6 avril 1964) groupe 8.

64. V. Lorenzelli, G. Randi, and F. Gesmundo, Atti Accad. Nazl. Lincei, Rend., Classe Sci. Fis., Mat. Nat. 38, (2), 214 (1965).

65. J. M. Smith. L. H. Jones, I. K. Kressin, and R. A. Penneman, Inorganic Chem., 4, 369 (1965).

66. D. H. Templeton and H. Rubin, (Crystallography, Department of Chemistry, University of California, Berkeley, California) private communication.

67. A. Davison, N. Edelstein, R. H. Holm, and A. H. Maki, Inorg. Chem. 2, 1227 (1963).

68. H. Hirsch, A. deCugnac, M. C. Gadet, and J. Pouradier, C. R. Acad. Sci., Paris, Ser. A, B 263B, (23), 1328 (1966).

69. W. Gordy, in Microwave Spectroscopy, Handbuch der Physik (Springer-verlad, Berlin, 1957), Vol. 28, p. 1.

70. M. A. Whitehead and H. H. Jaffe, Trans. Faraday Soc. 57, 1854 (1961).

71. J. B. Mann, (Physics, Los Alamos Scientific Laboratory, Los Alamos, New Mexico) private communication, September 1968.

72. W. J. Childs and L. S. Goodman, Phys. Rev. 141, 176 (1966).

73. H. G. Dehmelt, H. G. Robinson, and W. Gordy, Phys. Rev. 93, 480 (1954).

74. H. Kopfermann, Nuclear Moments (Academic Press Inc., New York, 1958).

75. J. B. Mann, Atomic Structure Calculations II. Hartree-Fock Wavefunctions and Radial Expectation Values: Hydrogen to Lawrencium, Los Alamos Scientific Laboratory Report, LA-3691, 1968.

76. F. Herman and S. Skillman, Atomic Structure Calculations (Prentice-Hall, New Jersey, 1963).

77. C. C. J. Roothaan, Rev. Mod. Phys. 23, 69 (1951).

78. C. C. J. Roothaan, Rev. Mod. Phys. 32, 179 (1960).

79. A. C. Wahl, P. J. Bertoncini, G. Das, and T. L. Gilbert, International Journal of Quantum Chemistry I S, 123 (1967).

80. R. M. Sternheimer, Phys. Rev. 146, 140 (1966).

81. A. J. Freeman and R. E. Watson, Phys. Rev. 132, 706 (1963).

82. R. M. Sternheimer, Phys. Rev. 159, 266 (1967).

83. M. F. Grawford and A. W. Schawlow, Phys. Rev. 76, 1310 (1949).

84. F. M. Kelly, Proc. Phys. Soc., 65A, 250 (1952).

85. L. G. Parratt, Probability and Experimental Errors in Science: An Elementary Survey (John Wiley and Sons, Inc., New York, 1961).

86. E. Clementi, Tables of Atomic Functions (International Business Machines Corporation, California, 1965), Table 01-15.

LEGAL NOTICE

This report was prepared as an account of Government sponsored work. Neither the United States, nor the Commission, nor any person acting on behalf of the Commission:

A. Makes any warranty or representation, expressed or implied, with respect to the accuracy, completeness, or usefulness of the information contained in this report, or that the use of any information, apparatus, method, or process disclosed in this report may not infringe privately owned rights; or

B. Assumes any liabilities with respect to the use of, or for damages resulting from the use of any information, apparatus, method, or process disclosed in this report.

As used in the above, "person acting on behalf of the Commission" includes any employee or contractor of the Commission, or employee of such contractor, to the extent that such employee or contractor of the Commission, or employee of such contractor prepares, disseminates, or provides access to, any information pursuant to his employment or contract with the Commission, or his employment with such contractor.

TECHNICAL INFORMATION DIVISION
LAWRENCE RADIATION LABORATORY
UNIVERSITY OF CALIFORNIA
BERKELEY, CALIFORNIA 94720